Pennsylvania
Department of Transportation

Electrochemical Testing of Lightweight Aggregates for MSE Wall Fill

FINAL REPORT

February 2026

Mansour Solaimanian
Jun Xiong

PENNSTATE

COMMONWEALTH OF PENNSYLVANIA
DEPARTMENT OF TRANSPORTATION

CONTRACT # 4400025950
WORK ORDER/RFQ # 220417

Technical Report Documentation Page

1. Report No. FHWA-PA-2026-PSU-220417	2. Government Accession No.	3. Recipient's Catalog No.
4. Title and Subtitle Electrochemical Testing of Lightweight Aggregates for MSE Wall Fill		**5. Report Date** February 2026 **6. Performing Organization Code**
7. Author(s) Mansour Solaimanian, Jun Xiong		**8. Performing Organization Report No.** LTI 2026-3
9. Performing Organization Name and Address Thomas D. Larson Pennsylvania Transportation Institute 201 Transportation Research Building The Pennsylvania State University University Park, PA 16802-4710		**10. Work Unit No. (TRAIS)** **11. Contract or Grant No.**
12. Sponsoring Agency Name and Address The Pennsylvania Department of Transportation Bureau of Planning and Research Commonwealth Keystone Building 400 North Street, 6th Floor Harrisburg, PA 17120-0064		**13. Type of Report and Period Covered** **14. Sponsoring Agency Code**

15. Supplementary Notes

Mr. Evan Zeiders acted as the project manager. Ms. Beverly Miller was the project technical advisor.

16. Abstract

Lightweight aggregates (LWAs), including expanded shale and foamed glass aggregate (FGA), are increasingly considered as alternative backfill materials for mechanically stabilized earth (MSE) walls due to their favorable engineering properties. However, questions remain regarding the applicability of conventional electrochemical test methods to LWAs and the interpretation of test results relative to corrosion performance of metallic reinforcements. This study was sponsored by PennDOT to evaluates the electrochemical characteristics of four LWAs, listed in PennDOT Bulletin 14 and Bulletin 15, through sulfate, chloride, pH, and electrical resistivity testing.

Testing was conducted using both standard AASHTO and PennDOT procedures and modified testing approaches to examine the influence of extraction methods, particle size, moisture condition, gradation, and compaction on measured results. Results indicate that sulfate and chloride measurements are strongly influenced by extraction protocol and particle size, with aggressive extraction producing higher measured ion concentrations. Chloride contents were generally low, while sulfate values for certain materials approached specification limits. pH values were generally moderately alkaline, although finer fractions occasionally exceeded specification ranges, indicating the importance of considering gradation effects during evaluation.

Electrical resistivity testing demonstrated that all LWAs exhibit high resistivity relative to specification thresholds and that resistivity is strongly affected by moisture content, compaction, and drainage behavior. Laboratory resistivity values may represent upper-bound conditions relative to field performance due to differences in compaction. Overall, the results support the suitability of LWAs for MSE wall applications when evaluated using appropriate testing procedures. Recommendations are provided regarding sample preparation, interpretation of electrochemical tests, and resistivity testing protocols to improve consistency and applicability of laboratory evaluations.

17. Key Words	18. Distribution Statement
Lightweight aggregates (LWA); MSE wall backfill; Electrical resistivity; Electrochemical testing; Corrosion risk	No restrictions. This document is available from the National Technical Information Service, Springfield, VA 22161

19. Security Classif. (of this report)	20. Security Classif. (of this page)	21. No. of Pages	22. Price
Unclassified	Unclassified	118	**$287,895.87**

Electrochemical Testing of Lightweight Aggregates for MSE Wall Fill

Final Report

Prepared by

Mansour Solaimanian

Jun Xiong

Larson Transportation Institute

The Pennsylvania State University

February 9, 2026

Table of Contents

Acknowledgement ix
Disclaimer ix
C H A P T E R 1 Introduction 1
1.1 Background 1
1.2 Objective and Scope of Work 2
1.3 Report Organization 3
C H A P T E R 2 Review of Literature 4
2.1 Lightweight Aggregates 4
2.2 Electrochemical Testing Methods 24
2.3 Summary and Implications for Current Research 41
C H A P T E R 3 Experimental Program 42
3.1 Factors Investigated in the Experiment 42
3.2 Materials 43
3.3 Equipment 49
3.4 Execution of the Experimental Plan 57
C H A P T E R 4 Summary of Results and Data Analysis 66
4.1 Data from Chemical Tests 66
4.2 Data from Electrical Resistivity Tests 74
4.3 Data from Additional Electrical Resistivity Tests 85
4.4 Summary of the Testing Data 91
4.5 Summary Findings 93
C H A P T E R 5 Summary, Conclusions, and Recommendations 95
SUMMARY 95
CONCLUSIONS 95
RECOMMENDATIONS 98
R e f e r e n c e s 104

List of Figures

Figure 2-1 Example GSD curves of FGA. 8
Figure 2-2 GSD of AASHTO specification and typical pre- and post-compaction FGA. 9
Figure 2-3 Comparison of quasi-elastic shear modulus G0 of FGA with shear modulus values of other coarse-grained materials (from Lenart and Kaynia 2019) 10
Figure 2-4 Direct shear test results (from Loux et al. 2019). 11
Figure 2-5 From left to right: Expanded shale, expanded slate, expanded clay; from top to bottom: coarse aggregates and fine aggregates (from Krc 2015). 16
Figure 2-6 Internal pores of expanded clay and shale LWA determined by X-ray computed tomography (from Lu et al. 2021, 2023). 17
Figure 2-7 Absorption vs. time for typical structural-grade ESCS aggregates 17
Figure 2-8 Recommended lightweight aggregate particle size distribution to produce high-quality concrete masonry units (from ASTM C331). 19
Figure 2-9 Dynamic elastic modulus of different lightweight aggregates and its dependence 20
Figure 2-10 Elastic modulus of expanded clay aggregates versus particle size and dry density (from Chandra and Berntsson 2002). 21
Figure 2-11 Stress-Strain curves from triaxial compression tests (1 t.s.f = 95.8 kPa) 22
Figure 2-12 Comparison between the corrosion rate of normal-weight aggregate and ESCS lightweight aggregates (from Fariborz et al. 2021). 24
Figure 2-13 Resistivity measurement using a two-electrode soil box 27
Figure 2-14 Resistivity versus moisture content (from Fishman et al. 2021a). 28
Figure 2-15 Comparisons of soil box test results relative to AASHTO T 288 31
Figure 2-16 Resistivity measurements from samples with different textures: 32
Figure 2-17 GSD curves of samples from MSE walls (from Parsons et al. 2020). 33
Figure 2-18 Resistivity vs. drained cycles (from Parsons et al. 2020) 34
Figure 2-19 Summary of test results for measuring pH 35
Figure 2-20 Comparisons of pH measurements relative to AASHTO T 289 36
Figure 2-21 Results of tests for measurement of salt content and observations 37

Figure 2-22 Correlation between measurements of salt content according to Tex-620-M and.... 38
Figure 2-23 Flowchart of the proposed EC testing protocol (from Fishman et al. 2021a)..... 40
Figure 3-1 Physical appearance of STALITE aggregate. 44
Figure 3-2 Physical appearance of NORLITE aggregate. 45
Figure 3-3 Physical appearance of NORTHEAST SOLITE aggregate..... 46
Figure 3-4 Physical appearance of AERO AGGREGATES. 48
Figure 3-5 Particle size distribution of the materials used in the study. 49
Figure 3-6 The equipment for sample preparation. 50
Figure 3-7 The equipment for sample extraction..... 51
Figure 3-8 The equipment for preparing sample solutions. 52
Figure 3-9 The equipment for measuring ion content. 53
Figure 3-10 The equipment for pH determination. 54
Figure 3-11 Custom Resistivity Boxes. 56
Figure 3-12 LCR meter. 56
Figure 3-13 The process of pH determination. 61
Figure 3-14 The process of resistivity measurement. 63
Figure 4-1 Testing results of sulfate content measurement (mg/L) grouped by test method. 68
Figure 4-2 Testing results of sulfate content measurement grouped by aggregate type..... 69
Figure 4-3 Testing results of chloride content measurement grouped by test method. 71
Figure 4-4 Testing results of chloride content measurement grouped by aggregate type. 72
Figure 4-5 Resistivity testing results for STALITE aggregate in drainage. 76
Figure 4-6 Relationships between resistivity and influencing factors of STALITE aggregates. . 77
Figure 4-7 Resistivity testing results of NORLITE aggregate in drainage..... 79
Figure 4-8 Relationships between resistivity and influencing factors of NORLITE aggregates. 80
Figure 4-9 Resistivity testing results of NORTHEAST SOLITE aggregate in drainage. 82
Figure 4-10 Relationships between resistivity and influencing factors for NORTHEAST SOLITE aggregates..... 82
Figure 4-11 Resistivity testing results of AERO AGGREGATES in drainage..... 84
Figure 4-12 Relationships between resistivity and influencing factors of AERO AGGREGATES. 84
Figure 4-13 Long-term resistivity monitoring results for STALITE samples..... 85

Figure 4-14 Long-term resistivity monitoring results for AERO AGGREGATES samples..... 86
Figure 4-15 Effect of compaction level on resistivity results for STALITE samples. 88
Figure 4-16 Effect of compaction level on resistivity results for AERO AGGREGATE 89
Figure 4-17 Effect of gradation conditions on resistivity results for STALITE. 90
Figure 4-18 Effect of gradation conditions on resistivity results for AERO AGGREGATE..... 91

List of Tables

Table 2-1 Typical Physical Properties of FGA (after Loux et al. 2021)..... 6
Table 2-2 Gradation Requirements for MSE Wall Backfill and Pre-compacted FGA Gradation.. 9
Table 2-3 Shear Strength Parameters (after Swan et al. 2016)..... 12
Table 2-4 TC Results for Trace Elements in FGA Compared to Established Requirements (from Arulrajah et al. 2015(a))..... 13
Table 2-5 Leachate Analysis Data for FGA Compared to Established Requirements..... 13
Table 2-6 AASHTO EC Requirements for MSE Wall Backfill and FGA Reported Values (from Loux et al. 2019)..... 14
Table 2-7 Major Manufacturers/Suppliers of FGA in the U.S. 14
Table 2-8 Physical Properties of ESCS Aggregates from Previous Studies..... 18
Table 2-9 Physical Properties of ESCS Aggregates from ASTM C331..... 19
Table 2-10 Source and Properties of ESCS Aggregates Used in Stoll and Holm (1985). 22
Table 2-11 EC Properties of ESCS Lightweight Fill..... 23
Table 2-12 Major Manufacturers/Suppliers of ESCS Aggregates to the PA Market..... 24
Table 2-13 AASHTO and PennDOT Requirements for Fill Materials in MSE Walls..... 25
Table 2-14 Summary of Resistivity Tests, Precision, and Bias (from Fishman et al. 2021b)..... 30
Table 3-1 Factors investigated for MSE wall fill with LWAs..... 42
Table 3-2 Types and sources of different materials for the tests. 43
Table 3-3 Physical properties and gradation of STALITE aggregate provided by supplier. 44
Table 3-4 Physical properties and gradation of NORLITE aggregate provided by supplier..... 46
Table 3-5 Physical properties and gradation of NORTHEAST SOLITE aggregate provided by supplier..... 47
Table 3-6 Physical properties of AERO AGGREGATES aggregate provided by supplier. 48
Table 3-7 The extraction methods considered in chemical testing..... 58
Table 3-8 Testing Matrix for Sulfate and Chloride Content Measurement. 59
Table 3-9 Testing Matrix for pH determination. 60
Table 3-10 Testing Matrix for Electrical Resistivity. 62

Table 4-1 Testing Results for pH. 73
Table 4-2 Testing data from sulfate content measurement. 91
Table 4-3 Testing data from chloride content measurement. 92
Table 4-4 Testing results for pH. 92
Table 4-5 Resistivity testing results for STALITE aggregate. 92
Table 4-6 Resistivity testing results for NORLITE aggregate..... 92
Table 4-7 Resistivity testing results for NORTHEAST SOLITE aggregate. 93
Table 4-8 Resistivity testing results for AERO AGGREGATES aggregate. 93

Acknowledgement

The authors greatly appreciate the financial support for this research project that was provided by the Pennsylvania Department of Transportation and the Federal Highway Administration. Ms. Beverly Miller from PennDOT acted as the project technical advisor and Mr. Evan Zeiders from PennDOT oversaw the execution of the project as the contract administrator. The support and their guidance were necessary for the success of the project and is sincerely appreciated. Thanks are also extended to Mr. Scott Milander of the Penn State Northeast Center of Excellence for Pavement Technology (NECEPT). Scott was instrumental in procuring the necessary equipment for conducting the laboratory tests. We are truly grateful to Stalite Lightweight Aggregate Company, Norlite Company, Northeast Solite Corporation, and Aero Aggregates of North America, LLC for providing us the materials needed for this research project. The participation of these companies in providing the aggregates was essential for conducting this project. Finally, we extend our appreciation to the staff of the Larson Transportation Institute at Penn State for their support.

Disclaimer

The contents of this report reflect the views of the authors, who are responsible for the facts and the accuracy of the data presented herein. The contents do not necessarily reflect the official views or policies of the Federal Highway Administration or the Commonwealth of Pennsylvania at the time of publication. This report does not constitute a standard, specification, or regulation.

CHAPTER 1

Introduction

1.1 Background

Mechanically Stabilized Earth (MSE) walls are widely utilized in civil engineering infrastructure. As lightweight aggregates (LWAs) are often proposed to facilitate cost effective use of MSE walls by mitigating settlement, balancing loads, and reducing lateral pressures, their application as backfill has gained considerable attention, particularly in longer retaining wall projects where MSE walls offer economic advantages over conventional systems. LWAs are beneficial due to their reduced density, improved thermal and acoustic insulation properties, and potential durability benefits compared to conventional aggregates.

The suitability of LWAs for MSE wall applications significantly depends on their chemical compatibility and electrochemical behavior, particularly regarding the potential for corrosion of embedded metallic reinforcement. Chloride and sulfate content within aggregates are critical indicators of the corrosivity potential, directly influencing the durability of these metallic elements. Additionally, the pH level of aggregates affects the corrosion rate of metallic components within MSE walls. Beyond chemical properties, resistivity is another essential parameter in assessing the electrochemical suitability of LWAs, as higher resistivity values typically correlate with lower corrosion rates. It is important to note that this research is focused on systems incorporating metallic reinforcement, which is vulnerable to such electrochemical degradation. In contrast, if extensible nonmetallic reinforcement were employed in practice, it would not be subject to the same corrosion concerns. In corrosive environments, it is best to use extensible reinforcement, which are polymeric in nature and considerably less susceptible to corrosion and degradation. Consequently, comprehensive electrochemical testing, including chloride and sulfate content analysis, pH measurement, and resistivity evaluation, is necessary to validate the compatibility of LWAs in metallic-reinforced MSE wall fills.

In this project, four distinct sources of LWAs were subjected to electrochemical testing procedures. These tests were conducted in accordance with multiple relevant standards and methodologies, considering various influencing factors to ensure accuracy and reliability of results. The findings from these tests will provide valuable insights into selecting appropriate LWAs and testing methods to optimize the structural and environmental performance of MSE wall systems.

1.2 Objective and Scope of Work

The objective of this research project was to encompass a comprehensive evaluation of the electrochemical properties of four types of LWAs intended for use as fill material in MSE walls. The testing program is designed to assess the suitability of these aggregates in terms of corrosion risk and material performance. The work included four major parts: (1) literature review, (2) development and execution of a testing plan, (3) analysis and interpretation of the data, and (4) guidance on the test protocols.

The review of literature was focused on the past and present research and guidance regarding the tests used for electrochemical testing of light weight aggregates. This review was used as the basis to develop an experimental program, which was shared and discussed with PennDOT. The testing plan mainly included chemical and resistivity testing. The chemical testing included the determination of sulfate content, chloride content, and pH levels. These tests aim to quantify the presence of potentially corrosive ions and assess the chemical environment created by the aggregates. On the other hand, the resistivity testing was performed to evaluate the aggregates' ability to resist electrochemical corrosion processes in different conditions, thus providing a comprehensive understanding of their protective characteristics. The plan was executed after approval by PennDOT and was the most core part of the research. Four different types of lightweight aggregates were procured and tested, one of the four processed from foamed glass aggregates.

All tests were carried out under controlled laboratory conditions, ensuring consistency and repeatability. Sample preparation, testing procedures, and data analysis followed standard protocols to ensure the reliability and comparability of results. The outcomes of this testing scope provide essential data for determining the electrochemical compatibility of each aggregate type with MSE wall systems and guiding both material selection and refinement of current testing standards for future construction applications.

1.3 Report Organization

This report is organized into five chapters, with the intent of presenting the research activities and findings in an organized sequence. Chapter 2 is allocated to the findings from the literature review. The experimental program of the research is covered in Chapter 3. The collected data and corresponding analysis are presented in Chapter 4. These two chapters form the largest portion of the research and required the longest time to execute. They cover details of the testing program and extensive work conducted on collection, analysis, and interpretation of data. Finally, a summary, conclusions, and general recommendations are presented in Chapter 5. Detailed data generated from this research is included as an appendix to this report.

CHAPTER 2

Review of Literature

This chapter documents the results of a literature review of electrochemical (EC) test methods and the physical, mechanical, chemical, and EC properties of foamed glass aggregate (FGA) and expanded shale, clay, or slate (ESCS) aggregate available in the market. The report will include recommendations for several EC test methods and sources of FGA and ESCS aggregates for subsequent testing.

2.1 Lightweight Aggregates

LWAs can be substituted for conventional mineral soil or aggregate to mitigate various challenging geotechnical site conditions, such as settlement, sensitive utilities, and slope stability. If settlement or sensitive utilities are a concern, the use of lightweight aggregate fill in lieu of conventional soil/aggregate fill can significantly reduce the effective stress increase experienced by the subgrade soils or utility. Thus, settlement in an underlying compressible layer or surcharging a utility is minimized. In practice, the concept of "soil balancing" is used to design a cross-section with a minimum net surcharge load on the subgrade. The substitution and strategic placement of lightweight aggregate fill can reduce the gravitational driving force causing slope instability and the lateral earth pressure causing retaining wall instability. LWAs have also found applications in insulation and green roofs due to their superior insulating properties. The most commonly used LWAs include FGA and ESCS aggregates.

2.1.1 Foamed Glass Aggregate (FGA)

FGA is a material that has been manufactured and used in Europe for several decades. It is produced from recycled glass. Like any recycled glass product, the production of FGA begins with obtaining a cullet, typically from a materials recovery facility (MRF) or a glass processor. The cullet must be dried and cleaned to remove impurities and ground very finely. Once it is a fine powder, it is

mixed with a foaming agent such as silica carbide (Aabøe and Øiseth 2004) using a pug mill or similar mixing device. This powder is run through a high-temperature furnace on a steel belt, whereby it expands (Aabøe et al. 2005). One cubic yard (yd^3) of glass cullet mix produces approximately 10 yd^3 of foamed glass. After leaving the furnace, the foam glass cake cracks into small fragments (<4 in) due to temperature shock (Zegowitz 2010).

Some of the foamed glass production in Europe was initiated to address waste glass from contaminated and toxic sources such as light bulbs, mercury lamps, windowpanes, car windshields, computer and television monitors, and industrial slag and fly ash. The heavy metals are removed from the cullet during the grinding process and likewise recycled (Aabøe and Øiseth 2004). This process was originally patented in Switzerland before the technology was brought to Scandinavia, where production commenced in 1999 (Frydenlund and Aabøe 2003). Foamed glass production in the U.S. is sourced from curbside-collected container glass (Loux et al. 2018).

Depending on the cell structure, two types of FGA exist. Closed-cell FGA are hermetically sealed with closed internal cells. It offers the following advantages: continuously ultra-lightweight, excellent drainage, defined properties for construction, great R-value (insulation resistance to heat flow) for the lifetime of the building, vermin proof, low capillarity, acid and chemical resistance, high compressive strength, economical, and ecological (Zegowitz 2010; Loux 2019; Mustafa et al. 2023; Nicks et al. 2024). On the contrary, open-cell FGA has a partially open and connected cell structure to allow water and air (gases) to penetrate and exchange, offering the following advantages: super lightweight even under saturation, freeze-thaw resistance, high capillarity, microporous absorbent, catalyst with outstanding properties for vegetation, hydroponics, filtration, and bioretention, and high compressive strength.

Properties of FGA vary due to variations in raw materials and the manufacturing process, including foaming agents and other mineral additives, as well as heating profiles and retention time within the kiln. The results reported in this section are primarily from testing completed on U.S.-manufactured samples of FGA. Some results reported in published literature are included (Frydenlund and Aabøe 2003; Aabøe et al. 2005; Skogstad et al. 2005; Zegowitz 2010; Arulrajah et al. 2015a; Betti et al. 2014).

2.1.1.1 Physical Properties

By volume, FGA is approximately 92% gas bubbles and 8% glass. The foaming reaction creates a thin glass wall around each gas bubble, making each piece of foamed glass aggregate have a cellular structure (Frydenlund and Aabøe 2003). The specific gravity of thoroughly pulverized FGA is approximately 2.27 as measured following ASTM D894 (GeoSystems 2013). The particle density varies between coarse particles (retained on No. 4 sieve) and fine particles (passing No. 4 sieve). Arulrajah et al. (2015a) reported a particle density of 28.9 pcf for coarse particles and 94.1 pcf for fine particles. FGA may be produced in a bulk dry unit weight of 8 to 15 pcf. For load-bearing geotechnical applications, the bulk dry unit weight of standard products is typically in the range of 13 to 15 pcf as delivered and 16.5 to 19.5 pcf post-compaction in the field (Loux et al. 2018).

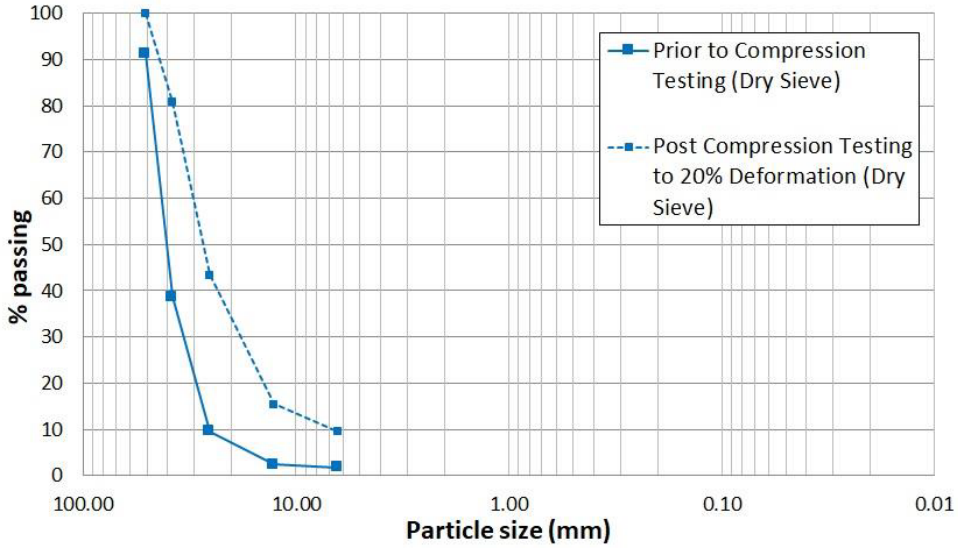
The gravimetric water content (GWC) is measured according to ASTM D2216. For FGA, GWC changes with time due to the cellular structure of the material as the exterior ruptured pores are filled with water; the water content can increase from 2% to 38% after being submerged for four days. Although the gravimetric water content is a high value, the volumetric water content is relatively low due to the lightweight nature of the aggregate (GeoSystems 2013). For example, Loux et al. (2018) reported a gravimetric water content of 25% and a volumetric water content of 6% for an FGA product. Table 2-1 shows the range of several physical properties of FGA.

Table 2-1 Typical Physical Properties of FGA (after Loux et al. 2021)

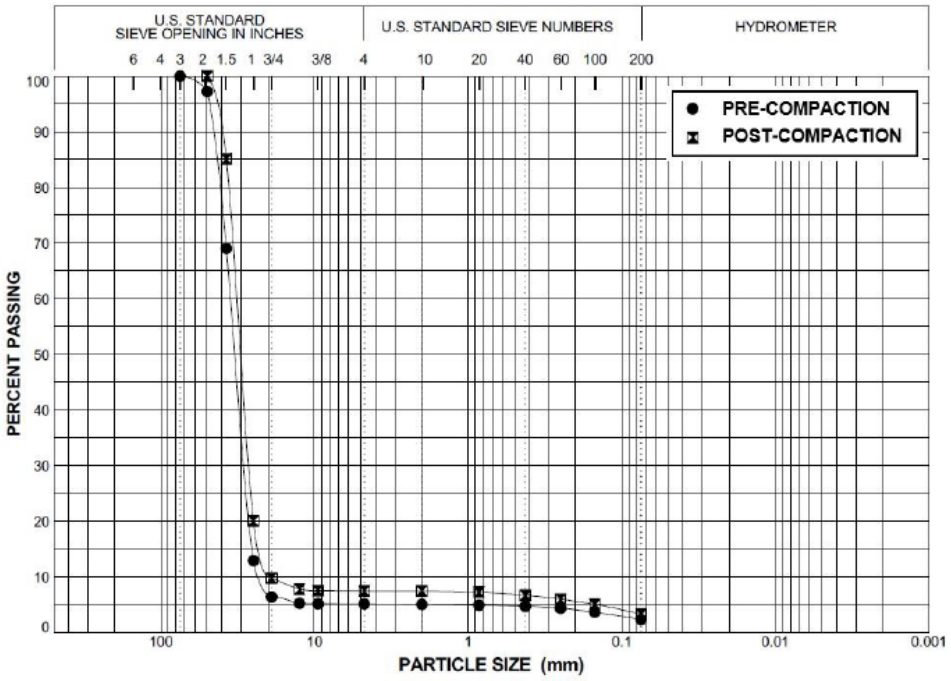
Properties	Values
Density	
Uncompacted dry bulk density (ASTM C29/C29M; AASHTO T19)	12 – 15 pcf
Estimated compacted dry density	
1.11 compression ratio (10% compaction of lift)	13 – 17 pcf
1.25 compression ratio (20% compaction of lift)	15 – 19 pcf
Buoyancy	
Estimated buoyant unit weight	15 pcf
Moisture content	
Volumetric	0 – 10% (6% typical)
Gravimetric (ASTM C566; AASHTO T255)	0 – 60% (25% typical)
Porosity	
Uncompacted	0.5
1.25 compression ratio	0.38
Stability	
Angle of repose	45°
Angle of internal friction – up to 1200 psf (ASTM D3080)	55°

2.1.1.2 Gradation

As-received FGA is classified as a poorly graded gravel (GP) according to the Unified Soil Classification System (USCS) (GeoSystems 2013). The aggregate particle sizes vary between 0.4 to 2.4 in (10 to 60 mm), with 15% by weight allowable under and over these limits. Changes in gradation may occur due to particle breakage and abrasion during material handling processes such as stockpiling, transportation, placement, and compaction. Figure 2-1(a) shows the grain size distribution (GSD) curves pre- and post-20% deformation in a confined compression test from Loux et al. (2018); Figure 2-1(b) shows the GSD curves pre- and post-field compaction from the Route 7 project in Kearny, NJ from Loux et al. (2019). Figure 2-1 shows that the aggregate materials would still classify as GP after crushing. Note that fines content is not shown in this figure, as lightweight aggregates typically contain negligible amount of fines.



(a) pre- and post-compression tests to 20% deformation (Loux et al. 2018)



(b) pre- and post-field compaction from the Route 7 project in Kearny, NJ (Loux et al. 2019).

Figure 2-1 Example GSD curves of FGA.

The American Association of State Highway and Transportation Officials (AASHTO) has set forth requirements for MSE backfill material in the Load Resistance Factor Design (LRFD) Bridge Construction Specifications (AASHTO 2017). Table 2-2 provides the AASHTO requirement for gradation in general accordance with AASHTO T 27 (AASHTO 2017) and some reported FGA values (Loux et al. 2019). Figure 2-2 shows the GSD requirement for AASHTO specification (Table 2-2) and the typical pre- and post-compaction GSD of FGA. This figure shows that the typical GSD of FGA is within the AASHTO limits shown in Table 2-2, even after minor breakdown of particles during field compaction. FGA is non-plastic and has a plasticity index (PI) of less than 6 in general (Loux et al. 2019).

Table 2-2 Gradation Requirements for MSE Wall Backfill and Pre-compacted FGA Gradation

Sieve Opening Size	AASHTO Gradation Requirements for MSE Wall Backfill (AASHTO 2017) Percent Passing	FGA Gradation (Pre-compaction) Percent Passing (Loux et al. 2019)	PennDOT Gradation Requirements for MSE Wall Backfill Percent Passing
4.0 in (100 mm)	100	100	100
3.0 in (75 mm)	-	-	100
2.5 in (63 mm)	-	85-100	-
3/4 in (19 mm)	-	-	20-100
3/8 in (9.5 mm)	-	0-15	-
0.0165 in (425 µm)	0-60	-	0-60
0.0029 in (75 µm)	0-15	-	0-10

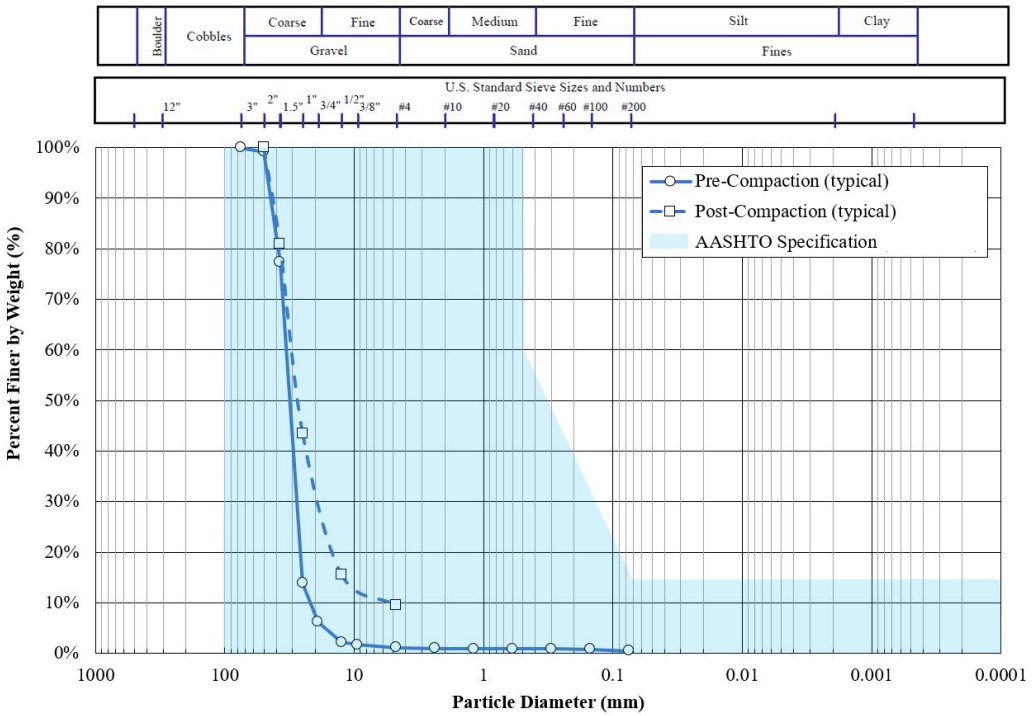


Figure 2-2 GSD of AASHTO specification and typical pre- and post-compaction FGA.

2.1.1.3 Elastic Modulus

The elastic modulus of compacted FGA varies with the applied stress. Betti et al. (2014) reported the elastic modulus in the range of 7,250 – 14,500 psi (50 – 70 MPa) from lightweight deflectometer tests for stress levels in the range of 1,045 psf – 2,090 psf (50 – 100 kPa). Lenart and Kaynia (2019) compared the quasi-elastic shear modulus G_0 of FGA measured from a series of large-scale triaxial tests with those of other coarse-grained geomaterials reported in the literature, including resonant column tests on ballast particles with D50=40 mm from Prange (1981), triaxial tests on both

crushed rock with D50=30 mm and round gravel with D50=10 mm from Kokusho and Esashi (1981), and triaxial tests on undisturbed gravel with D50=10 mm from Nishio et al. (1985). Figure 2-3 shows that G_0 of FGA is similar to or slightly smaller than other materials; it is closest to the data for gravel proposed by Tanaka et al. (1987) and Nishio et al. (1985). Like other coarse-grained materials, the quasi-elastic shear modulus of FGA exhibits high dependence on confining pressure.

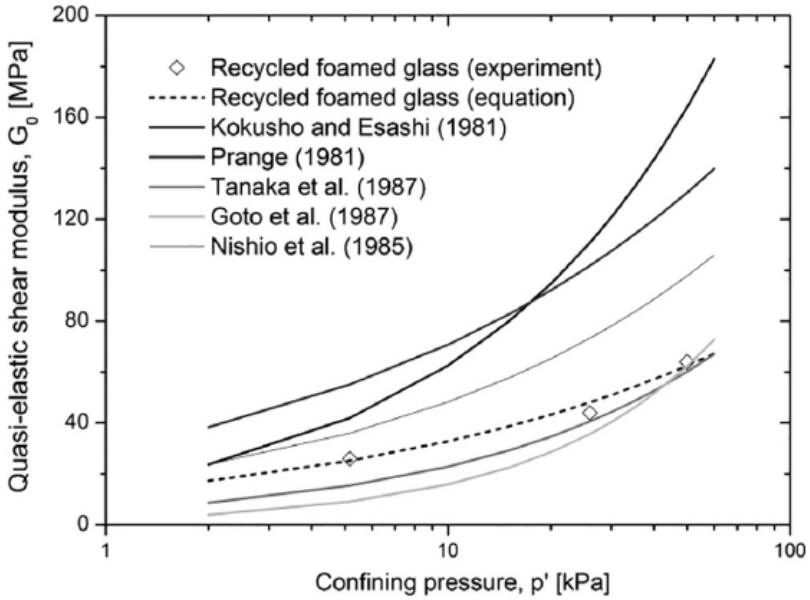


Figure 2-3 Comparison of quasi-elastic shear modulus G0 of FGA with shear modulus values of other coarse-grained materials (from Lenart and Kaynia 2019).

2.1.1.4 Shear Strength

AASHTO requires a minimum internal friction angle of 34 degrees or higher for MSE backfill materials (AASHTO 2017); however, no testing is required for backfills where 80% of particle sizes are greater than 0.75 in (20 mm). FGAs generally meet this gradation threshold pre-compaction (Figure 2-1(b)) but may not meet the threshold post-compaction (Figures 2-1(a) and 2-2). Due to the granular and angular nature of FGA particles, FGAs generally exhibit friction angles much higher than 34 degrees. For example, Loux et al. (2019) reported peak and large displacement internal friction angles of 56 and 54 degrees, respectively, and peak and large displacement cohesions of 60 psf (2.87 kPa) and 20 psf (0.96 kPa), respectively, for a normal stress range of 50 – 1200 psf (2.4 – 57.5 kPa), as shown in Figure 2-4, using a 12 in by 12 in (600 mm by 600 mm) large direct shear box. The FGA was compacted under dry conditions to a dry density of approximately 15 pcf (240 kg/m^3)

for each test. Similar shear strength values of FGA were also reported by Arulrajah et al. (2015a and b).

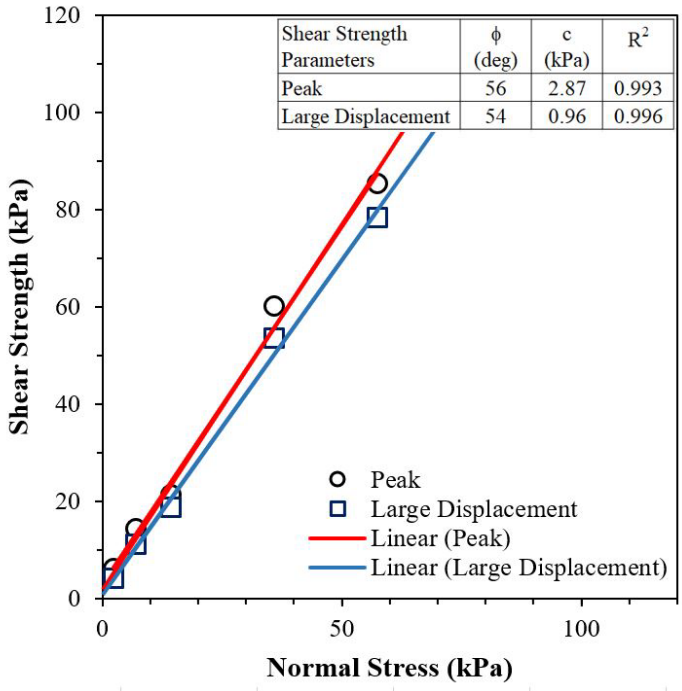


Figure 2-4 Direct shear test results (from Loux et al. 2019).

Based on a series of large-scale direct shear box tests, Swan et al. (2016) reported the shear strength parameters of FGA for different confining stress levels, as shown in Table 2-3, where the modified FGA refers to the FGA that had undergone modified Proctor compaction ASTM D1557 (2012). Table 2-3 shows that the shear strength parameters for the low normal stress range (300 – 1,200 psf) are very similar to those presented in Table 2-1 and Figure 2-4. Swan et al. (2016) showed that there is a transition point around the normal stress of 2,000 psf where the shearing behavior of the FGA particles transitions from a frictional response (high friction angle) to a crushing response (lower friction angle and an increase in cohesion). Based on the measured shear strength parameters for the high normal stress range (3,000 – 8,900 psf), there is an increase in frictional strength as a function of modified particles due to the modified compaction energy prior to shear displacement. If this material were a naturally formed gravel material having a similar particle distribution, one would anticipate cohesion closer to zero for the applied range of normal stresses. The measured cohesion indicates a strength that develops independent of normal stress that is a function of additional particle degradation due to the shearing of the FGA particles (Swan et al. 2016).

Swan et al. (2016) also investigated the effects of compaction energy and confining pressure on the GSD of FGA. They concluded that FGA material is a very brittle material with its mechanical properties varying as a function of particle breakage. The material transforms from a uniformly graded material to a very well-graded material as a function of compaction energy through either impact or direct shear testing. Static loading under vertical stress greater than 4,000 psf has a moderate effect on the particle distribution and produces finer particles approaching a well-graded distribution. The effect of vibratory compaction has very little effect on the particle distribution, allowing the FGA to maintain a uniform gradation with slightly finer particles.

Table 2-3 Shear Strength Parameters (after Swan et al. 2016).

Tested Material	Range of Normal Stress (psf)	Peak Friction Angle (°)	Peak Cohesion (psf)
As-received FGA	300 – 1,200	56	44
As-received FGA	750 – 3,000	29	957
As-received FGA	3,000 – 8,900	27	960
Modified FGA	3,000 – 8,900	31	1076

2.1.1.5 Environmental and Electrochemical Properties

For the use of FGA in engineering applications such as backfill, embankment fills, pavements, and pipe bedding, environmental effects have to be considered to ensure that environmental contamination will not arise (Rahman et al. 2014(a)). Table 2-4 presents total concentration (TC) results for trace elements in FGA and compares the values with allowable TC values for soil, waste materials, and backfill materials reported. The data in Table 2-4 implies that for all cases, the contaminant constituents for FGA are far below the threshold limits specified for these applications (Arulrajah et al. 2015(a)).

Table 2-4 TC Results for Trace Elements in FGA Compared to Established Requirements (from Arulrajah et al. 2015(a))

Contaminant	Foamed recycled glass (mg/kg)	Soil (Rahman et al., 2014b) (mg/kg)	Waste material (EPA, 2009) (mg/kg)	Backfill material (EPA, 2007) (mg/kg)
Arsenic	7	0.1 – 40	500	20
Barium	6	100 - 3000	6250	-
Chromium	10	5- 1500	500	1
Copper	9	2 - 60	5000	100
Mercury	< 0.05	10 - 150	75	1
Nickel	8	0.01 – 0.5	3000	60
Lead	28	2 - 100	1500	-
Selenium	< 3	0.1 - 5	50	10
Vanadium	< 5	3 - 500	-	-
Zinc	< 5	25 - 200	35000	200

Table 2-5 presents the leachate analysis data of FGA and compares it to the requirements for fill material, drinking water and hazardous waste. Based on the U.S. Environmental Protection Agency (EPA), a material is designated as hazardous if any metal is present in concentrations greater than 100 times that of the drinking water standards (Wartman et al. 2004). A comparison of the leaching results indicates that all metal contaminants are within allowable limits for using FGA as a fill material. Only for lead and arsenic, the leachate concentration gets close to the threshold defined by EPA Victoria for solid inert waste. The data in Table 2-5 suggests that FGA will not pose any risk to the groundwater tables or water streams beyond what is commonly accepted for fill material and solid inert waste.

Table 2-5 Leachate Analysis Data for FGA Compared to Established Requirements (from Arulrajah et al. 2015(a))

Contaminant	ASLP: acet. (mg/L)	ASLP: Borate (mg/L)	Threshold for solid inert waste (EPA, 2009) (mg/L)	Drinking water standards (EPA, 1999) (mg/L)	Hazardous waste designation (Wartman et al. 2004) (mg/L)
Arsenic	0.22	0.1	0.35	0.05	5.0
Barium	0.09	< 0.1	35.0	2.0	100.0
Cadmium	0.05	< 0.02	0.1	0.005	1.0
Chromium	0.09	< 0.1	2.5	0.1	5.0
Lead	0.42	< 0.1	0.5	0.015	5.0
Mercury	< 0.001	< 0.01	0.05	0.002	0.2
Selenium	< 0.01	< 0.1	0.5	0.05	1.0
Silver	< 0.01	< 0.1	5.0	0.05	5.0

For MSE walls constructed with steel reinforcements, AASHTO (2017) sets EC requirements for retaining wall backfills. EC properties of FGA have been rarely reported in the literature. Loux et al. (2019) reported the EC properties of FGA based on the testing of two samples and compared these measured properties with AASHTO EC requirements; Table 2-6 shows that the reported EC properties of FGA are well within the limits of AASHTO (2017). The FGA test results reported by Loux were obtained following AASHTO standard test methods, including required sample size and preparation procedures. A detailed discussion of the validity of these EC tests on FGA is presented in Section 2.2.

Table 2-6 AASHTO EC Requirements for MSE Wall Backfill and FGA Reported Values (from Loux et al. 2019)

Parameter	AASHTO (2017) Requirement for MSE Wall Backfill	Reported values for FGA
pH	5 – 10	9.2 – 9.33
Resistivity	≥ 30 Ω·m	15,600 Ω·m
Chlorides	< 100 ppm	< 10 ppm
Sulfates	< 200 ppm	11 ppm

2.1.1.6 Major Manufacturers and Suppliers

Table 2-7 lists major manufacturers and suppliers of FGA in the U.S.

Table 2-7 Major Manufacturers/Suppliers of FGA in the U.S.

Manufacturer/Supplier	Contact Information
Aero Aggregates of North America, LLC https://www.aeroaggna.com/	1500 Chester Pike, Eddystone, PA 19022 Phone: (833) 261-8499
Foam Glass Aggregates https://foamglassaggregate.com/	3646 Roland Ave. Baltimore, MD 21211 Phone: (443) 345-1578
AGSCO https://www.agsco.com/	Chicago 1755 N. Butterfield Rd, Libertyville, IL 60048 Phone: 847.261.0422 New Jersey 60 Chapin Rd, Pine Brook, NJ 07058 Phone: (973) 685-4444
Columbia Green Technologies https://columbia-green.com/foam/	79 SE Taylor Street, Ste 201 Portland, OR 97214 USA Phone: (503) 327-8723

2.1.2 Expanded Shale, Clay, or Slate (ESCS) Aggregates

ESCS aggregate is a ceramic lightweight aggregate prepared by expanding and vitrifying select shales, clays, and slates in a rotary kiln at temperatures over 2,000 ºF. The manufacturing process for ESCS aggregates was originally developed in 1908 by Stephen J. Hayde, who patented it in 1918 (Thomas and John 2007; Thienel et al. 2020). High-quality shales, clays, or slates are selected as raw materials that are placed in a rotary kiln where gases evolve within the material, leading to expansion and creating a cellular structure within the aggregate particles. As the material cools down, it transforms into a hardened, high-quality ceramic aggregate. Since their development, ESCS aggregates have been used extensively in asphalt road surfaces, concrete bridge decks, high-rise buildings, concrete masonry, and other geotechnical applications (Selman and Abbas 2022; Das et al. 2023)

Due to the specific manufacturing process and inherent characteristics of the raw materials, ESCS aggregates possess unique properties, including light weight, structural strength, dimensional stability, thermal insulation, and environmental inertness, making them valuable in many sustainable construction and infrastructure projects (Thomas and John 2007; Arioz et al. 2008; Boarder et al. 2016; Mohammed et al. 2022).

2.1.2.1 Physical Properties

Depending on the source and the production method, ESCS aggregates exhibit considerable differences in particle shape and texture. The shape of ESCS Aggregates can vary from highly angular to almost perfectly spherical, whereas the textures may range from fine pore, relatively smooth skins to highly irregular surfaces with large, exposed pores (Zukri et al. 2018). The rotary kiln produces the most rounded aggregates, especially when using a system of pre-shaping of the clay, shale, or slate granulate (Sveindottir et al. 1998). Typically, the particle shape of expanded clay is rounded, expanded shale is rounded-irregular, and expanded slate is angular-irregular (Nodehi 2021). Figure 2-5 shows the ESCS aggregates used in the experimental work by Krc (2015).



Figure 2-5 From left to right: Expanded shale, expanded slate, expanded clay; from top to bottom: coarse aggregates and fine aggregates (from Krc 2015).

When selected shales, clays, or slates are heated in rotary kilns to temperatures over 2,000 ºF, a cellular structure with non-interconnected spherical pores is developed when gases are evolved, causing expansion that is retained upon cooling (Holm and Valsangkar 1993). The expanded ESCS aggregates contain a relatively uniformly distributed system of pores with a size range of approximately 5 to 300 μm (Thomas and John 2007). ESCS aggregate's oven dry specific gravity commonly ranges from 1.25 to 1.40. Due to the low specific gravity and high interparticle void content, the bulk dry density of ESCS aggregates is commonly below 45 pcf. Compaction of the expanded aggregates in a similar way to crushed stone provides a highly stable interlocking network that will develop in-place moist densities of less than 65 pcf (Holm and Valsangkar 1993). With cellular structures, lightweight aggregates absorb more water than their heavy aggregate counterparts. However, ESCS aggregates' porous structures differ depending on the raw materials. Therefore, water absorption varies in different ESCS aggregates. For example, Lu et al. (2021) found that expanded shale with a finer pore structure resulted in lower water absorption than using expanded clay with coarser pores through X-ray computed tomography. Given the expanded shale/slate had lower porosity than the expanded clay (Figure 2-6), the use of the former could achieve moderate to high strength, while the latter was more suitable for producing low to moderate-strength concrete (Youm et al. 2016; Bogas et al. 2019; Lu et al. 2021; Lu et al. 2023).

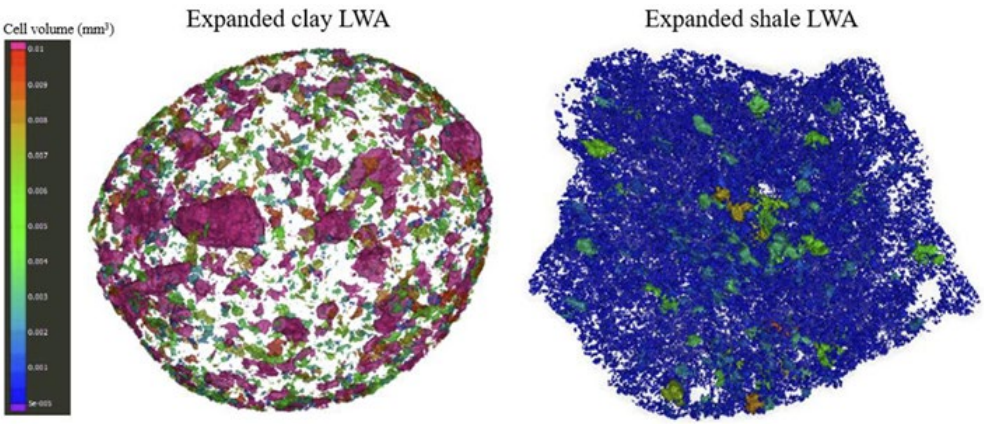


Figure 2-6 Internal pores of expanded clay and shale LWA determined by X-ray computed tomography (from Lu et al. 2021, 2023).

Based upon a 24-hour absorption test conducted in accordance with the procedures of ASTM C127 and ASTM C128, structural-grade ESCS lightweight aggregates will absorb from 5% to more than 25% moisture by mass of dry aggregate. By contrast, normal-weight aggregates generally absorb less than 2% moisture (Thomas and John 2007). The important distinction in moisture content is that with lightweight aggregates, the moisture is largely absorbed into the interior of the particles, whereas with ordinary aggregates, it is primarily surface moisture. The rate of absorption of lightweight aggregates is dependent on the characteristics of pore size, continuity, and distribution, particularly for those close to the surface.

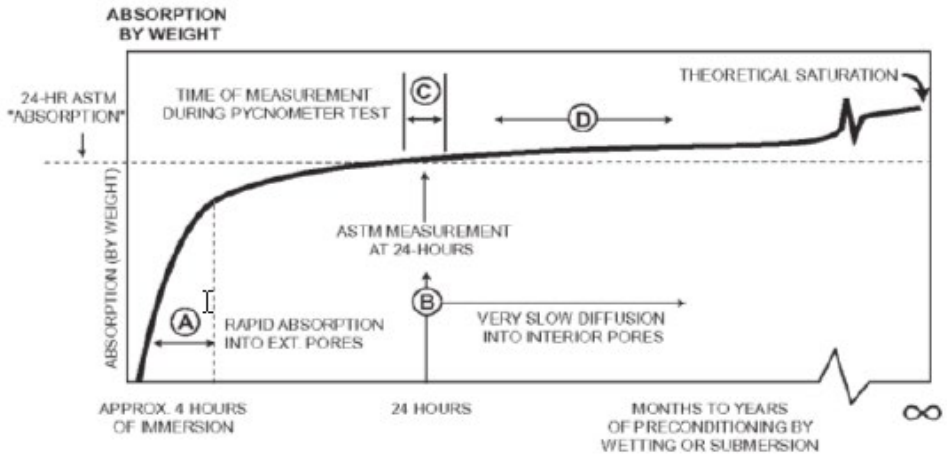


Figure 2-7 Absorption vs. time for typical structural-grade ESCS aggregates (from Thomas and John 2007).

As Figure 2-7 shows, the absorption rate can be divided into several regimes. Region A corresponds to a rapid water entry by capillary absorption by close-to-surface pores within the first few hours. Region B corresponds to a very slow diffusion into interior pores. Region C corresponds to when the moisture content is approximately equal to that obtained by the ASTM procedure (24-hour immersion), then the slope of the line reflecting further absorption is a very slow diffusion process. This is the basis for providing accurate relative density values during the relatively short time to conduct pycnometer tests at 24 hours. Region D corresponds to absorption developed over an extended period of time.

Understanding the physical properties of ESCS aggregates is crucial for designing safe and durable structures, optimizing material usage, and ensuring efficient construction practices. The physical properties of ESCS aggregates obtained from previous studies are compiled in Table 2-8.

Table 2-8 Physical Properties of ESCS Aggregates from Previous Studies.

Authors	Aggregate type	Specific Gravity	Density (pcf)	Bulk Density (pcf)	Water absorption (%)
Chia and Zhang (2002)	Expanded clay/shale	-	74.9	39.0 – 42.1	7.3
Zhang and Poon (2015)	Expanded clay	-	-	74.4	9.41
Shafigh et al. (2014)	Expanded clay	0.66	-	17.0	26.5
Rumsys, D. et al. (2017)	Expanded clay	-	49.9	30.5	25
Wu T. et al. (2016)	Expanded clay		74.9	41.4	10
Ardakani A, and Yazdani M (2014)	Expanded clay	0.48	-	16.0	26
Boudaghpour S, and Hashemi S (2008)	Expanded clay	-	-	25.0	17
Zukri A. et al. (2018)	Expanded clay	0.45	62.4	18.3	30
Yoon J. Y. et al. (2015)	Expanded clay	-	74.9	43.2	17
	Expanded shale	-	81.2	48.2	14
	Expanded slate	-	87.4	48.0	5

2.1.2.2 Gradation

With a prime consideration of lower densities, concrete masonry units can be manufactured with ESCS aggregates, with a blend of ESCS aggregates, or a blend of ESCS aggregates and normal-weight aggregates. Because the blended ESCS aggregates may come from different sources, the proper combined aggregate gradation is important in producing quality concrete masonry units. (Barbosa et al. 2012; Lotfy et al. 2015; Agrawal et al. 2021). Based on ASTM C331, the gradation recommendations of lightweight aggregates, including ESCS aggregates, are shown in Figure 2-8 and

Table 2-9. With the recommended gradation, the aggregates will have an ideal interstitial void system and a fine surface, and the concrete units with the aggregates will be of superior quality (Thomas and John 2007).

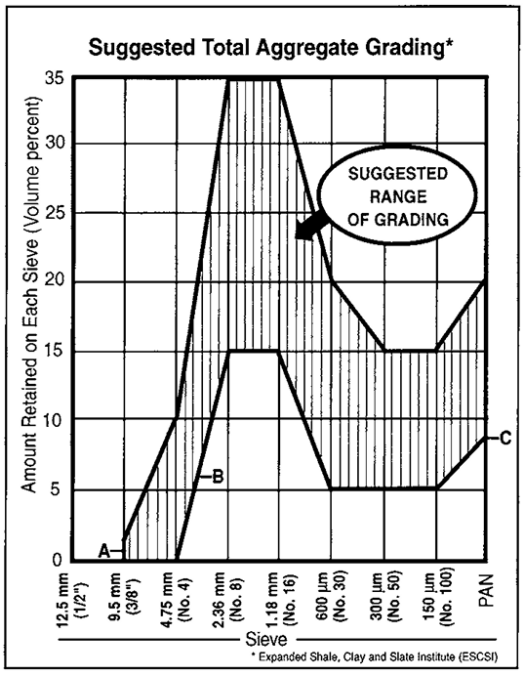


Figure 2-8 Recommended lightweight aggregate particle size distribution to produce high-quality concrete masonry units (from ASTM C331).

Table 2-9 Physical Properties of ESCS Aggregates from ASTM C331.

Sieve Opening Size	Amount Retained on Each Sieve (volume %)
3/8 in (9.50 mm)	0 – 2
0.19 in (4.75 mm)	0 – 10
0.093 in (2.36 mm)	15 – 35
0.046 in (1.18 mm)	15 – 35
0.024 in (600 µm)	5 – 20
0.012 in (300 µm)	5 – 15
0.006 in (150 µm)	5 – 15
Pan	8 – 20

2.1.2.3 Elastic Modulus

In general, the elastic modulus is the ratio of normal stress to the corresponding strain under a compressive load that is below the proportional limit of the material. However, due to the small dimensions and anisotropy of ESCS particles, the elastic modulus of ESCS cannot be determined by the standard test methods (Ardakani and Yazdani 2014). Nilsen et al. (1995) presented a method that

is based on composite materials theory to estimate the elastic modulus of lightweight aggregates and obtained the elastic modulus of three different expanded shale types of lightweight aggregates, using the Mori-Tanaka method. Chandra and Berntsson (2002) studied the elastic modulus of individual particles of different lightweight aggregates, including expanded clay. The diameter of the particles was 1/2 – 2/3 in. Because of the small dimensions of the particles, only the dynamic modulus was measured (Figure 2-9). They concluded that the dynamic elastic modulus is dependent on the particle density. Based on the previous studies, Ardakani and Yazdani (2014) determined the static elastic modulus of expanded clay aggregate using the micromechanics method and the Mori-Tanaka model. The results indicated the elastic modulus of aggregates ranged from 87 ksi (0.6 GPa) to 913 ksi (6.3 GPa), and there is a linear relation between the elastic modulus and the particle density of lightweight expanded clay aggregates (Figure 2-10).

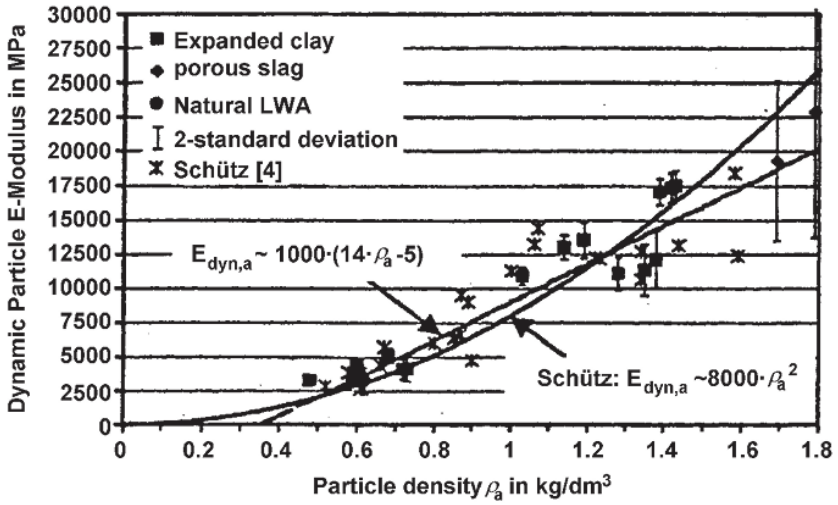


Figure 2-9 Dynamic elastic modulus of different lightweight aggregates and its dependence on particle density (from Chandra and Berntsson 2002).

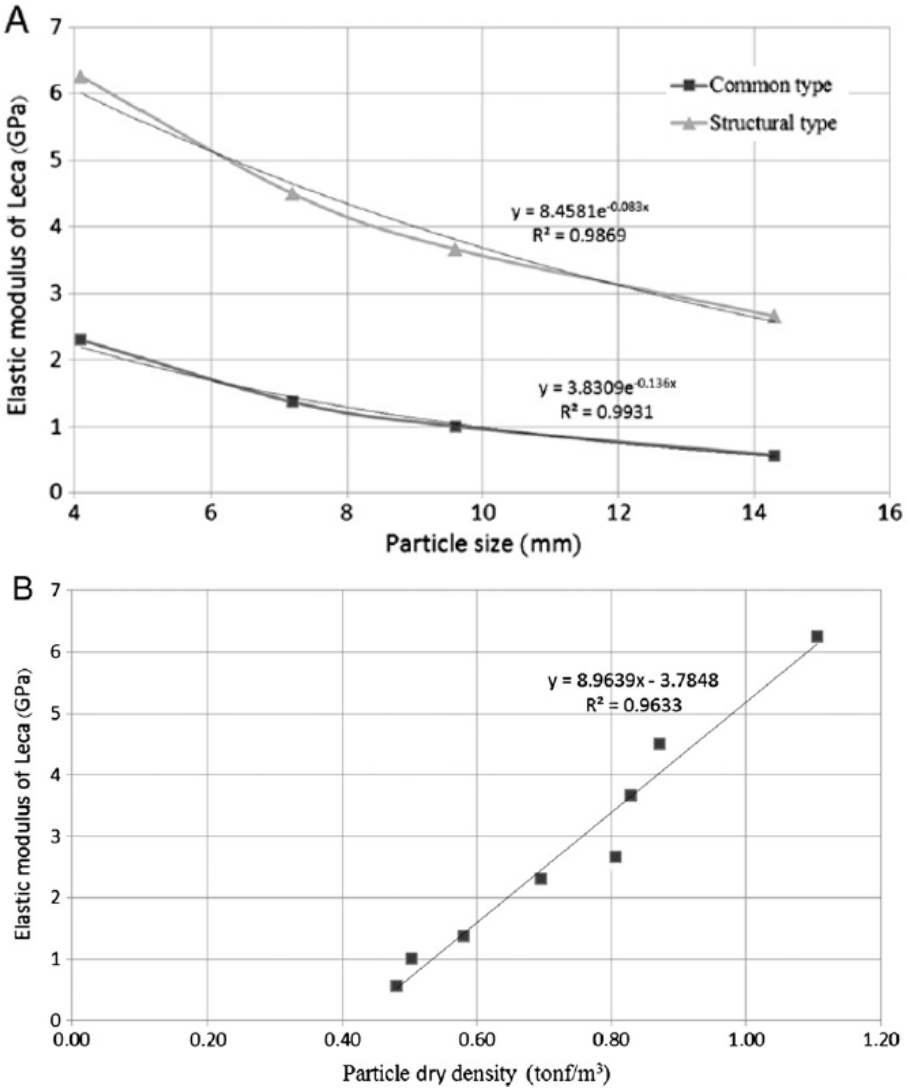


Figure 2-10 Elastic modulus of expanded clay aggregates versus particle size and dry density (from Chandra and Berntsson 2002).

2.1.2.4 Shear Strength

ESCS lightweight aggregate provides a cohesionless, granular fill that develops stability from inter-particle friction. Stoll and Holm (1985) conducted extensive triaxial compression tests on ESCS aggregates from six production plants and concluded that the consistently high friction angles varied with gradation, moisture content, and compaction levels. The physical properties of the expanded shale aggregates used in the tests are shown in Table 2-10.

Table 2-10 Source and Properties of ESCS Aggregates Used in Stoll and Holm (1985).

Number	Source of aggregate	Gradation passing/retained	Water content at time of test (%)		Dry unit weight (pcf)	
			Compact	Loose	Compact	Loose
1	Saugerties New York	3/4 in. /No. 4	5.3	7.1	~52	~46
2	Aquadale N. Carolina	3/4 in. /No. 4	7.2	6.7	53.4	47.6
3	Bremo Virginia	3/4 in. /No. 4	4.0	6.0	49.2	41.7
4	Green Cove Florida	3/4 in. /No. 4	8.1	8.4	50.6	46.4
5	Green Cove Florida	3/8 in. to Pan	8.2	8.4	61.9	53.9
6	Hubers Kentucky	3/8 in. /No. 8	0.1	1.4	53.0	47.1

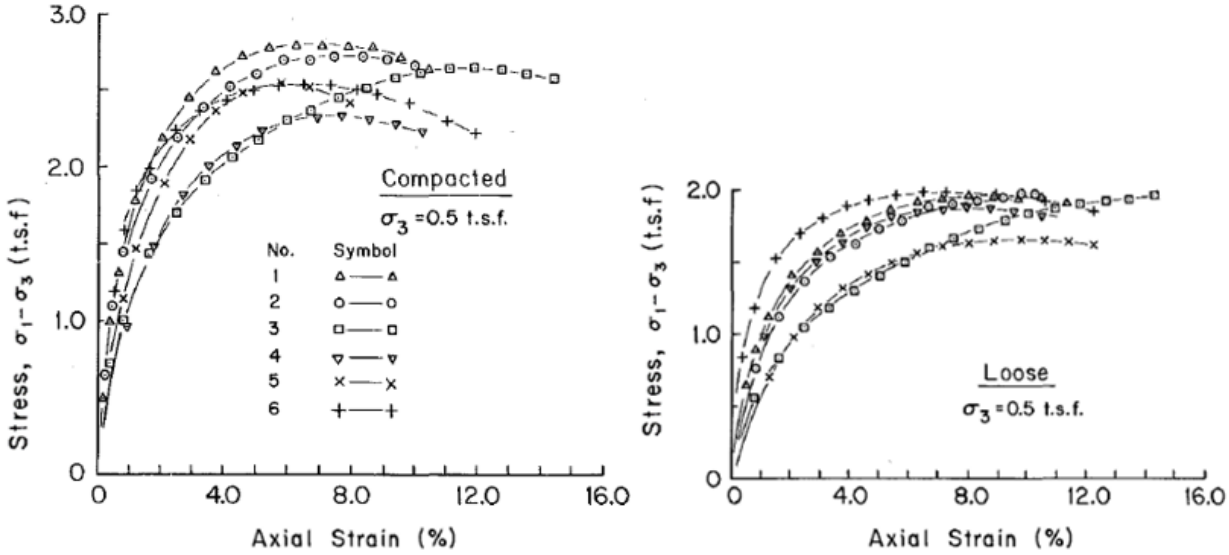


Figure 2-11 Stress-Strain curves from triaxial compression tests (1 t.s.f = 95.8 kPa) (from Stoll and Holm 1985).

Figure 2-11 shows the stress-strain curves obtained from six sets of tests from Stoll and Holm (1985). For the compacted ESCS aggregates, the angle of internal friction corresponding to the peak stress difference varies from 44.5 to 48°, whereas for the loose material, the range of the friction angle is from 39.5 to 42°. In general, the curves shown in Figure 2-11 are similar to those obtained for many common gradations of ordinary aggregates for fill. However, the lightweight aggregates weigh roughly half as much as their naturally occurring counterparts. Additionally, an extensive direct shear testing program conducted by Valsangkar and Holm (1990) confirmed high internal friction angles for plane-strain conditions.

2.1.2.5 Environmental and Electrochemical Properties

ESCS aggregate's lightweight properties, resource efficiency, and durability contribute to its environmentally friendly characteristics. It aligns with sustainable building practices and offers benefits across various applications. For example, Borthakur et al. (2022) found that ESCS aggregates aged with heavy metals, which are abundant in urban stormwater, develop antibacterial properties that will remove pathogens long-term. Wall and Castrodale (2019) reported the EC properties of ESCS aggregates used in the 11th Street Bridge Project in Washington, D.C. The project was to replace two bridges built in the 1960s with three new bridges that separate local and freeway traffic. ESCS lightweight aggregate was used as a backfill for MSE walls on the project. The project specifications for lightweight aggregate included specific limits on pH, chlorides, and resistivity along with the other requirements. Table 2-11 shows that the EC properties of ESCS lightweight fill meet the Federal Highway Administration (FHWA) requirements for MSE wall backfill, which are similar to AASHTO requirements for MSE wall backfill for steel reinforcements. Fariborz et al. (2021) showed that ESCS aggregates had extremely low chloride and sulfate content and substantially lower corrosion rates for measured resistivity than natural materials (Figure 2-12).

Table 2-11 EC Properties of ESCS Lightweight Fill (Wall and Castrodale 2019).

Properties	FHWA Specification	11th St. Test Result
pH	5.0 – 10.0	8.3
Chlorides	< 100 ppm	< 1 ppm
Sulfates	< 200 ppm	32.1 ppm
Resistivity	> 3,000 ohm-cm	35,209 ohm-cm
Organic Content	1% Maximum	0%

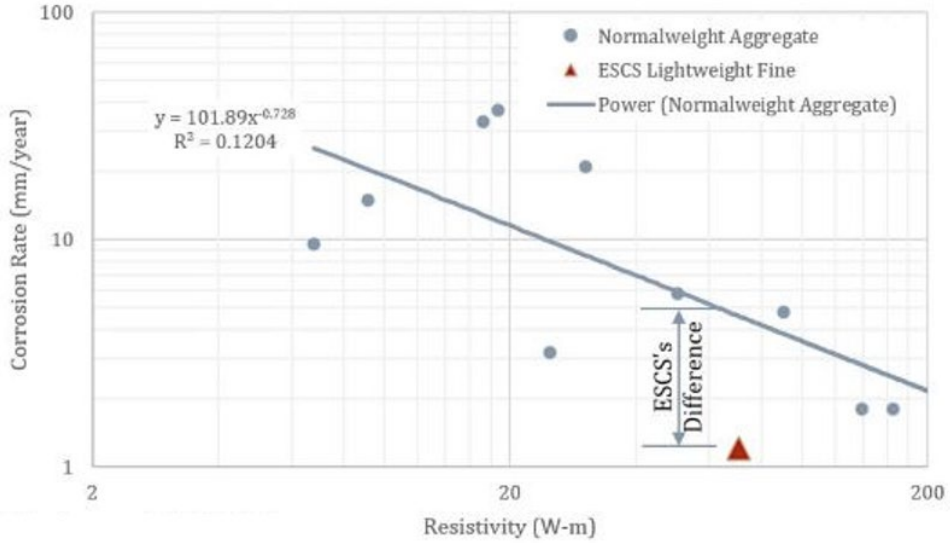


Figure 2-12 Comparison between the corrosion rate of normal-weight aggregate and ESCS lightweight aggregates (from Fariborz et al. 2021).

2.1.2.6 Major Manufacturers and Suppliers

The ESCS Institute (https://www.escsi.org/) lists major manufacturers and suppliers of ESCS aggregates in the U.S., and Table 2-12 lists suppliers to the PA market.

Table 2-12 Major Manufacturers/Suppliers of ESCS Aggregates to the PA Market.

Manufacturer/Supplier	Contact Information
Arcosa Lightweight https://www.arcosalightweight.com/	6618 N Tidewater Rd Mooresville, IN 46158 Phone: (317) 831-0710
Stalite https://www.stalite.com/	205 Klumac Road Salisbury, North Carolina 28144 Phone: (704) 637-1515
Northeast Solite https://www.norliteagg.com	628 South Saratoga Street Cohoes, NY 12047 Phone: (518) 235-0030

2.2 Electrochemical Testing Methods

Most transportation agencies evaluate the EC properties of earthen materials using current AASHTO laboratory test standards, which were adopted in the early 1990s. Specified test methods to measure the EC properties of geomaterials are AASHTO T 288 (resistivity measurement), AASHTO T 289 (pH measurement), AASHTO T 290 (soluble sulfate content measurement), and AASHTO T 291 (soluble chloride content measurement); these tests only use particles passing the No. 10 sieve (2 mm). These electrochemical test methods were originally developed for and are

primarily intended for conventional aggregate materials. These methods are referenced in the AASHTO LRFD Bridge Design Specifications for evaluating backfill materials used in mechanically stabilized earth (MSE) wall systems, which have historically been based on conventional aggregates. The recommended limits of EC properties by AASHTO for fills with steel reinforcement are listed in Table 2-13. As indicated in the special provisions on MSE wall systems, PennDOT has adopted the same limits for sulfate and chloride contents but required more stringent limits for pH to be 6.0-10.0 and set the minimum resistivity to be 2,000 ohm-centimeters with no chloride or sulfate testing required for resistivity higher than 5,000 ohm-centimeters.

Table 2-13 AASHTO and PennDOT Requirements for Fill Materials in MSE Walls.

Parameter	Acceptable Range	AASHTO Standard	Acceptable Range	PennDOT Standard
Minimum resistivity (Ω·cm)	> 3,000	T 288	> 2000-5000	Standard Special Provision of Mechanically Stabilized Retaining Wall Systems
pH	5−10	T 289	6-10	
Sulfate content (ppm)	< 200	T 290	< 200	
Chloride content (ppm)	< 100	T 291	< 100	

Note: Ω·cm = ohm·centimeter, ppm = parts per million

In a comprehensive NCHRP research project (21-11), Fishman et al. (2021a) compared various alternatives to the aforementioned AASHTO tests in terms of precision, repeatability, and sample preparation procedures and proposed a protocol describing best practices for sampling, testing, and characterizing the steel corrosion potential of earthen materials. A summary of these tests and the major findings of Fishman et al. (2021a), with an emphasis on resistivity measurement, is presented in this section. The NCHRP research conducted by Fishman et al., was focused on conventional aggregate materials, and was used as the basis for the electrochemical evaluation methods referenced in current specifications.

2.2.1 Resistivity Measurement

Resistivity test methods can be divided into two general types: (1) measurements of voltage drop in response to an applied current passing through specimens that are compacted in a soil box

(galvanostatic test), or (2) conductivity measurements on aqueous solutions extracted from solid samples (leachates). Typically, the process for measuring the resistivity from soil box tests includes (a) drying, separating, and adding moisture to the specimen, (b) compacting the material into the box, (c) connecting the soil resistance meter to the two- electrode resistivity box, and (d) obtaining a measurement of resistance, which is then converted to resistivity via a geometric "box factor." Generally, leaching tests for measurement of resistivity include (a) preparing measured amounts of material for testing, which are then (b) added to a measured volume of distilled or deionized water, and (c) measurements of conductivity are carried out on the extracts. Differences in various tests include dilution ratios (i.e., mass of water per mass of soil), methods of mixing, and how long the mixture stands before making measurements.

AASHTO T 288 considers a soil box test (Figure 2-13), and a sample size that includes about 1,500 grams (g) of air-dried materials finer than No. 10 sieve is required for testing. The process is as follows:

- The soil sample is placed in an acrylic plastic soil box (Figure 2-13a) in layers and compacted by applying finger pressure (Figure 2-13b). The soil box has inner dimensions of 6 in (150 mm) × 4 in (100 mm) × 1¾ in (45 mm) (length × width × height).
- To provide proper electrical contact between the resistivity meter and the soil, two stainless steel plates with dimensions of 6 in (150 mm) × 1¾ in (45 mm) are affixed to the side walls of the soil box (distance between the stainless-steel electrodes = 4 in (100 mm)).
- A measured amount of distilled or DI water with a resistivity greater than 20,000 Ω·cm, is gradually added to the soil sample.
- The resistivity meter is then connected to the stainless-steel electrodes, as shown in Figure 2-13e, and an alternating current consisting of a square wave with a frequency of 97 hertz (Hz) passes through the soil sample.
- The electrical resistance is measured from the corresponding voltage drop between the two electrodes. The resistivity of the soil sample is computed by multiplying the resistance by the soil box factor, which is a function of the geometry of the box and calculated by dividing the cross-sectional box area perpendicular to electron flow by the average distance between the two electrode plates.
- The process is repeated by remixing the soil sample with increasing amounts of distilled or deionized water to produce resistivity measurements at various moisture contents (up to

saturation state, shown in Figure 2-13d. A plot of resistivity versus moisture content renders the minimum resistivity and corresponding moisture content (Figure 2-14).

AASHTO T 288 is used to determine earthen materials' minimum resistivity (ρ_{min}) at a saturated or slurry state. However, a slurry state does not represent a condition that often occurs during the effective service life of earth-retaining structures. Hence, the minimum resistivity obtained from such a test is generally not representative of resistivity conditions most often experienced during typical service conditions of metal elements embedded in earthen materials. However, near-saturated conditions may occur under certain circumstances, such as failure of the impervious membrane, drainage system failure, or flooding. (Fishman et al. 2021b). In the test standard AASHTO T 288, only particles finer than No. 10 sieve are incorporated. Resistivity measurements for earthen materials are affected by soil texture; thus, including only the finer portion of the sample within the test specimen renders resistivity measurements that are different from what would be measured if all the particle sizes inherent to the sample were included. AASHTO T 288 notes, "When less than 5 percent of a material passes the No.10 sieve, this method may not be indicative of the corrosion potential of the material." AASHTO T 288 may not be appropriate for determining the corrosivity of coarser types of earthen materials and does not consider practical limits on moisture contents that may be experienced in the field.

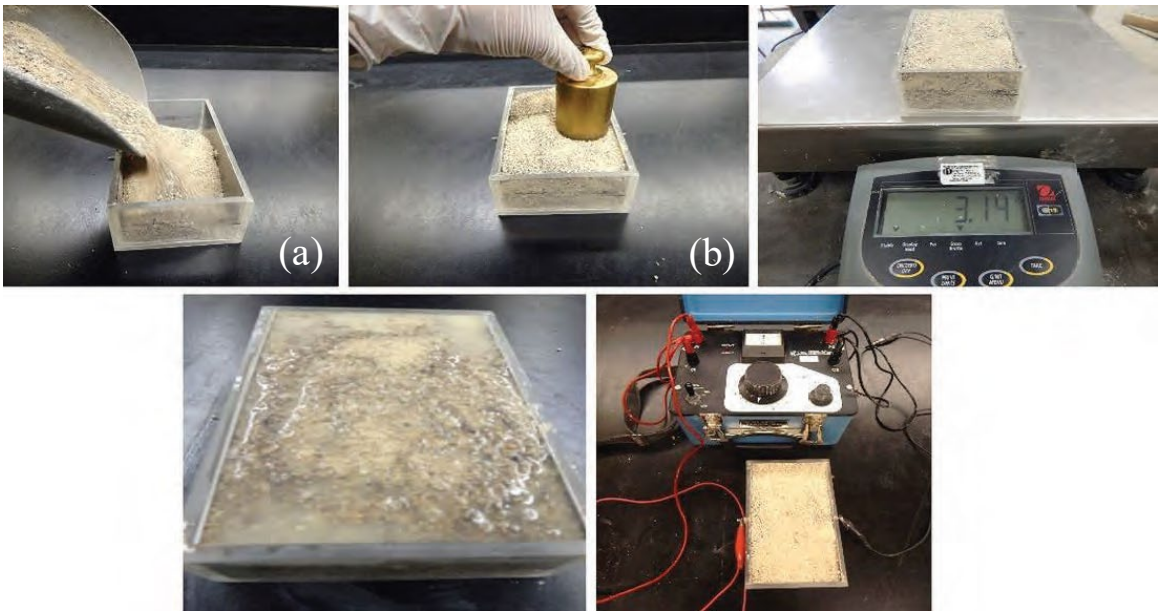


Figure 2-13 Resistivity measurement using a two-electrode soil box (from Fishman et al. 2021a).

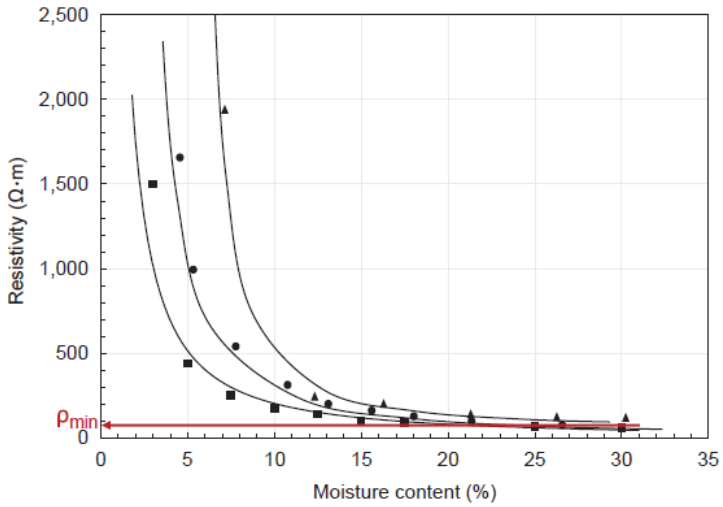


Figure 2-14 Resistivity versus moisture content (from Fishman et al. 2021a).

The Texas Department of Transportation (TxDOT) and the University of Texas at El Paso (UTEP) recognized the need to characterize the resistivity of the full blended gradation of MSE backfill and conducted research regarding the issue. Arciniega (2017) took several gradations of sandy limestone [based on AASHTO Gradation Number (GN)], measured the minimum resistivity, and found that coarser-graded blends (lower GN) had a higher minimum resistivity than finer-graded (higher GN); to accommodate the increased maximum aggregate size, 2-times and 4-times larger boxes were used. Cabrera (2018) found that the corrosion rate increased with a decrease in the resistivity of an aggregate backfill through a time-lapse study and that finer-graded materials exhibited higher corrosion rates than coarser-graded ones. Arciniega et al. (2018) proposed a numerical model to blend resistivity values of the gradational constituents of a backfill aggregate to predict bulk resistivity, arguing that current test methods do not accurately characterize MSE backfill resistivity.

Moisture condition affects the resistivity of MSE backfill by influencing the electron flow path. If the backfill material pores are 100% filled with air (i.e., dry condition) and if the air is assumed to be infinitely resistive, electrons will tend to travel through aggregate particles and their contact points. With the introduction of moisture, pores are partially filled with fluid, and because of the adhesion of the fluid to the aggregate particles, pore fluid coats aggregate particles. As soon as this coating forms, ions from the particle and the air are dissolved into the pore fluid, which decreases the resistance to electron flow in the pore fluid so that electron transport occurs mostly around aggregate particles and through their contact points. This adjustment to the electron flow path affects aggregate

resistivity. In fully saturated aggregate backfill, most of the electron flow will often occur via interconnected pore spaces because the resistivity of the pore fluid with dissolved ions tends to be much lower than that of the aggregate particles (Parsons et al. 2020).

Alternative test methods should be considered to address the effect of larger particles and moisture conditions on resistivity measurement (Fishman et al. 2021b). Alternatives to AASHTO T 288 in measuring soil resistivity include ASTM G187, Tex-129-E, Tex-129-M, ASTM WK24621, SC-T-143, and Tex-620-M. Table 2-14 summarizes the salient features of these tests and the statics describing the precision and bias of each test with respect to AASHTO T 288 from testing replicates with various gradations, as reported by Fishman et al. (2021a). The replicates were from 27 samples obtained from 25 sites. The composition of the test materials can be summarized as follows:

- Three samples were predominately (i.e., more than 50%) fine sand.
- Six samples were predominantly coarse to medium sands.
- Two samples were mixtures of fine and coarse particles, where none of the components were equal to or greater than 50% of the total.
- Sixteen samples were predominately gravel, varying from sandy gravels to clean and open-graded gravels with no sand content.
- None of the samples had more than 5% passing No. 200 sieve.

In Table 2-14, the ratio between results from an alternative test method to that from AASHTO T 288 is defined as the bias for the alternative test method. Figure 2-15 shows comparisons of soil box test results relative to AASHTO T 288 from Fishman et al. (2021a).

Tex-129-M and ASTM WK24621 are new test methods being considered for implementation by the Texas DOT and ASTM, respectively. Tex-129-M is an improvement compared to Tex-129-E, as it applies to testing coarse-graded samples, including gravel. For Tex-129-E, larger particles are crushed to render specimens with all particles passing a No. 8 sieve. However, the geochemical behavior and EC properties of crushed particles are not representative of the larger-sized particles from which they were derived and the EC and geochemical activity that occurs on the surfaces of the larger particles (Borrock et al. 2013). The test procedure described in Tex-129-M allows all particle sizes up to a maximum of 1¾ inches to be included in the test specimen, and, relative to Tex-129-E, larger-sized boxes are employed to accommodate testing coarse samples.

ASTM WK24621 also applies to coarse-graded samples and solves many of the shortcomings of using AASTHO T 288 for aggregate resistivity. An unsieved aggregate sample is compacted into

a two-electrode resistivity box (much larger in dimension than that for AASHTO T 288), soaked in (typically) deionized water for 24 h, drained, and then tested for resistivity. This proposed method allows for the testing of as-received samples. Unlike the AASHTO T 288 procedure, this proposed method does not include the removal, remixing, and reinstallation of aggregate in the test box; this addresses the issue of mass loss and aggregate displacement. Allowing drainage in the soil box to measure resistivity at drained conditions represents typical working conditions of MSE wall backfill in the field and is, hence, more advantageous than AASHTO T 288 since MSE wall backfill is rarely in a saturated or slurry state in the field.

Table 2-14 Summary of Resistivity Tests, Precision, and Bias (from Fishman et al. 2021b).

Test	Salient details	Precision		Bias w.r.t. AASHTO T-288	
Soil box tests	**Measure resistivity (ρ) of compacted specimens**	**μ^1_{COV}[3]**	**σ^2_{COV}**	**μ**	**σ**
AASHTO T 288	Sample passing No. 10 sieve, incremental addition of water (10% by weight), curing for 12 hours, compacting the specimen into the soil box, and measuring the resistance. Keep adding water until reaching ρ_{min} or ρ_{sat}	4.6	4.5	-	-
ASTM G 187	Scalp material greater than ¼ inch, saturating the specimen while compacting in a soil box and measuring resistivity at saturation, ρ_{sat}. Saturation is determined visually	5.3	4.5	1.4	0.4
ASTM WK24261	Include particle sizes up to 1 ¾ inches, curing for 24 hours, compacted specimen into the soil box. The specimen is allowed to drain before making the resistance readings	7.4	5.8	3.8	5.1
Tex-129-E	Similar to AASHTO T-288 except the material is separated on a No. 8 sieve before testing	3.2	4.3	1.1	0.2
Tex-129-M	Include particle sizes up to 1 ¾ inches, the sample is removed from the box after each measurement and remixed with additional water, the test continues until the additional moisture cannot be absorbed and the specimen has reached either ρ_{min} or ρ_{sat}	4.8	2.8	2.3	1.9
Leaching tests	**Measure conductance of aqueous solution**	**μ_{COV}**	**σ_{COV}**	**μ**	**σ**
SCT 143[15]	Include particle sizes up to 1 ¾ inches,diluting the sample at a 1:1 ratio, agitating for 3-minutes at the 30-minutes, 2-hour, and 4-hour intervals, standing for 20 hours, and filtering the sample before conductivity measurements	4.9	4.5	1.9	1.7
Tex-620-J	Sample passing No. 40 sieve, diluting the sample at a 10:1 ratio, heating to 140°F while stirring every hour for 12 hours, measuring the conductivity of the mixture	4.9	1.9	1.6	0.9
Tex-620-M	Include particle sizes up to 1 ¾ inches, diluting the sample at a 10L:1kg ratio, mixed continuously for 60 minutes, not allowed to stand before the conductivity measurements	4.5	3.1	5.2	3.4

Note: [1]μ = Mean, [2]σ = Standard Deviation, [3]COV = coefficient of variation ($\frac{\sigma}{\mu}$)

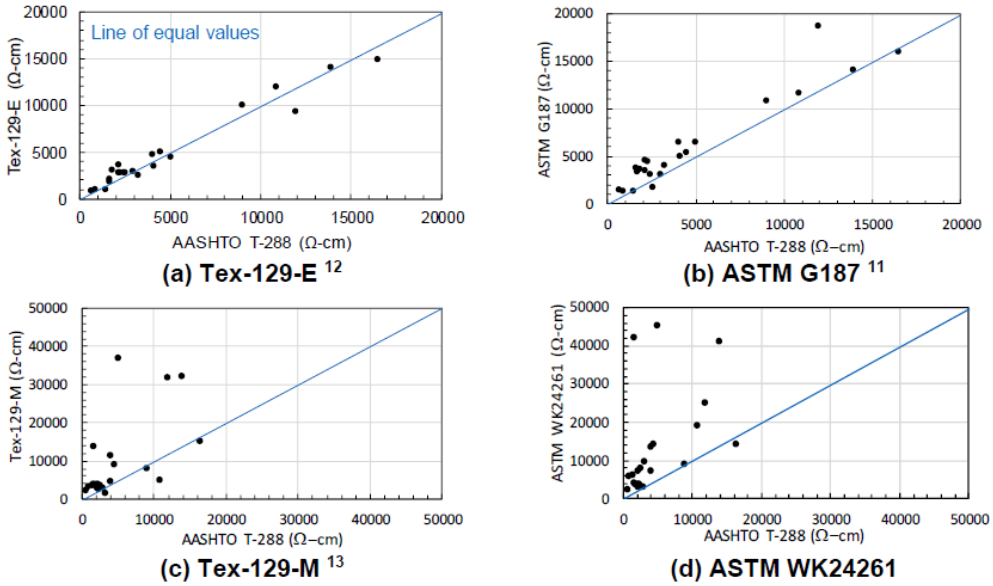


Figure 2-15 Comparisons of soil box test results relative to AASHTO T 288 (from Fishman et al. 2021a).

According to Table 2-14, the mean bias is close to one for Tex-129-E with a COV of approximately 18%. These statistics are manifested in the relatively narrow band and proximity to the line of equal values depicted in Figure 2-15(a). The results from Tex-129-E and AASHTO T 288 are expected to be close because of the similarities between these test methods. The two tests differ regarding the sieve sizes used to separate the specimen from the sample (No. 8 vs. No. 10) and the 12-hour curing period prescribed by AASHTO T 288 for the first moisture increment. For the materials tested in this study, these differences did not have a significant impact on the results. Other test procedures show mean bias values that are noticeably higher than 1.00 (as high as 5.2 in Tex-620-M) with significantly higher COVs. The mean bias is greater for test procedures that involve coarser gradations (i.e., ASTM G187, Tex-129-M, and ASTM WK24261). ASTM G187 includes particle sizes up to 1/4", but Tex-129-M and ASTM WK24261 include particle sizes up to 1¾ in. This is reflected in the mean bias values, which are higher for results obtained from ASTM WK24261 and Tex-129-M than those from ASTM G187. The bias from ASTM WK24261 is higher than that from Tex-129-M due to the manner in which measurements are taken after the sample is drained for ASTM WK24261 (Fishman et al. 2021b).

Table 2-14 shows that the mean bias for the tests on compacted soil specimens and leachate tests are 2.15 and 2.95, respectively. The observed differences between results were expected because the effects of tortuosity are not included with conductivity measurements from leachates. In addition,

biases from tests on leachate are all greater than one, even for samples that are separated into finer components (e.g., for Tex-620-J, the sample is separated on a No. 40 sieve). This is due to the different dilution ratios, and methods of mixing and extracting leachates used in different leaching tests compared to soil box tests (Fishman et al. 2021b).

The data from each test method are grouped according to the fineness of the samples (fine sand, coarse sand, and gravel) and are shown in Figure 2-16. Figure 2-16 shows that, as the coarseness of the sample increases, the mean bias, and the COV increase. For soil box tests on fine sand specimens, the average bias is close to one with a relatively low COV (average COV = 8%). On the other hand, for coarse sand and gravel specimens, the biases are 1.6 and 3.1, respectively, and COVs in excess of 30% are observed.

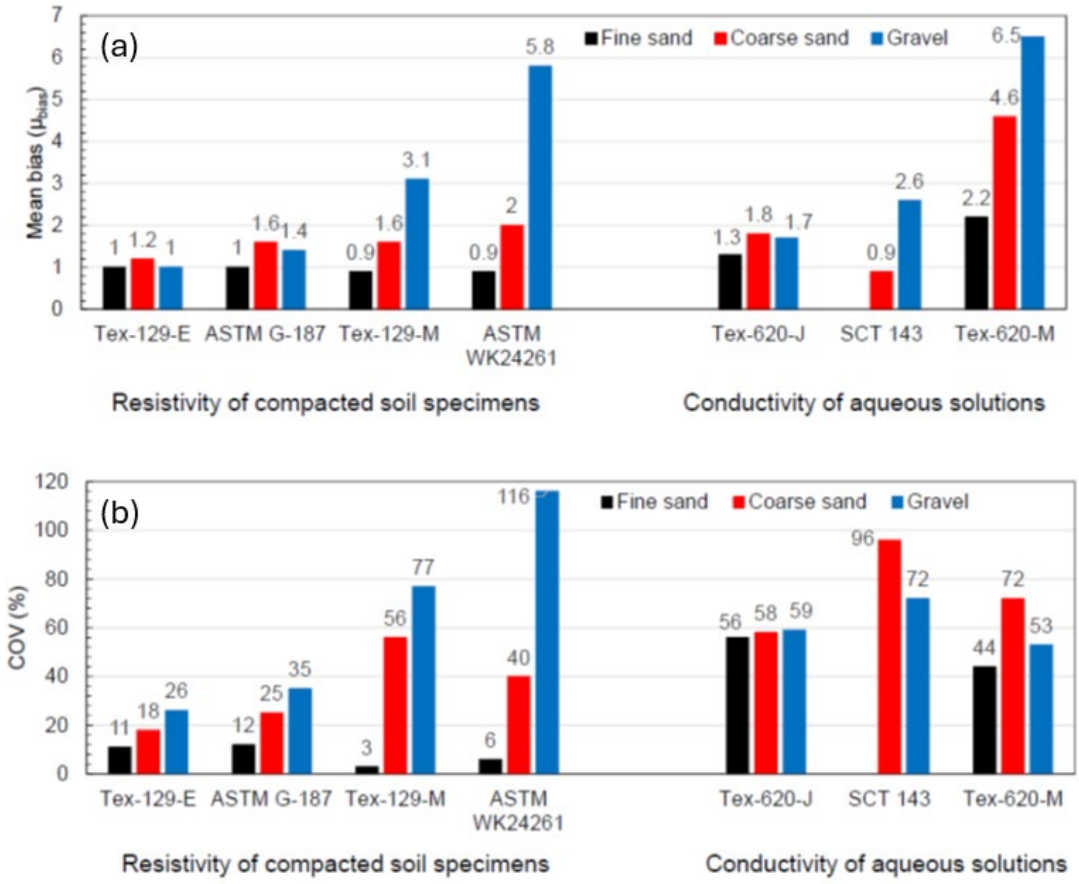


Figure 2-16 Resistivity measurements from samples with different textures: (a) mean bias; (b) coefficient of variation (from Fishman et al. 2021a).

Parsons et al. (2020) compared the resistivity measurements of five aggregate backfill materials collected during construction from MSE wall projects in eastern Kansas using the AASHTO

T 288 and ASTM WK24261 methods. The laboratory testing results were compared with field resistivity measurements of two MSE wall backfills post-construction. Figure 2-17 shows the test materials' GSD curves. Parsons et al. (2020) concluded that the ASTM WK24261 test method appeared to simulate field conditions behind MSE walls more accurately. The soak/drain cycling tests were conducted to simulate the natural process of rainwater cycling through the aggregate. Figure 2-18 shows that resistivity increased for these samples with cycling. This suggests that moving water through the backfill may flush out some of the constituents that promote electrical current flow, and the resistivity may increase with time and with the number of rainfall and drainage events. Based on their research findings, Parsons et al. (2020) recommended a minimum electrode spacing of eight times the maximum particle size and a minimum height of the test box three times the maximum particle size.

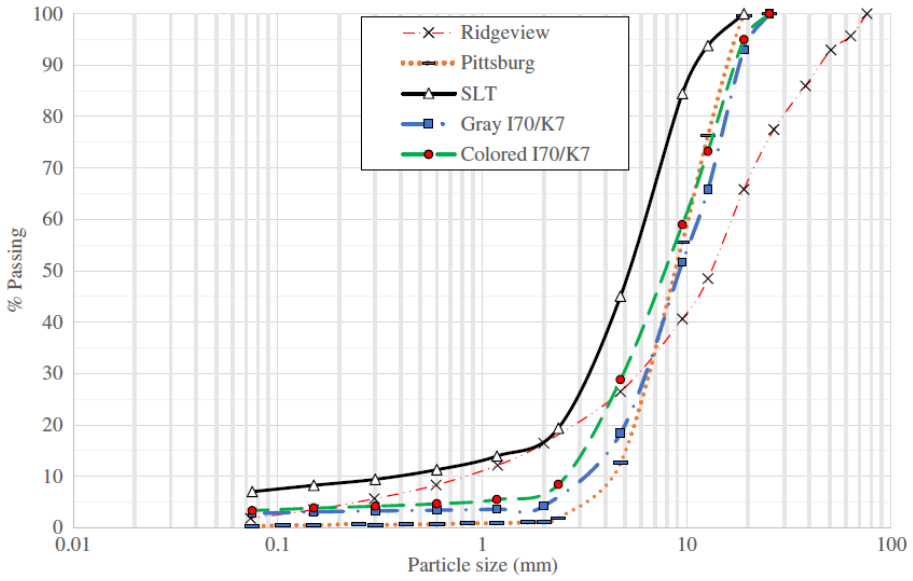


Figure 2-17 GSD curves of samples from MSE walls (from Parsons et al. 2020).

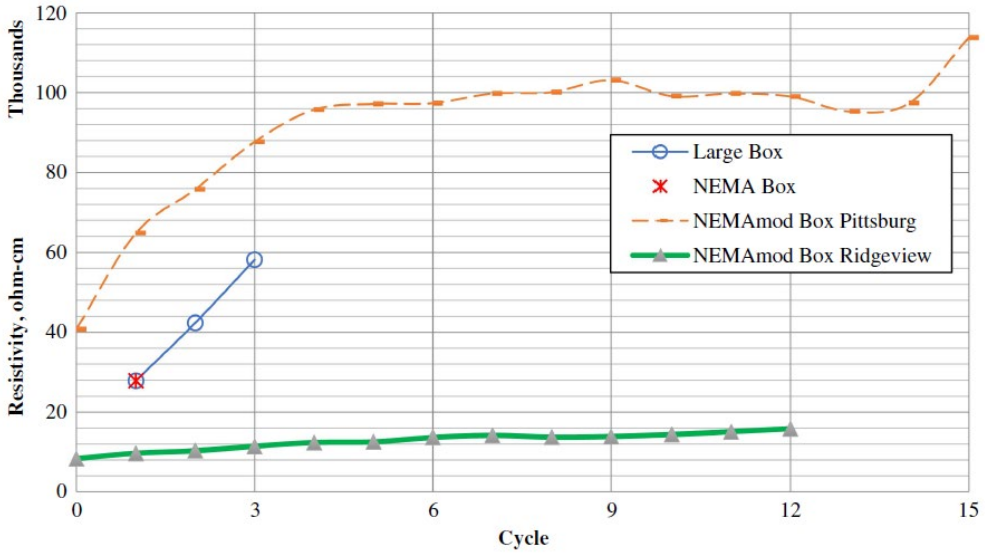


Figure 2-18 Resistivity vs. drained cycles (from Parsons et al. 2020)

2.2.2 pH Measurement

AASHTO T 289 describes procedures and apparatus for determining a pH value for corrosion testing using a pH meter. The principal use of the test is to supplement soil-resistivity measurements and thereby identify conditions under which the corrosion of metals in the soil may be sharply accentuated. This standard is divided into two parts. The first part involves obtaining and preparing the sample to size for testing, which is similar to AASHTO 288. The second part describes the test method for determining the pH of soil.

Figure 2-19 summarizes the statistics describing the precision observed in testing replicates and the bias of each test procedure with respect to AASHTO T 289. Precision was observed in testing replicates from the same replicas as those described for resistivity testing. Figure 2-20 shows the pH values from the alternative methods compared to those from AASHTO T 289. Fishman et al. (2021a) described in detail the following variables in different test procedures for measuring pH.

- Whether or not the sample is air-dried.
- Particle sizes included in the test specimen.
- Dilution ratios used in the sample preparation.
- Methods of mixing water with the sample, including whether or not the mixture is heated.
- The period that the soil-water mixture is allowed to stand before the first measurement.

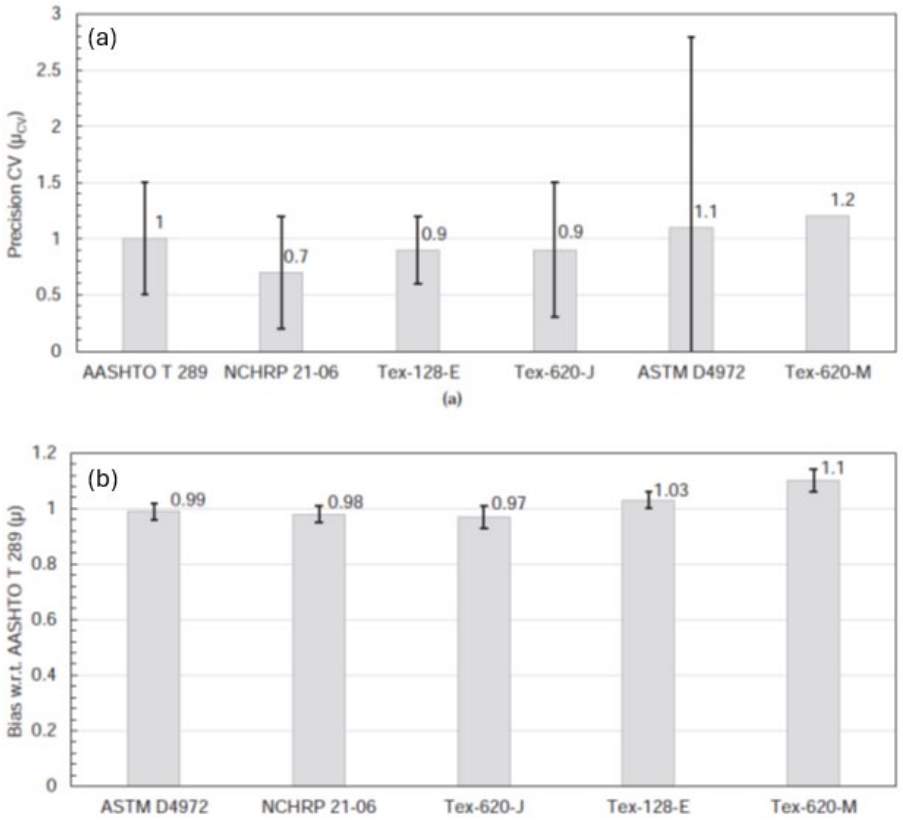


Figure 2-19 Summary of test results for measuring pH: (a) precision; (b) bias with respect to AASHTO T 289 (from Fishman et al. 2021a).

Figure 2-19(b) shows that, except for Tex-620-M, the biases of results from all the test methods with respect to data from AASHTO T 289 were close to 1. The biases of the results from Tex-620-M were observed to increase with respect to sample coarseness; that is, the bias from testing a gravel sample was higher than that from a sample that included coarse or fine sand. Fishman et al. (2021a) drew the following conclusions from the results shown in Figures 2-19 and 2-20:

- Measurements of pH from Tex-620-M are less repeatable as compared with measurements from other test methods investigated in this study.
- In general, Tex-620-M renders pH values that are higher than those obtained from the other test methods investigated in the study.
- Results from NCHRP 21-06 (Vilda 2009) are more repeatable as compared with AASHTO T 289 and do not have a significant bias with respect to results obtained from AASHTO T 289.

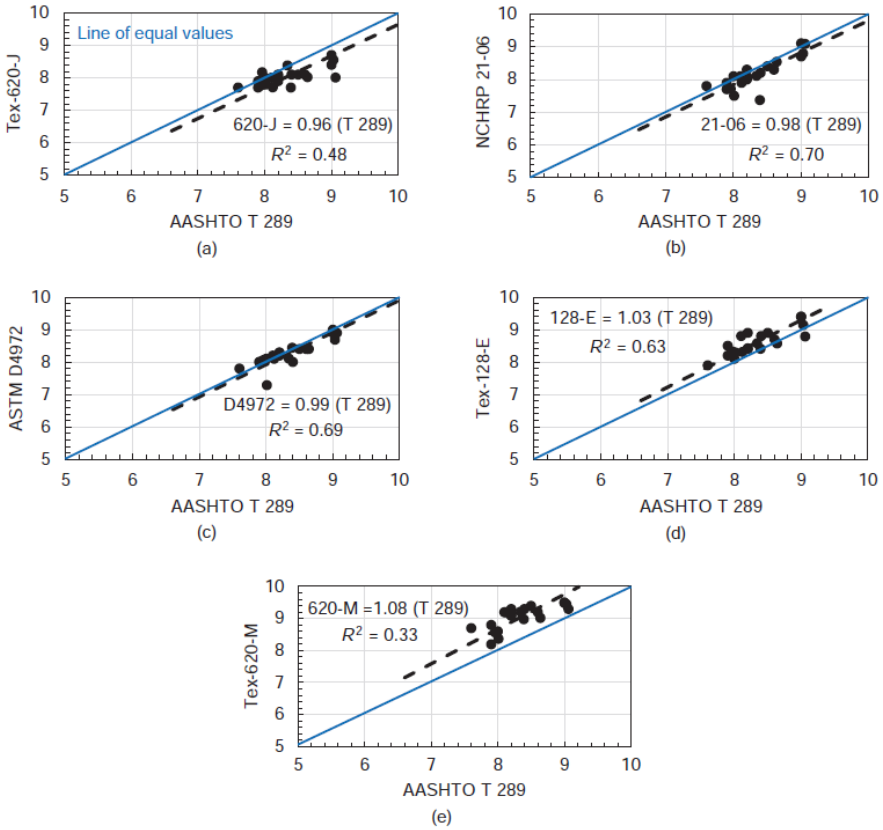


Figure 2-20 Comparisons of pH measurements relative to AASHTO T 289: (a) Tex-620-J; (b) NCHRP 21-06 (Vilda 2009); (c) ASTM D4792; (d) Tex-128-E; and (e) Tex-620-M (from Fishman et al. 2021a).

2.2.3 Salt Content Measurement

AASHTO T 290 covers the determination of the water-soluble sulfate ion content in soil. This standard is divided into two parts. The first part specifies the procedure for sampling and preparing the sample to size for testing, which is similar to AASHTO T 288. The second part delineates two test procedures (Gravimetric and Turbidimetric) for determining the sulfate ion content in soils. The selection of the method is dependent on the sulfate ion concentration and the accuracy desired.

AASHTO T 291 describes the procedures for sampling and testing soil for chloride ion content. This standard is divided into two parts. The first part specifies the procedure for sampling and preparing the sample to size for testing, which is similar to AASHTO 288. The second part delineates two test procedures for determining the water-soluble chloride ion content in soil. Two methods are given. Method A is based on the Mohr procedure for determining chloride ion content with silver nitrate. Method B utilizes a pH/mV Meter. By comparing the mV readings to the calibration curve determines the chloride ion content.

Figure 2-21 summarizes the precision of measurements of salt content observed in tests of replicates. The samples and replicates are the same as those used in evaluating the precision of resistivity and pH tests. Only samples with salt content greater than 10 mg/kg (ppm) were included for computations of the CV statistics in Figure 2-21. Fishman et al. (2021a) drew the following conclusions from the results shown in Figure 2-21:

- Differences between precision and repeatability across the tests are more distinct between the tests for chloride than between those for measurements of sulfate.
- For sulfate measurements, AASHTO T 290 rendered repeatability equal to or better than the other test methods that were evaluated.
- Measurements of chloride from Tex-620-M are less repeatable than measurements from other methods.

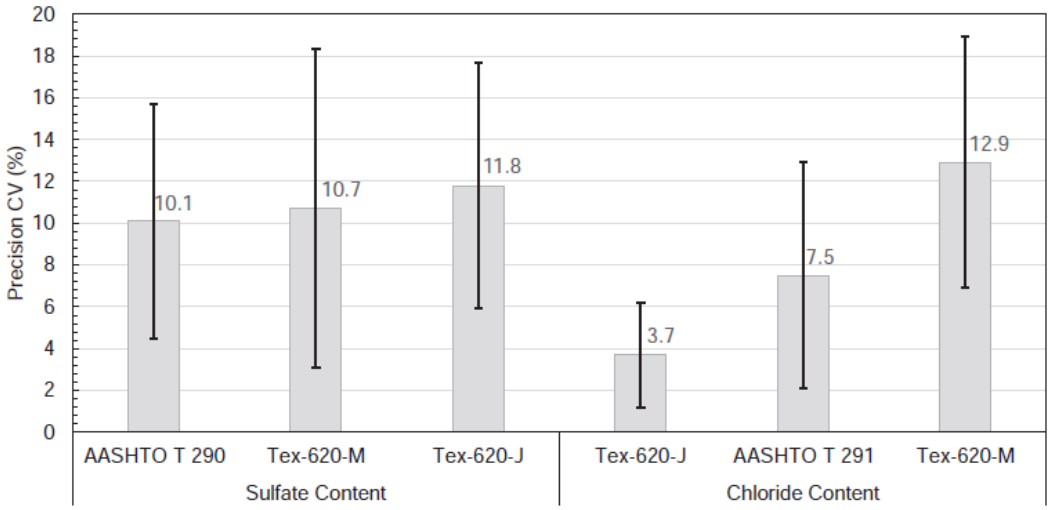


Figure 2-21 Results of tests for measurement of salt content and observations of precision [includes only results from samples with sulfate and chloride content greater than 10 mg/kg (ppm)] (from Fishman et al. 2021a).

Fishman et al. (2021a) tested 26 samples: 21 according to AASHTO and Texas modified procedures and five according to Tex-620-M only. Five coarse samples were not tested according to the AASHTO standards because of the lack of sufficient constituents passing No. 10 sieve. Figure 2-22 compares the salt content obtained from Tex-620-M and the AASHTO procedures. Except for samples with a high content of particles passing the No. 10 sieve, the Tex-620-M procedure rendered lower salt content as compared with the AASHTO tests. This was due to the larger particle sizes included in the Tex-620-M tests compared to the AASHTO tests, which are performed on the finer

fraction of the sample (that passing No. 10 sieve). The black dashed line, which shows the best fit for sulfate measurements by Tex-620-M ($R^2 = 0.79$), indicates that the sulfate content measured by Tex-620-M was approximately 71% of that measured by the AASHTO tests. Similarly, the chloride content measured by Tex-620-M ($R^2 = 0.76$) was approximately 51% of that measured by the AASHTO tests.

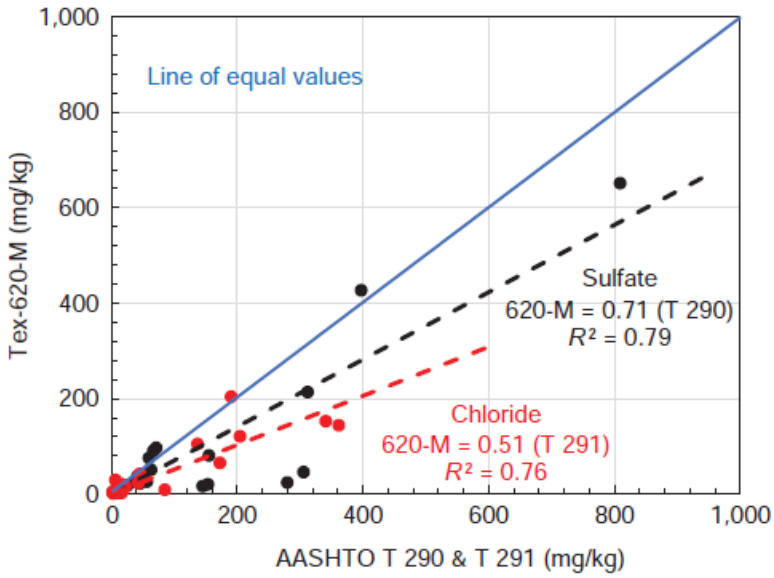


Figure 2-22 Correlation between measurements of salt content according to Tex-620-M and AASHTO T 290 and T 291 (from Fishman et al. 2021a).

2.2.4 EC Testing Protocol Proposed by Fishman et al. (2021a)

Based on the results of the aforementioned extensive investigation, Fishman et al. (2021a) developed an EC testing protocol. Four factors were considered in selecting methods for the proposed protocol, including a) precision and repeatability of the test methods as described, b) compatibility between parameters (e.g., salt contents and resistivity), c) correlations between geochemical and EC properties, corrosivity and corrosion rates, and d) the utility of the test results. All these factors support the implementation of the AASHTO and alternative test procedures that describe testing with the as-received gradation, such as the Texas-modified procedures within the proposed protocol. Figure 2-23 presents a summary of the proposed protocol in the form of a flowchart. In general, the proposed protocol describes applying the current AASHTO test methods for samples with a grading number (GN) > 3, or if the percent passing No.10 sieve is greater than 25%. Otherwise, if the GN < 3, and the percent passing No.10 sieve is less than 25%, the alternatives that consider the as-received gradation

of the samples, such as Texas-modified procedures, are recommended (i.e., Tex-129-M and Tex-620-M), which use particle sizes up to 1¾ in (45 mm).

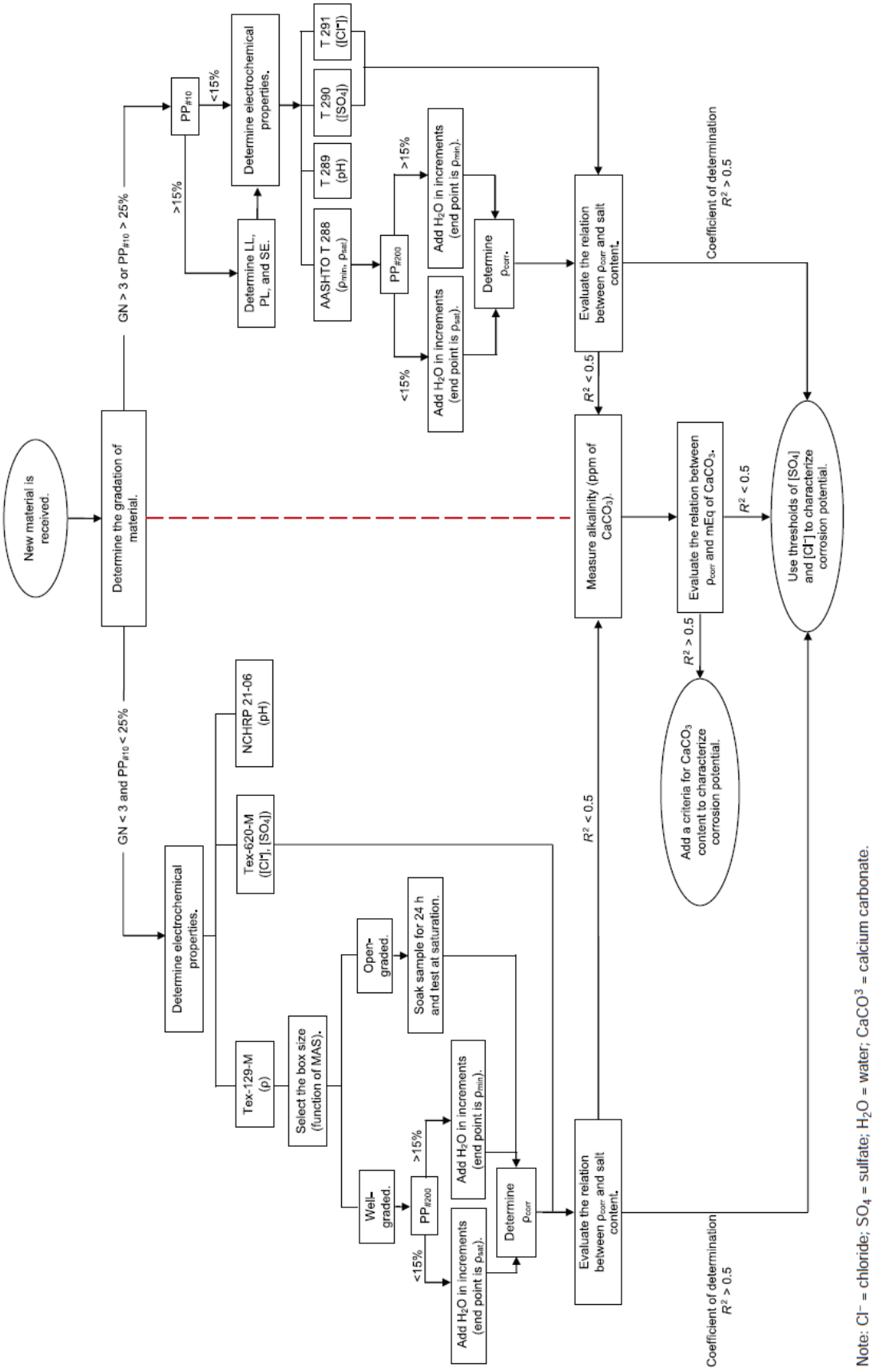


Figure 2-23 Flowchart of the proposed EC testing protocol (from Fishman et al. 2021a).

2.3 Summary and Implications for Current Research

Very few studies have investigated/reported the EC properties of FGA and ESCS aggregates. No studies were found to have investigated the precision and bias of AASHTO test methods and their various alternatives on FGA and ESCS aggregates. While the EC testing protocol proposed by Fishman et al. (2021a) is applicable to FGA and ESCS aggregates in terms of gradation, the applicability of various tests involved in the protocol to FGA and ESCS aggregates is uncertain. As these aggregates are made of recycled materials or industrial by-products, the composition and chemical and EC properties of these materials are significantly different from soils. For example, the measured resistivity, pH, and salt contents of FGA and ESCS aggregates may substantially vary if the samples are soaked for different periods (e.g., 24 hours vs. 48 hours) due to the absorption properties of the materials. Hence, special test considerations and sample preparations need to be developed for proper measurement of the EC properties of these materials in the field conditions.

For subsequent investigation of EC properties of FGA and ESCS aggregates in this research, the FGA products from Aero Aggregates of North America, LLC (https://www.aeroaggna.com/) and the ESCS aggregates from the suppliers in Table 2-12 were used since they are major LWA suppliers to the PA market. The EC testing protocol proposed by Fishman et al. (2021a) were applied in testing the selected FGA and ESCS aggregates.

CHAPTER 3

Experimental Program

3.1 Factors Investigated in the Experiment

Several key factors related to chemical and electrochemical properties were investigated to determine the suitability of LWAs for MSE wall applications. Specifically, sulfate and chloride contents were evaluated to identify aggregates' potential for initiating and accelerating corrosion processes. The pH value was measured to determine the aggregate's alkalinity or acidity, which directly impacts the corrosion rate. Finally, electrical resistivity was investigated as a critical parameter for assessing aggregates' ability to resist electrical current, which influences the electrochemical processes leading to corrosion.

Table 3-1 outlines each investigated factor, providing a description of their implications for aggregate suitability in MSE wall fills.

Table 3-15 Factors investigated for MSE wall fill with LWAs.

Factor	Description
Sulfate content	Measures sulfate concentration, which can accelerate corrosion by reacting chemically with metals, leading to deterioration and potential structural failure.
Chloride content	Measures chloride concentration, a primary contributor to corrosion risk, particularly affecting steel reinforcement by promoting corrosion reactions.
pH value	Determines alkalinity or acidity of aggregates. A suitable pH range is necessary to maintain the passive protective layer on metallic reinforcements and minimize the corrosion rate.
Resistivity	Reflects aggregate’s ability to resist electrical current flow. Higher resistivity values generally indicate lower corrosion potential, reducing the electrochemical reactions that facilitate corrosion processes.

3.2 Materials

In this study, four types of LWAs were obtained from different manufacturers. These materials are listed in PennDOT Bulletins 14 and 15, the approved list of aggregates and suppliers, respectively. It was the intention to select materials that were in the PennDOT approved list before moving forward with evaluation of their potential applicability as MSE wall fill. The types of materials and their sources are shown in Table 3-2. The diversity of the sourced LWAs allowed for a broad and comparative assessment of material behavior under consistent testing conditions.

Table 3-16 Types and sources of different materials for the tests.

LWA Type	Supplier Name	Supplier Code	Material Class	Location
Expanded shale	STALITE	CSCNCA14	LW3/4	Salisbury, NC
	NORLITE	NOHNYA14	LW3/4	Cohoes, NY
	NORTHEAST SOLITE	NOTNYA14	LW3/4	Saugerties, NY
Foamed glass aggregate	AERO AGGREGATES	AERO1 15	Foamed Glass Agg. (FGA)	Eddystone, PA

Manufacturers provided not only LWA samples but also accompanying documentation detailing the physical properties of the materials. These parameters served as important references for analyzing the results of subsequent chemical and electrochemical testing. The materials were delivered in sealed containers to ensure integrity during transport and handling. Upon receipt, all samples were labeled and stored to preserve their condition prior to testing. Detailed descriptions of the individual material are presented in the following sections.

STALITE

STALITE aggregate is a manufactured lightweight aggregate produced from argillite slate. The raw material is expanded in a rotary kiln at high temperatures, creating a porous but durable ceramic aggregate.

This aggregate is used in various civil engineering applications, including structural concrete, highway embankments, and MSE wall fills. The material is known for its relatively uniform gradation and angular particle shape, which contribute to its mechanical stability under load. The production process yields consistent material with predictable behavior in compaction and load transfer, making

it suitable for use in MSE wall backfill systems. The physical appearance of Stalite aggregate is shown in Figure 3-1.



Figure 3-24 Physical appearance of STALITE aggregate.

The key physical characteristics and gradation of Stalite aggregate are shown in Table 3-3. Sieve sizes finer than #4 sieve are not shown in the table since there were no values specified for these finer sieves.

Table 3-17 Physical properties and gradation of STALITE aggregate provided by supplier.

Property	**Designated as 3/4" (19 mm)**	
Typical Density (Unit Weight)	(lbs/cf)	(kg/m³)
Dry Loose (ASTM C29)	48	768
Dry Rodded (ASTM C29)	55	880
Saturated Surface Dry Loose (ASTM C29)	50	800
Maximum Dry Density (ASTM D4253)	60	960
Damp Loose (ASTM C29)	48-52	768-832
Typical Relative Density (Specific Gravity)		
Dry (ASTM C127)	1.45	
Saturated Surface Dry (ASTM C127)	1.50	
Range in Saturated Surface Dry (ASTM C127)	1.47-1.54	
Sieve Sizes	% Passing	
1" (25 mm)	100	
3/4" (19 mm)	90-100	
1/2" (12.5 mm)	-	
3/8" (9.5 mm)	10-50	
#4 (4.75 mm)	0-15	

NORLITE

NORLITE aggregate is produced by expanding and vitrifying select shale in a rotary kiln. The shale is crushed, screened, and then fed into a rotary kiln where it is rapidly heated and expanded.

NORLITE is used in both structural and geotechnical applications, including retaining walls, embankments, and slope stabilization projects. Its angular and rough-textured particles allow for good interlock and compaction characteristics. The aggregate meets relevant ASTM standards for structural lightweight fill materials and is used in DOT-approved applications. It is often selected where weight reduction and shear strength are important design factors. The physical appearance of Norlite aggregate is shown in Figure 3-2.



Figure 3-25 Physical appearance of NORLITE aggregate.

The key physical characteristics and gradation of Norlite aggregate are shown in Table 3-4. Sieve sizes finer than #4 sieve are not shown in the table since there were no values specified for these finer sieves.

Table 3-18 Physical properties and gradation of NORLITE aggregate provided by supplier.

Property	Designated as 3/4” (1 9mm)
Dry Loose Unit Weight (pcf)	40.2
Damp Loose Unit Weight (pcf)	45.7
Sieve Size	% Passing
1” (25 mm)	100
3/4” (19 mm)	90-100
1/2” (12.5 mm)	85
3/8” (9.5 mm)	10-50
#4 (4.75 mm)	0-15

NORTHEAST SOLITE

NORTHEAST SOLITE is a lightweight aggregate produced by firing select shale at high temperatures in a rotary kiln, resulting in a porous, ceramic-like material. The aggregate is commonly used in geotechnical applications, including MSE wall backfill, due to its low density and granular structure. The material exhibits moderate water absorption and is also reported to have chemical stability suitable for use with metallic reinforcement. The physical appearance of Northeast Solite aggregate is shown in Figure 3-3.



Figure 3-26 Physical appearance of NORTHEAST SOLITE aggregate.

The key physical characteristics and gradation of Northeast Solite aggregate are shown in Table 3-5. Sieve sizes finer than #4 are not shown in the table (except #200 sieve) since there were no values specified for these finer sieves.

Table 3-19 Physical properties and gradation of NORTHEAST SOLITE aggregate provided by

supplier.

Property	Designated as 3/4” (19 mm)
Dry Loose Unit Weight (pcf)	54
Damp Loose Unit Weight (pcf)	60
Sieve Size	% Passing
1” (25 mm)	100
3/4” (19 mm)	97
1/2” (12.5 mm)	54
3/8” (9.5 mm)	34
#4 (4.75 mm)	8
#200 (75 µm)	2

AERO AGGREGATES

AERO AGGREGATES aggregate is produced by processing 100% post-consumer recycled glass in a rotary kiln with a foaming agent, producing a closed-cell, foamed glass aggregate (FGA). Foamed glass aggregates can generally be classified as either open-cell or closed-cell materials, depending on their pore structure. The Aero Aggregates FGA evaluated in this study is a closed-cell foamed glass aggregate, characterized by predominantly isolated pores and relatively low water absorption. Therefore, the results presented in this study for foamed glass aggregate are specific to closed-cell FGA. The material’s dry bulk density is only approximately 15 pcf. According to manufacturer specifications, AERO AGGREGATE is approximately 85% lighter than conventional aggregates and exhibits a highly frictional surface texture. The material is inert, non-leaching, rot-resistant, non-flammable, and structurally stable under freeze-thaw cycles. Applications include embankment fill, load distribution platforms, insulation beneath slabs, and MSE wall fill systems. AERO AGGREGATE can be placed in lifts and does not require conventional compaction equipment. In accordance with PennDOT Publication 408, Section 218, FGA it is compacted using four passes of tracked equipment at specified ground pressure. This unconventional compaction method ensures stability while still allowing the material to provide drainage and thermal insulation benefits and to reduce load on underlying soils. The physical appearance of Aero Aggregates FGA is shown in Figure 3-4.



Figure 3-27 Physical appearance of AERO AGGREGATES.

The key physical characteristics of Aero Aggregates are shown in Table 3-6.

Table 3-20 Physical properties of AERO AGGREGATES aggregate provided by supplier.

Property	Value
Dry Loose Unit Weight (pcf)	12-15
Dry Compacted Unit Weight (pcf)	13.3-16.7
Specific Gravity	0.4
Porosity (Uncompacted)	0.5
Porosity (1.25 Compression Ratio)	0.38

In this study, four types of lightweight aggregates were selected for investigation. Three of the materials (STALITE, NORLITE, and NORTHEAST SOLITE) are expanded shale/slate aggregates produced through high-temperature kiln processing. The fourth material (AERO AGGREGATES) is a foamed glass aggregate manufactured from recycled glass. These aggregates represent a range of manufacturing processes and physical characteristics. Results from sieve analysis of the materials are plotted as particle size distribution curves (Figure 3-5). The sieve analysis was conducted three times for each material, and the average results are shown in Figure 3-5. These graphs indicate how different aggregates compare in size distribution relative to one another and also show the gradation of the material as used in the resistivity testing under this research and presented in this report. For LWA of a given source, the particle size distribution may or may not be an important factor in terms of electrical resistivity and corrosion potential. Sometimes the aggregates received from the manufacturer may be on the very coarse or very fine side of gradation and the question is if this wide variation in size matters in terms of corrosion potential. The impact of gradation variations

on the test results will be the subject of further investigation during the next step of this research. All four materials were included in the experimental program for electrochemical evaluation related to MSE wall fill applications.

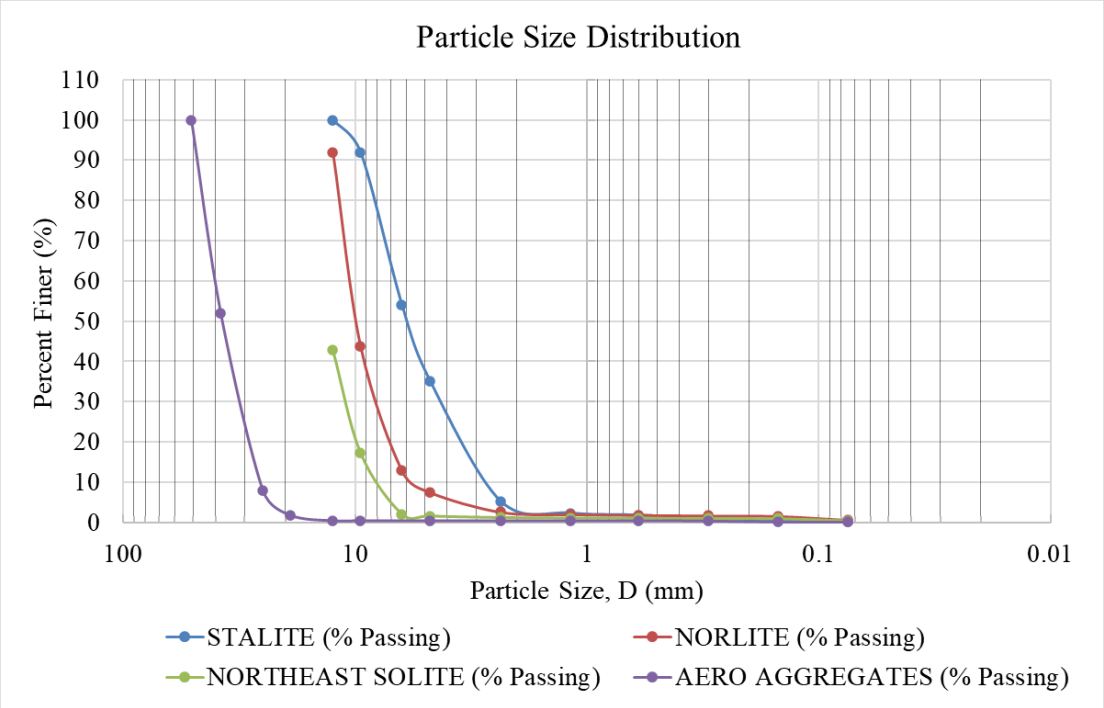


Figure 3-28 Particle size distribution of the materials used in the study.

3.3 Equipment

3.3.1 Equipment for Chemical Testing

The chemical testing program consisted of two main sections: the determination of sulfate and chloride contents, and the measurement of pH. Each set of tests required a combination of standard laboratory apparatus and specialized instruments to ensure reliable results.

3.3.1.1 Equipment for Sulfate and Chloride Measurement

The determination of sulfate and chloride contents in LWA requires a combination of sample preparation tools, clarification equipment, and analytical instruments. The process involves reducing aggregate particle size to facilitate ion extraction, isolating the liquid phase to remove suspended solids, and using precise colorimetric techniques for quantification. The selected equipment is intended to standardize each stage of the procedure from sample preparation through measurement,

so that results are accurate, reproducible, and comparable across different materials. The main equipment used in the measurement of sulfate and chloride content is described as follows.

Pulverizing Machine

The pulverizing machine was used to crush aggregate samples into smaller particles, increasing the available surface area for dissolution of sulfate and chloride ions during extraction. This step improves the efficiency and completeness of ion release from both surface deposits and internal voids. The pulverizing machine used in the tests is shown in Figure 3-6(a).

Sieve Set and Mechanical Sieve Shaker

Standardized mesh sizes were employed to separate and verify the particle-size fraction specified in the testing method. The sieving process was carried out in accordance with relevant standard procedures (i.e., ASTM C136 for sieve analysis of fine and coarse aggregates) to ensure consistency and repeatability. Consistent particle size ensures uniform extraction conditions across all samples. The sieving process was conducted as Figure 3-6(b) shows.



(a) Pulverizing machine



(b) Sieve shaker

Figure 3-29 The equipment for sample preparation.

Vibration Machine

The vibration machine is a platform capable of providing continuous mechanical shaking to samples for a pre-set period. In this study, it was used to maintain constant agitation for the samples in extraction process. The vibration ensured that aggregate particles remained in suspension and

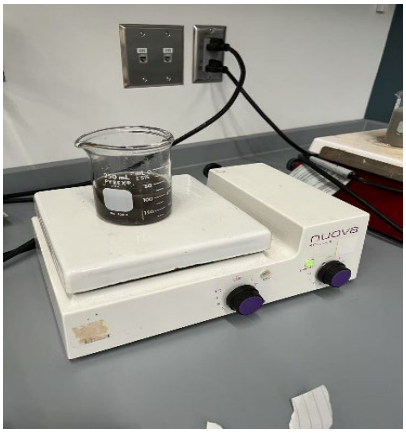
maintained consistent contact with the extraction solution. The vibration machine used in the tests is shown in Figure 3-7(a).

Hot Plate Stirrer

It is a laboratory device that combines magnetic stirring with the capability to apply controlled heating to the sample. The unit uses a rotating magnetic field to spin a stir bar inside the container, providing consistent mixing, while the integrated hot plate delivers heating to the liquid. The hot plate stirrer used in the tests is shown in Figure 3-7(b).



(a) Vibration machine



(b) Hot plate stirrer

Figure 3-30 The equipment for sample extraction.

Centrifuge

Centrifuge was used to separate suspended solids from the liquid extract, producing a clear supernatant that can be analyzed without interference from particulates. Balanced loading of the rotor was maintained to prevent operational vibration and ensure consistent separation. The centrifuge used in the tests is shown in Figure 3-8(a).

Membrane Filters

0.2-μm membrane filters were used to further remove residual fine particles after centrifugation. Filtration prevents light scattering in the spectrophotometer, ensuring that absorbance measurements reflect only the target analyte-reagent reaction. The membrane filters used in the tests are shown in Figure 3-8(b).



(a) Centrifuge



(b) Membrane filters

Figure 3-31 The equipment for preparing sample solutions.

TNTplus® Sulfate & Chloride Testing Kits

TNTplus® Sulfate & Chloride Testing Kits are pre-measured reagent vials developed by Hach company for the colorimetric determination of sulfate and chloride in aqueous samples. As Figure 3-9(a) shows, each kit contains sealed glass vials with precisely dosed reagents, buffers, and catalysts required by the method, minimizing direct handling of chemicals and reducing operator exposure. Each testing kit is designed for a specific concentration range to optimize sensitivity and accuracy.

Hach DR 1900 and 2800 Spectrophotometers

Hach DR 1900 and 2800 Spectrophotometer are visible-range spectrophotometers designed for water and environmental testing and are compatible with Hach TNTplus® reagent vials. With the automated wavelength selection and TNTplus barcode recognition, they can provide consistent calibration and data readout for sulfate and chloride testing. The Hach DR 1900 and 2800 spectrophotometers used in the tests are shown in Figure 3-9(b).



(a) TNTplus® Sulfate & Chloride Testing Kits



(b) Hach DR 1900 and 2800 spectrophotometers

Figure 3-32 The equipment for measuring ion content.

Laboratory Glassware and Analytical Balance

Regular laboratory glassware was used through the tests, including beakers, measuring cylinders, pipettes, and droppers. These were used for preparing extraction solutions, transferring liquids accurately, and mixing samples with reagents, minimizing contamination risks. High-precision balance (readability to 0.01 mg) was used for weighing aggregate samples and reagents.

3.3.1.2 Equipment for pH Determination

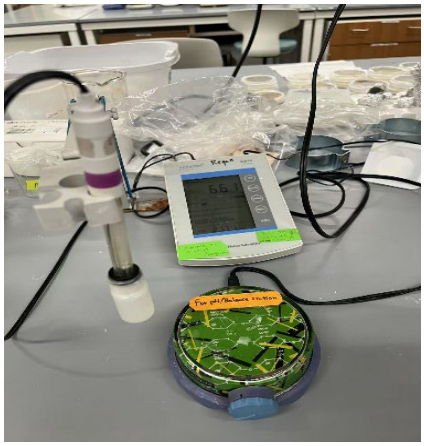
Measuring the pH of aggregate samples provides insight into the chemical environment they create when in contact with water, which can influence the corrosion potential of metallic reinforcements. This analysis requires equipment that can prepare stable aqueous sample, calibrate and operate pH measurement instruments, and prevent cross-contamination between tests. The selected tools ensure accurate readings by maintaining calibration integrity and consistent sample handling. The main equipment used in the determination of pH value is listed as follows:

pH Meter

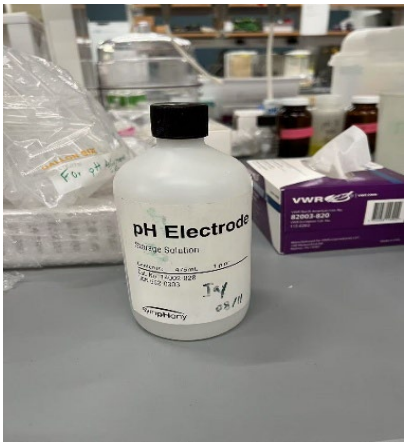
A portable pH meter equipped with a glass combination electrode and automatic temperature compensation was used to measure the hydrogen ion concentration in the solution prepared from aggregate samples. The pH meter was calibrated at the start of each testing session. Electrodes were rinsed between measurements and stored according to manufacturer guidance. The pH meter used in the tests is shown in Figure 3-10(a).

Neutral Buffer Solution (pH 7.00)

Standardized buffer solution was used to calibrate and verify the pH meter at neutral conditions before sample measurement. Calibration at pH 7 is essential for minimizing systematic errors around the expected range of aggregate pH values and ensuring measurement accuracy. The neutral buffer solution used in the tests is shown in Figure 3-10(b).



(a) pH Meter



(b) Neutral Buffer Solution

Figure 3-33 The equipment for pH determination.

Laboratory Glassware and Analytical Balance

Regular laboratory glassware including beakers, stirring rods, and measuring cylinders was used for preparing sample solutions, mixing calibration buffers, and rinsing electrodes between measurements to prevent cross-contamination.

By utilizing the equipment mentioned above, the integrated use of sample preparation equipment, filtration and clarification tools, and analytical instruments in the chemical tests allowed for consistent and reproducible chemical testing results across all lightweight aggregate types evaluated in this study.

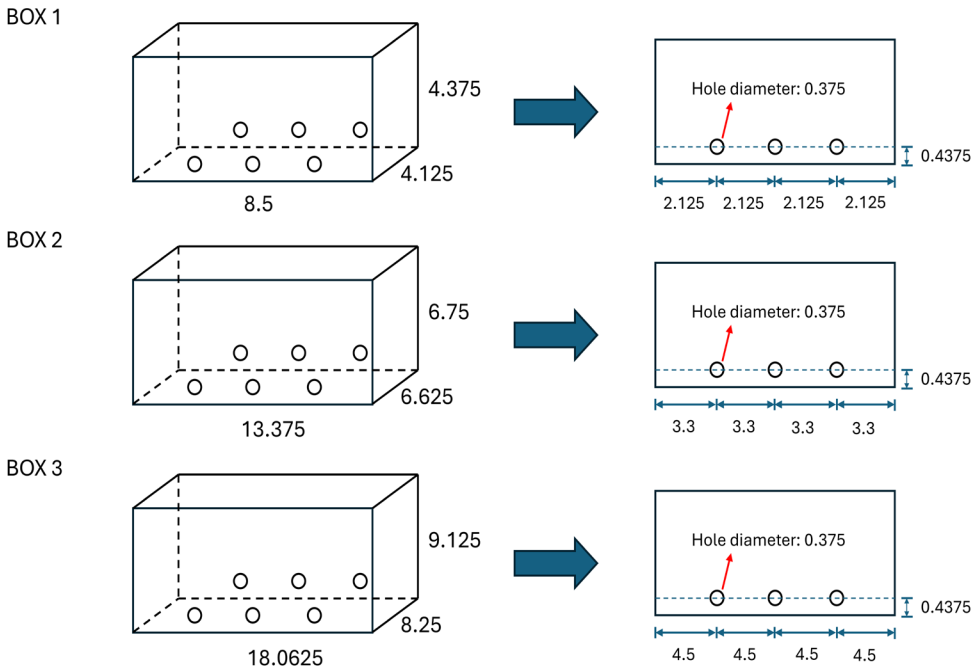
3.3.2 Equipment for Resistivity Testing

Resistivity testing was performed on aggregates in their as-received gradation to reflect field conditions more accurately. Standard AASHTO soil box apparatus, designed primarily for fine-grained soils, was not suitable for these samples because its limited dimensions could not accommodate coarse particles without altering their natural packing structure. Forcing coarse

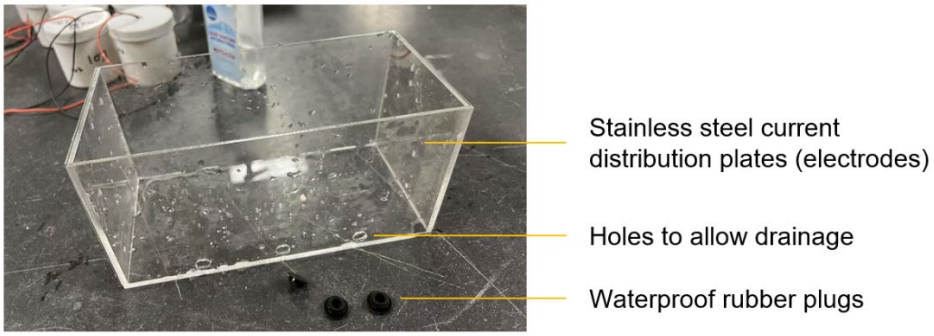
aggregates into an undersized box can lead to particle bridging, uneven contact between sample and electrodes, and artificially high resistivity values. To overcome these limitations, a set of custom-designed resistivity boxes was fabricated in this study, along with supporting equipment, to enable consistent measurement across varying conditions. The main equipment used in the resistivity testing is listed as follows:

Custom-Made Resistivity Boxes

Three boxes of different dimensions were fabricated to accommodate as-received aggregate gradations. The increased size allowed the natural particle arrangement to be preserved during testing, minimizing edge effects and ensuring representative resistivity values. Circular drainage openings were installed near the base of each box to allow controlled water drainage, enabling resistivity measurements at different moisture contents. Rubber stoppers provided a watertight seal when the box needed to retain water for saturation tests. In addition, each box was fitted with stainless steel plates at opposite ends to serve as electrodes. Stainless steel was selected for its corrosion resistance and stable electrical contact properties over repeated wet and dry testing cycles. The design of custom resistivity boxes and supporting components are shown in Figure 3-11.



(a) The design of custom resistivity boxes (Unit: inches).



(b) Custom box and supporting equipment.

Figure 3-34 Custom Resistivity Boxes.

B&K Precision Model 895 LCR Meter

A LCR meter is designed to measure inductance (L), capacitance (C), and resistance (R) over a wide range of values. In this study, it was configured for resistance measurement to determine the electrical resistivity of LWAs. The instrument uses an AC test signal, and for this application, a frequency of 97 Hz was selected (within the typical 80-100 Hz range recommended for granular material resistivity testing) to minimize electrode polarization effects and to provide stable readings. The Model 895 features a measurement range from 0.01 Ω to 100 MΩ, enabling accurate capture of resistivity values across both saturated and drier conditions. The meter's digital interface provides direct readouts, selectable measurement modes, and data stability indicators, which facilitated quality control during testing. The B&K Precision Model 895 LCR Meter used in the tests is shown in Figure 3-12.

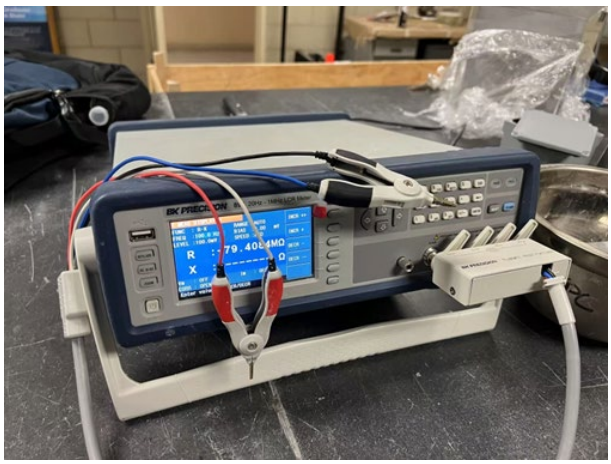


Figure 3-35 LCR meter.

3.4 Execution of the Experimental Plan

The experimental program was carried out in accordance with the objectives defined for evaluating the electrochemical properties of the selected LWAs. Following the acquisition and preparation of the materials, and the assembly of the necessary equipment, the testing procedures were implemented in a systematic manner to ensure consistency, accuracy, and comparability of results. For each targeted parameter (sulfate and chloride content, pH value, and resistivity) potential influencing factors were identified in advance, and multiple test conditions were designed to capture their effects. These conditions allowed for direct comparison between different material responses under varying environmental or procedural scenarios, providing a more comprehensive understanding of performance. Each test was performed on all four aggregate types under controlled laboratory conditions. The following subsections describe the execution of the chemical and resistivity testing procedures, along with the variable conditions, and adjustments applied to accommodate the unique characteristics of the LWAs under study.

3.4.1 Chemical Testing

3.4.1.1 Sulfate and Chloride Content Measurement

For chemical measurements, sample preparation began with the use of a pulverizing machine to break down aggregate particles, followed by mechanical sieve separation to obtain the required particle-size fraction for analysis.

The samples prepared were then subjected to extraction procedures. Extraction is required to transfer water-soluble ions from the solid aggregate matrix into an aqueous phase suitable for colorimetric measurement and to minimize matrix effects (which means the influence of other substances in the sample). In LWAs, chloride and sulfate may occur as surface residues, pore-water species, or salts lodged within micro-voids, so reducing particle size is important to promote mass transfer and approach equilibrium. Aqueous extraction also standardizes the chemical environment so that reagents react in the correct chemical proportions with the target ions. In the extraction procedure, water-soluble ions were leached from the aggregate samples into solution for subsequent analysis. It is recognized that preparing the material by crushing and sieving to specified particle sizes does not precisely replicate the “as-installed” condition of the backfill; however, this approach is necessary for proper evaluation: finer particles ensure that soluble ions trapped in pores are released, and standardized gradations provide reproducible, comparable results across materials. For the step

of extraction, we considered and implemented three different approaches based on different standards as Table 3-7 shows.

Table 3-21 The extraction methods considered in chemical testing.

Extraction method	Description	Reference
Intermittent shaking for one hour	Weigh 10 g aggregate samples and add 30 mL of distilled water. Stopper and shake the solution vigorously for 20s. After 1 hour, repeating shaking.	AASHTO T290 and 291
Continuous shaking for one hour	A comparative method developed for this study, in which the sample container was placed on a vibration machine and subjected to continuous shaking throughout the extraction period to maintain constant particle suspension and solution contact.	Proposed in this study
Heated continuously stirring for one hour	Involving heating of the suspension during constant agitation in a hot plate stirrer to accelerate ion release and approach equilibrium more rapidly.	Tex-620-J

These methods were selected for comparison to evaluate the influence of agitation intensity and temperature on ion recovery from lightweight aggregates. In addition to varying the agitation and heating conditions, the extraction method also considered different aggregate particle sizes in accordance with requirements from multiple standards. The different particle sizes included passing No. 10 sieve (AASHTO T290/291), passing No. 8 sieve (PA Test Method (PTM) No. 128), and passing No. 50 sieve (AASHTO T260). These particle-size variations were included because different gradations can influence the dissolution rate of ions. Finer fractions generally provide greater surface area for interaction with the extraction solution, while coarser fractions may better represent in-situ conditions for as-received aggregates. By combining three agitation/heating approaches with three particle-size conditions, the experiment was designed to assess how both mechanical/thermal extraction conditions and sample gradation affect measured sulfate and chloride concentrations.

Following extraction, the liquid phase was clarified first by centrifugation to separate suspended solids, then passed through 0.2-μm membrane filters to remove residual particulates that would scatter light and bias absorbance readings. This two-stage clarification is essential for reproducible photometric measurements, reducing turbidity influence and ensuring that absorbance changes arise from reagent reactions rather than optical interference.

Sulfate testing kits (TNT864) were used to measure the content of sulfate in the filtered solution sample. The kits use the turbidity method, where sulfate ions react with barium chloride to form insoluble barium sulfate. The resulting turbidity is measured photometrically at a specified wavelength. Chloride testing kits (TNT879) use the ferric thiocyanate colorimetric method, where chloride ions displace thiocyanate from mercury thiocyanate, and the released thiocyanate reacts with ferric ions to form a reddish-brown complex measured photometrically. The Hach DR 1900 and 2800 spectrophotometers were then used with testing kits to determine the content of sulfate and chloride in the sample.

Subsequent analysis of the test results indicated that the differences between the "intermittent shaking" method and the "continuous shaking" method were minimal in terms of measured ion concentrations. As a result, the mixing procedure for later stages of testing was standardized to continuous shaking for one hour to improve operational consistency and simplify the workflow, while retaining the heated continuous stirring method as a separate condition for comparative purposes. Therefore, a testing matrix for sulfate and chloride content measurement was developed as Table 3-8 shows.

Table 3-22 Testing Matrix for Sulfate and Chloride Content Measurement.

Extraction method / Materials	PTM No. 128	AASHTO T290/291 (× heating)	AASHTO T290/291 (√ heating)	AASHTO T260 (×heating)	AASHTO T260 (√ heating)
STALITE	√	√	√	√	√
NORLITE	√	√	√	√	√
NORTHEAST SOLITE	√	√	√	√	√
AERO AGGREGATES	√	√	√	√	√

3.4.1.2 pH Value Determination

Different particle sizes were evaluated to examine the influence of aggregate size on the measured pH. Unlike the sulfate and chloride tests, no heating was applied during extraction for pH determination, as the objective was to measure the material's behavior under conditions more representative of natural field environments. The testing matrix for pH determination was developed as Table 3-9 shows.

Table 3-23 Testing Matrix for pH determination.

Materials \ Extraction method	Original size	Passing No. 10 sieve	Passing No. 50 sieve
STALITE	√	√	√
NORLITE	√	√	√
NORTHEAST SOLITE	√	√	√
AERO AGGREGATES	√	√	√

The pH determination procedure consisted of two main steps:

Calibrating the pH Meter

Prior to any measurements, the pH meter equipped with a glass combination electrode and automatic temperature compensation was calibrated. The electrode was first rinsed thoroughly with distilled water to remove any residues from previous tests, and then gently blotted dry with tissue to avoid damage to the sensing surface. Calibration solutions (buffers) were prepared and poured into clean beakers dedicated for calibration use. A neutral buffer solution (pH 7.00) was used for the initial calibration point. The electrode was immersed in the buffer until the reading stabilized, and the calibration was accepted if the slope and offset values met the manufacturer's specifications. The calibrating process of pH meter is shown in Figure 3-13(a).

Measuring The Sample's pH

The preparation of the sample solution followed the procedure outlined in AASHTO T289, which involves combining a measured mass of aggregate with a specified volume of deionized water in a clean container. The solution was stirred into slurry and was transferred to a clean beaker. The electrode was immersed into the slurry until a stable reading was obtained. Between each measurement, the electrode was rinsed and checked periodically against the pH 7.00 buffer to verify calibration stability during the testing sequence. The pH measuring process is shown in Figure 3-13(b).



(a) pH meter calibration



(b) pH measurement

Figure 3-36 The process of pH determination.

3.4.2 Electrical Resistivity Testing

In this study, electrical resistivity was measured on the aggregates in their as-received gradation, to reflect the particle size distribution and packing conditions that would occur in field backfill applications. There are numerous factors that can influence the resistivity of granular materials, but two were found to be the most consistently discussed and experimentally validated: electrode spacing and pre-soaking time.

The influence of electrode spacing arises from the fact that the measured resistance in granular materials is a function of the path length of the electrical current between electrodes, as well as the cross-sectional area through which the current passes. Increasing the electrode spacing increases the path length, generally resulting in higher measured resistance for the same material and moisture condition. Conversely, smaller spacings tend to reduce resistance values but may be more sensitive to local heterogeneity and particle contact effects. In this experiment, electrode spacing was inherently varied by using the three custom-fabricated resistivity boxes described previously, each with different internal dimensions and therefore different electrode separations.

The role of pre-soaking time is associated with the degree to which water can infiltrate the pores and micro-voids of the aggregate particles, as well as fill the inter-particle void spaces. Short pre-soaking times may not allow full saturation of internal pores, especially for lightweight aggregates with high porosity, resulting in higher resistivity readings. Longer pre-soaking times generally reduce resistivity by increasing the continuity of conductive paths through both surface films and internal moisture, until a saturation is reached. To capture this effect, pre-soaking times of 5 minutes, 10 minutes, 30 minutes, 1 hour, 2 hours, and 12 hours were investigated for each aggregate type and box

size. Therefore, by considering the two influencing factors, a testing matrix for resistivity test was developed as Table 3-10 shows.

Table 3-24 Testing Matrix for Electrical Resistivity.

Material \ Condition	Soaking time (5 mins)			Soaking time (10 mins)			Soaking time (30 mins)			Soaking time (1 hour)			Soaking time (2 hours)			Soaking time (12 hours)		
	Electrode spacing			Electrode spacing			Electrode spacing			Electrode spacing			Electrode spacing			Electrode spacing		
	S	M	L	S	M	L	S	M	L	S	M	L	S	M	L	S	M	L
STALITE	√	√	√	√	√	√	√	√	√	√	√	√	√	√	√	√	√	√
NORLITE	√	√	√	√	√	√	√	√	√	√	√	√	√	√	√	√	√	√
NORTHEAST SOLITE	√	√	√	√	√	√	√	√	√	√	√	√	√	√	√	√	√	√
AERO AGGREGATES	√	√	√	√	√	√	√	√	√	√	√	√	√	√	√	√	√	√

For each test, a measured quantity of the as-received aggregate was first placed into a clean container, and distilled water was added until the material was fully submerged. The sample was mixed thoroughly to dislodge entrapped air and promote uniform wetting, then left undisturbed for the designated pre-soaking period (5 min to 12 h), allowing water to infiltrate both the inter-particle voids and the internal pore structure of the aggregates. At the end of the pre-soaking period, the aggregate was transferred into the selected resistivity box, which corresponded to one of the three electrode spacings under investigation. Placement was carried out in several layers, with each layer compacted using finger pressure to achieve a packing arrangement without crushing particles or altering their shape. The top surface was leveled to ensure full and even contact with both stainless-steel electrodes mounted at the ends of the box.

With the drainage hole sealed, the box was connected to the LCR meter, set to operate at 97 Hz AC for resistance measurement. The resistance of the fully saturated specimen was recorded once the reading had stabilized. Following the saturated measurement, the rubber plug on the drainage hole was opened to allow free water to exit under gravity. Resistance readings were then taken continuously throughout the drainage phase, as the removal of free water and reduction in moisture content led to a progressive increase in resistance. The process continued until the resistance reached a maximum stable value, corresponding to the nearly dry condition for that packing configuration.

Finally, the recorded resistance values (R) were converted to bulk resistivity (ρ) using the geometric parameters of the test box, namely the electrode spacing (L) and the cross-sectional area (A) of the specimen, applying Ohm's law in the form $\rho = R \times A / L$. The resulting resistivity values were compiled for each combination of pre-soaking time and electrode spacing, enabling direct comparison across the full matrix of test conditions. The typical measuring process is shown in Figure 3-14.



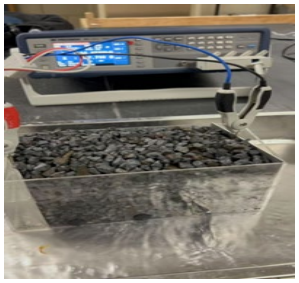
(a) Pre-soaking of the sample



(b) Place the sample in the testing box



(c) Measure the resistance



(d) Allow the water drainage

Figure 3-37 The process of resistivity measurement.

3.4.3 Additional Resistivity Testing

3.4.3.1 Long-term Effect of Moisture Change

To comprehensively investigate the influence of moisture variation on the electrical resistivity of lightweight aggregates over time, a long-term monitoring of resistivity test was conducted. Two representative materials, Stalite expanded shale and AERO AGGREGATE, were selected for this extended observation. The test used the medium sized custom box, consistent with the setup of the short-term resistivity tests. Two pre-soaking conditions of 5 minutes and 12 hours were applied, representing the extremes of practical field moisture exposure. The resistivity of each sample was

recorded continuously for 48 hours, with the monitoring extended if stabilization had not yet been achieved. This approach allows the resistivity evolution to be linked to gradual drainage and redistribution of moisture within the aggregate mass.

To relate the change of resistivity to moisture variation, a parallel measurement of moisture content was conducted using an identical companion box for each aggregate and soaking condition. Both boxes underwent the same drainage process simultaneously. At determined time intervals of 1 hour, 2 hours, 4 hours, 8 hours, 12 hours, 24 hours, and 48 hours, samples were taken from the companion box for gravimetric moisture content determination following AASHTO T 255 procedures. Each subsample was weighed before and after oven drying to calculate its water content.

This design ensured that the resistivity monitoring box remained undisturbed during the entire test while still allowing an assessment of corresponding moisture evolution over time. The combined resistivity-moisture datasets will provide insight into the coupling between drying behavior and electrical conduction within lightweight aggregates, as well as potential differences between expanded shale and foamed glass materials under varying degrees of saturation.

3.4.3.2 Effect of Compaction Level on Resistivity

To investigate how different degrees of compaction influence the electrical resistivity of lightweight aggregates, additional tests were performed using Stalite and AERO AGGREGATE materials. The purpose of this test was to quantify the relationship between particle packing density, pore space, and resulting resistivity, providing insight into the sensitivity of electrochemical behavior to placement conditions.

All tests were conducted using the medium size resistivity box, with a constant pre-soaking time of 12 hours to ensure a uniform moisture condition prior to compaction. The compaction level was the only variable parameter in this experiment, categorized into three conditions: loose, medium, and dense, representing typical field placement variability. Loose compaction means samples were placed in a single lift without any applied pressure or tamping, allowing the natural settling of particles under gravity. Medium compaction means samples were placed in three layers and compacted using moderate finger pressure, following the same procedure as described in previous section. Dense compaction means samples were placed in three layers, with each layer compacted using 25 uniform rodding strokes, ensuring a higher degree of particle interlock and reduced void space.

This study of compaction was designed to capture how particle contact and pore volume reduction influence electrical conduction in lightweight aggregates.

3.4.3.3 Effect of Gradation Condition on Resistivity

To isolate the influence of particle size distribution on electrical resistivity, additional tests were performed on Stalite and AERO AGGREGATE under controlled gradation conditions using the medium size box and a constant pre-soaking time of 12 hours. For each material, three gradation conditions were considered: the as-received gradation and two adjusted gradations, referred to as coarse and fine conditions.

For Stalite, the as-received particle size distribution showed approximately 54% passing the 1/4-in sieve. The coarser gradation was obtained by removing all material passing the 1/4-in. sieve, so that only particles larger than 1/4 in. were retained. Conversely, the finer gradation was produced by removing all particles larger than 1/4-in. and testing only the fraction passing the 1/4-in. sieve. This approach effectively brackets the field gradation with two extreme cases: a coarse skeleton composed solely of large particles, and a relatively dense packing composed solely of the finer fraction.

For Aero Aggregate, the as-received gradation indicated that about 52% of the particles passed the 1 1/2-in. sieve. The coarser Aero Aggregate gradation was therefore prepared by removing all material passing 1 1/2 in., retaining only particles larger than 1 1/2 in. The finer gradation was obtained by removing all particles larger than 1 1/2 in. and using only the fraction passing the 1 1/2-in. sieve. Because Aero Aggregate consists of relatively large particles, these two gradations represent upper- and lower-bound particle size conditions that can be realistically formed without crushing the material.

CHAPTER 4

Summary of Results and Data Analysis

The testing program produced a comprehensive dataset covering the chemical and electrical properties of four different lightweight aggregates, evaluated under a range of controlled laboratory conditions. For each target parameter (sulfate and chloride content, pH value, and electrical resistivity), multiple test scenarios were implemented to capture the influence of key variables such as extraction method, particle size, electrode spacing, and pre-soaking time. The results are presented in the following sections through a combination of summary tables and graphical plots, enabling both direct comparison between materials and identification of trends associated with the selected test conditions. This integrated presentation provides not only the measured values but also the context necessary to interpret material performance in relation to applicable specifications and potential field behavior.

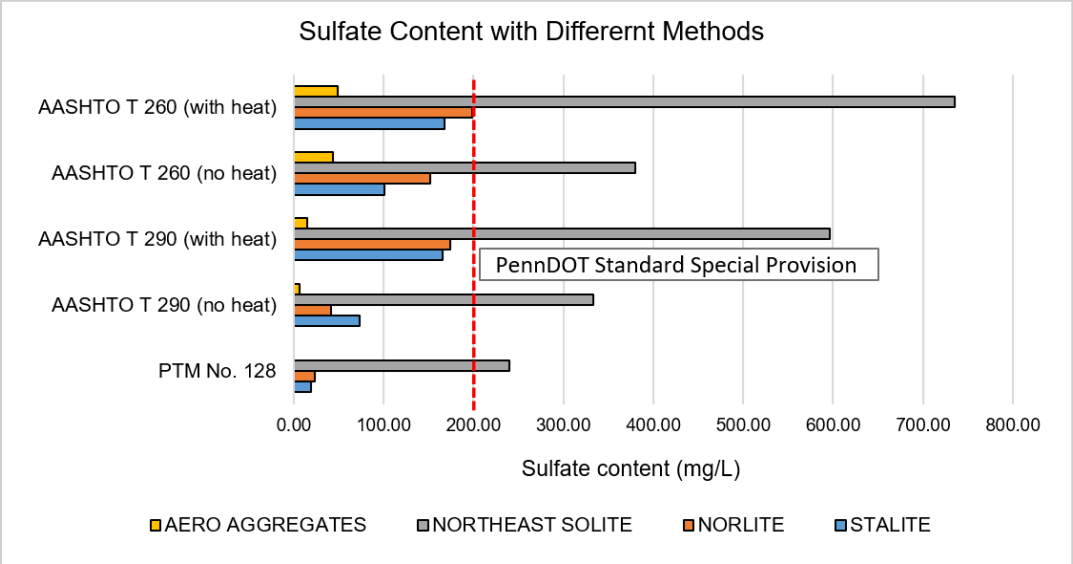
4.1 Data from Chemical Tests

4.1.1 Results of Sulfate and Chloride Content Measurement

The experimental data for sulfate and chloride content measurement are presented in Figures 4-1 and 4-2 for sulfate and Figures 4-3 and 4-4 for chloride. The results are analyzed in two ways: first, by comparing different testing methods for the same material; and second, by comparing different materials under the same testing method. This dual classification approach allows both method-driven variability and intrinsic material differences to be assessed in parallel.

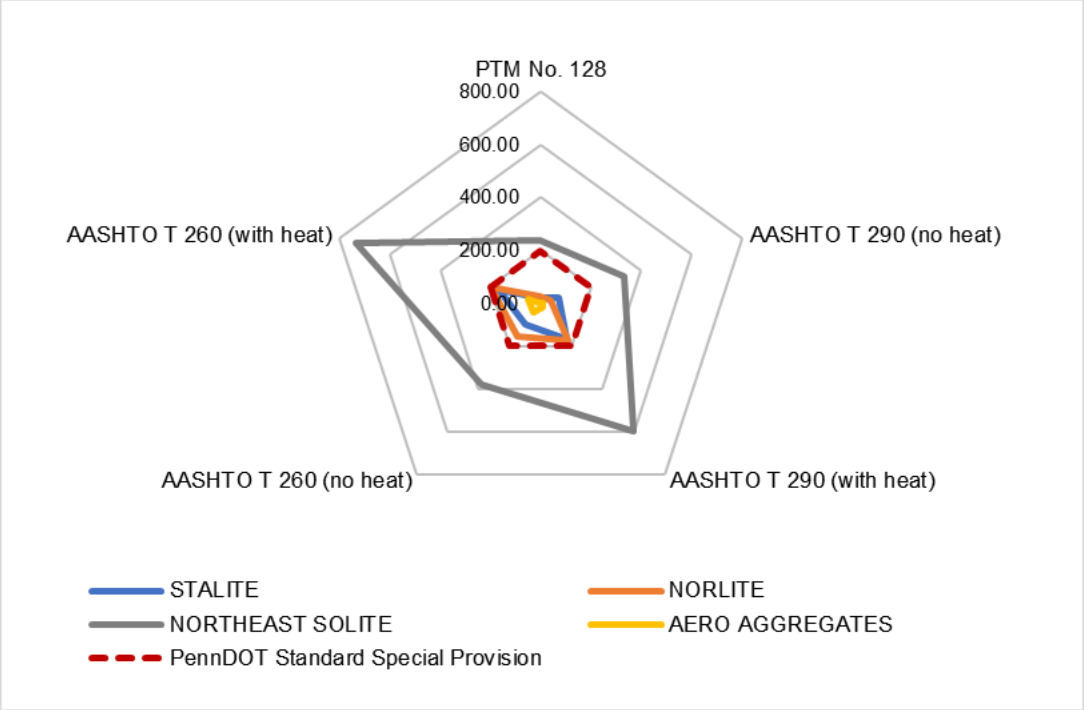
For sulfate content, the method-based comparison reveals that heating generally increases measured concentrations, with the effect being mostly pronounced for AASHTO T 260. Under heated AASHTO T 260, Northeast Solite reaches the highest sulfate level, and measures over 750 mg/L. This level is well in excess of the 200 mg/L control threshold. Heated AASHTO T 290 also produces elevated sulfate content levels for this material. The sulfate content of approximately 600 mg/L for this material is three times higher than the limit. Norlite and Stalite produce mid-range sulfate

concentrations, typically between 150 mg/L and 250 mg/L depending on the applied method. This finding is highly important and emphasizes the need to ensure that the specified threshold values for acceptance and rejection are appropriate for a selected test method. For the preceding case, if the same limit is adopted (i.e., 200 mg/L), then one test will result in rejecting the aggregate while the other delivers it as acceptable. The sulfate content for the Aero Aggregates FGA remains consistently low across all methods, and well below the control threshold. PTM No. 128 yields the lowest sulfate content for all materials, often close to or below 100 mg/L, reflecting its milder extraction procedure. When results are organized by material, the ranking, in terms of the sulfate content, is consistent: NORTHEAST SOLITE $>$ (STALITE $\approx$ NORLITE) $>$ AERO AGGREGATES. The radar plots confirm this stability and illustrate how the severity of the test method amplifies the measured values.



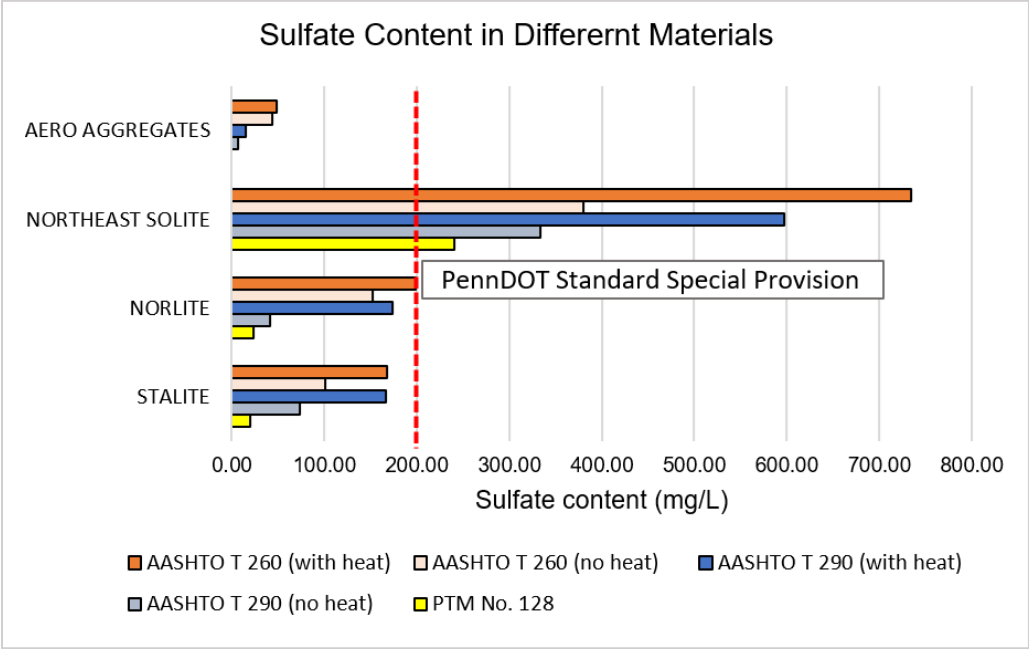
(a) Bar plot of the sulfate content measurement grouped by test method.

Note: PTM test results are not available for the AERO AGGREGATES, as the material could not be prepared to meet the particle size requirements of the PTM method.

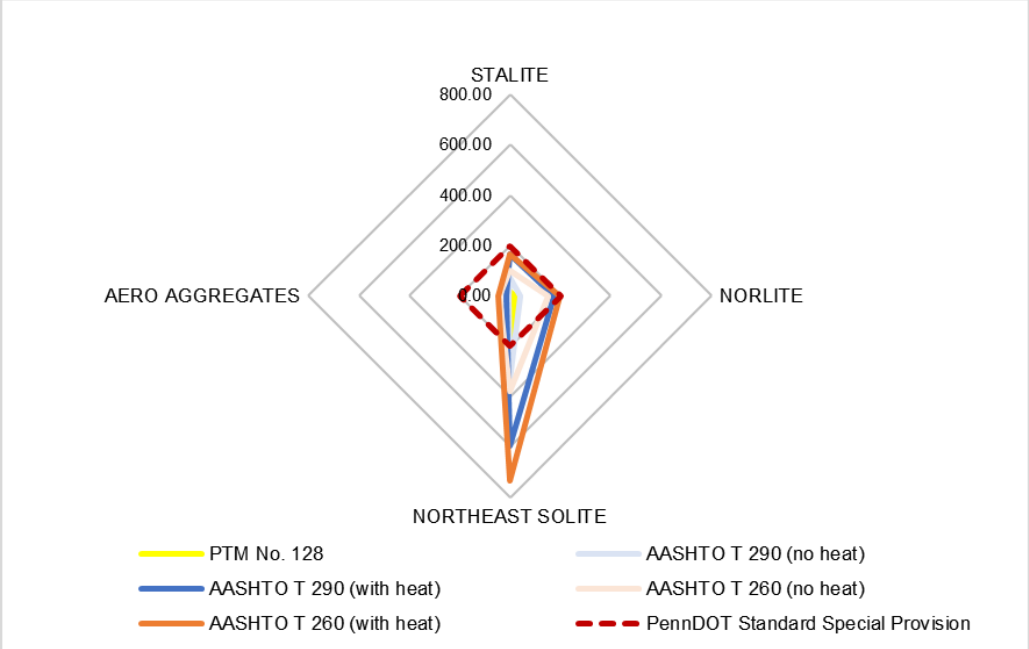


(b) Radar plot of the sulfate content measurement grouped by test method.

Figure 4-38 Testing results of sulfate content measurement (mg/L) grouped by test method.



(a) Bar plot of the sulfate content measurement grouped by aggregate type.



(b) Radar plot of the sulfate content measurement grouped by aggregate type.

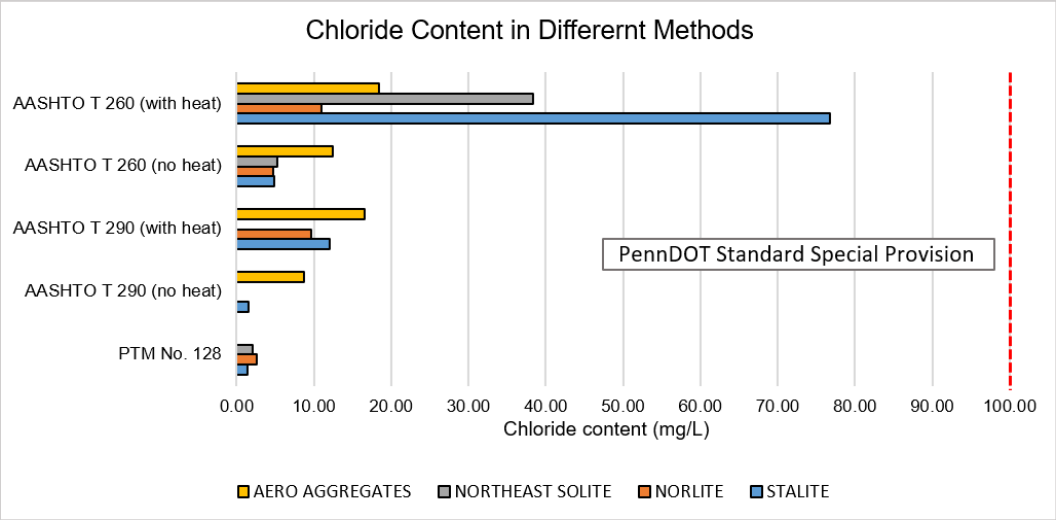
Figure 4-39 Testing results of sulfate content measurement grouped by aggregate type.

For chloride content, the absolute concentrations are much lower, and all results remain below the 100 mg/L control threshold. Nevertheless, method effects are still visible. Heated AASHTO T 260 stands out, with Stalite showing the highest chloride content at approximately 80 mg/L, which is

close to the threshold but still compliant, while Northeast Solite records around 40 mg/L. Norlite and Aero Aggregates consistently remain below 20 mg/L for all methods. The AASHTO T290 method, whether heated or unheated, yields modest chloride concentrations, and PTM No. 128 also produces the lowest values. Viewed by material, the ranking is less distinct than for sulfate, but Stalite's elevated chloride under heated AASHTO T 260 is a clear outlier. It must be noted that in some cases, particularly for the gentler methods and for materials like Aero Aggregates, the measured chloride content was below the measurable limit of 1 mg/L. This indicates presence of extremely low chloride content.

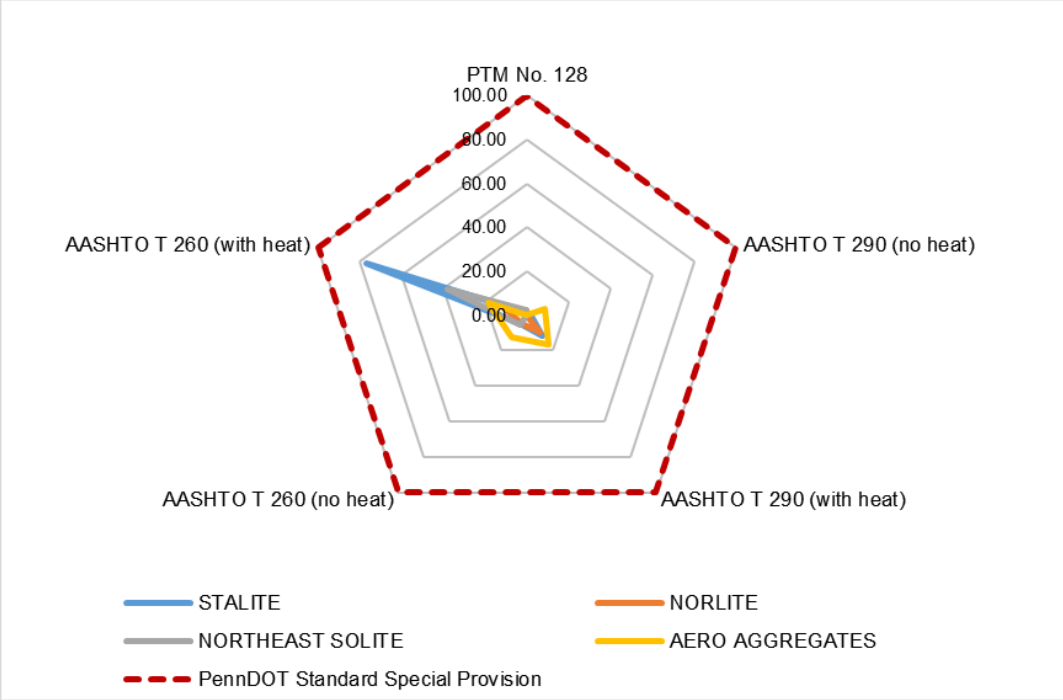
The differences between test methods can be attributed mainly to the intensity of the extraction conditions. Heating accelerates dissolution of soluble ions trapped in pores or bound within hydration products, increasing their mobility into the extraction solution. Finer particle sizes also enhance ion release by increasing the surface area in contact with the solution and improving mass transfer. Conversely, milder methods such as PTM No. 128 may underestimate potential ion content because they extract only the most readily soluble fraction. As a result, more aggressive methods tend to simulate worse-case leaching conditions, while gentler methods reflect more likely field conditions.

Overall, the data indicates that for sulfate, both method choice and material type are critical in relation to the 200 mg/L control limit: aggressive methods, particularly heated AASHTO T 260, can push certain materials well above the allowable threshold, with NORTHEASET SOLITE presenting the most significant concern. For chloride, although all results are below the 100 mg/L limit, heated extraction can still reveal notable differences between materials, especially in identifying those with relatively higher chloride release potential. These findings would suggest that sulfate control is the more pressing durability consideration for MSE wall fill using LWAs, and that method severity must be carefully matched to the intended application either for routine compliance screening or for worst-case condition assessment.



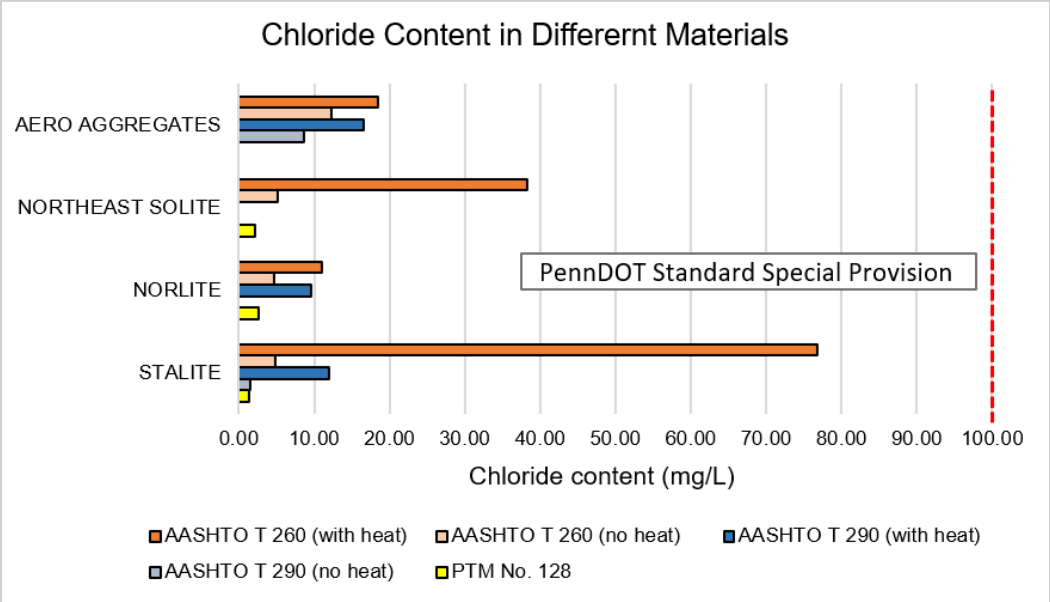
Note: In some cases, no bar appears for chloride measurements because the test results were below the measurable range of the TNT879 method (detection limit = 1 mg/L). These under-range results were confirmed by three repeat tests, all of which indicated concentrations below the detection threshold.

(a) Bar plot of the chloride content measurement grouped by test method.

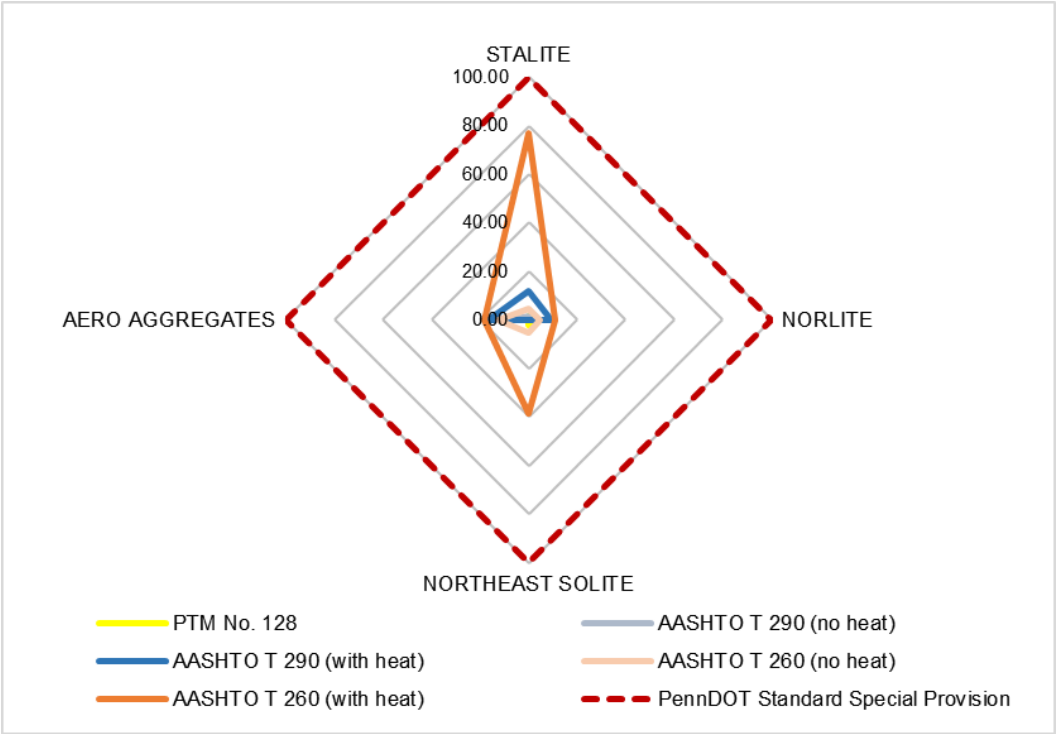


(b) Radar plot of the chloride content measurement grouped by test method.

Figure 4-40 Testing results of chloride content measurement grouped by test method.



(a) Bar plot of the chloride content measurement grouped by aggregate type.



(b) Radar plot of the chloride content measurement grouped by aggregate type.

Figure 4-41 Testing results of chloride content measurement grouped by aggregate type.

In summary, sulfate and chloride testing showed that both extraction method and particle size can noticeably influence measured concentrations, with finer fractions and heated procedures

generally yielding higher values. While sulfate content occasionally approached specification thresholds, especially for Northeast Solite aggregates, chloride concentrations were consistently low and often below detection limits, suggesting limited risk from chlorides in different conditions.

4.1.2 Results of pH Determination

The experimental data for pH determination are presented in Table 4-1, which reports results for four LWA materials across three particle size conditions: as-received gradation, particles passing the No. 10 sieve, and particles passing the No. 50 sieve. This design allows the influence of particle size reduction on measured pH to be assessed, reflecting potential differences in surface area exposure and dissolution behavior. For Aero Aggregates, only a single data point is reported for the passing No. 10 and passing No. 50 sieves. During sample preparation, pulverization of the Aero Aggregates material resulted in rapid fragmentation into very fine particles, making it impractical to reliably produce and isolate discrete particle size fractions corresponding to the specified sieve sizes.

Table 4-25 Testing Results for pH.

Extraction method / Materials	As-received gradation	Passing No. 10 sieve	Passing No. 50 sieve	Max % pH Increase Relative to As-received Particle Size
STALITE	9.04	9.64	10.12	12%
NORLITE	7.35	8.51	9.24	26%
NORTHEAST SOLITE	7.68	8.45	8.99	17%
AERO AGGREGATES	9.35	10.89		16%

Across all materials, the measured pH values fall in a relatively narrow range, between approximately 7.3 and 10.9. Aero Aggregates exhibits the highest pH among all materials, with values of 9.35 for the as-received gradation and 10.89 for the finest fraction (passing No. 50 sieve). The marked increase in pH with decreasing particle size for this material suggests that finer grinding enhances the release of alkaline species from the aggregate surface or internal pores. Stalite also shows an upward trend with smaller particle sizes, from 9.04 (as-received) to 10.12 (No. 50 sieve), indicating a similar surface reactivity effect. Norlite and Northeast Solite display lower absolute pH values, with more modest increases across particle size fractions.

When comparing materials at the same particle size, Aero Aggregates and Stalite tend to get higher pH value, while Norlite and Northeast Solite are consistently lower. This suggests intrinsic

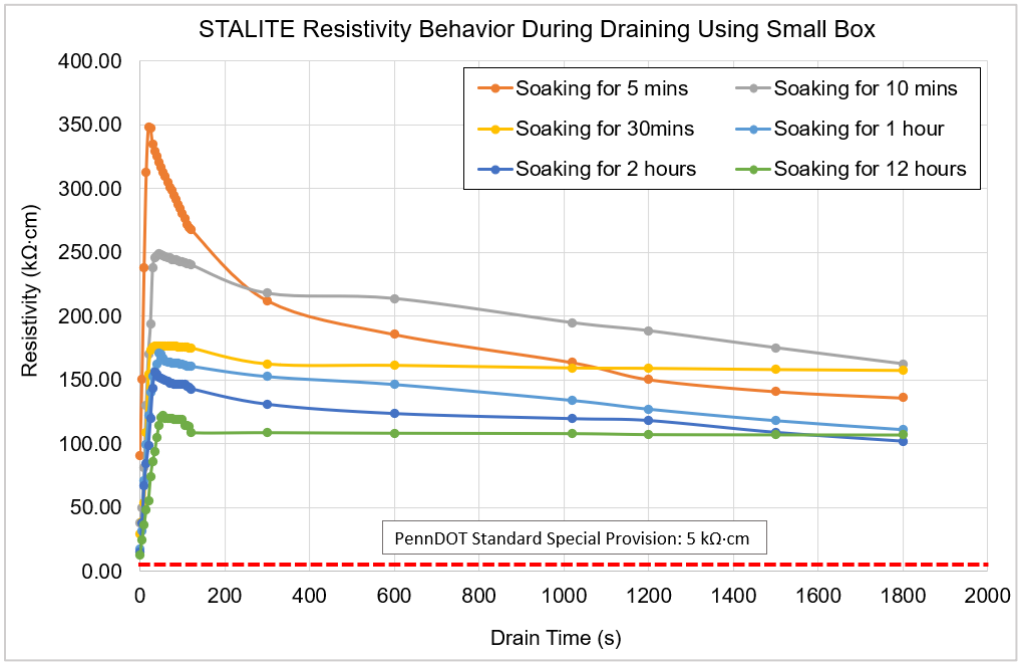
compositional differences, which are likely related to raw material chemistry or production processes, which influence the alkalinity of pore solutions. Additionally, the data indicates that particle size reduction generally produces a measurable increase in pH for all materials, although the magnitude of this effect varies. This is consistent with the increased surface area and shortened diffusion paths in finer particles, which accelerate dissolution of alkaline constituents during the extraction procedure.

These results imply that pH levels in LWAs can vary both by material type and particle size, with potential implications for long-term durability in field applications. Materials such as Aero Aggregates, which show high pH in fine fractions, may provide a more alkaline environment, potentially influencing corrosion processes or chemical stability in contact with other construction materials.

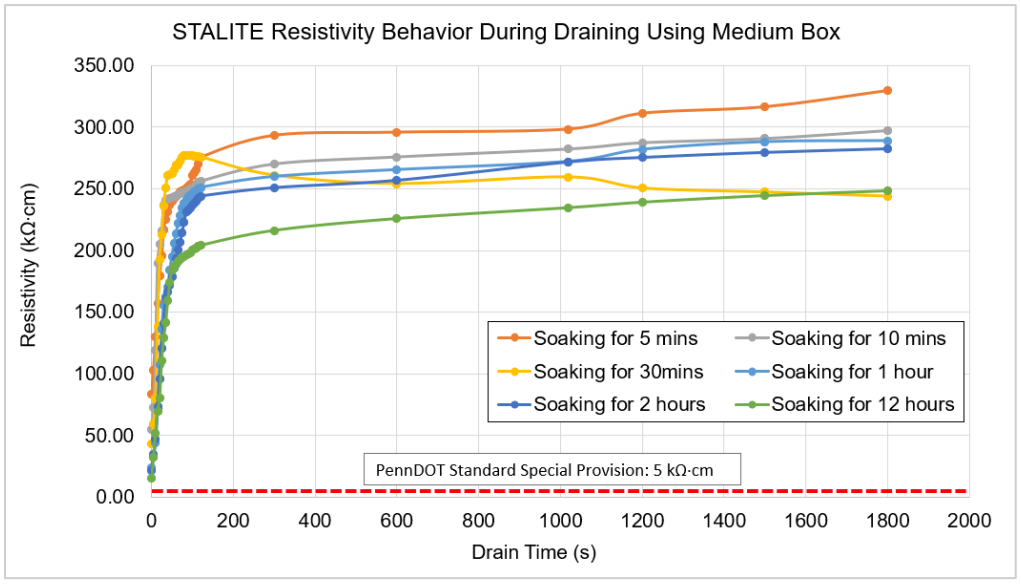
Overall, the pH testing demonstrated that reducing particle size tends to increase the measured alkalinity, although the changes were moderate in scale. Measured pH values generally fell within ranges typical for aggregate materials; however, some lightweight aggregate samples exhibited pH values outside the PennDOT MSE backfill specification range of 6.0 to 10.0. In particular, the finer fractions of Stalite (passing the No. 50 sieve) and Aero Aggregates (passing the No. 10 sieve) exceeded the specified pH limits. These results indicate that while particle size influences the reported pH, and many lightweight aggregates provide a relatively benign chemical environment, finer particle fractions may approach or exceed specification limits and therefore should be considered when evaluating corrosion risk for MSE wall applications.

4.2 Data from Electrical Resistivity Tests

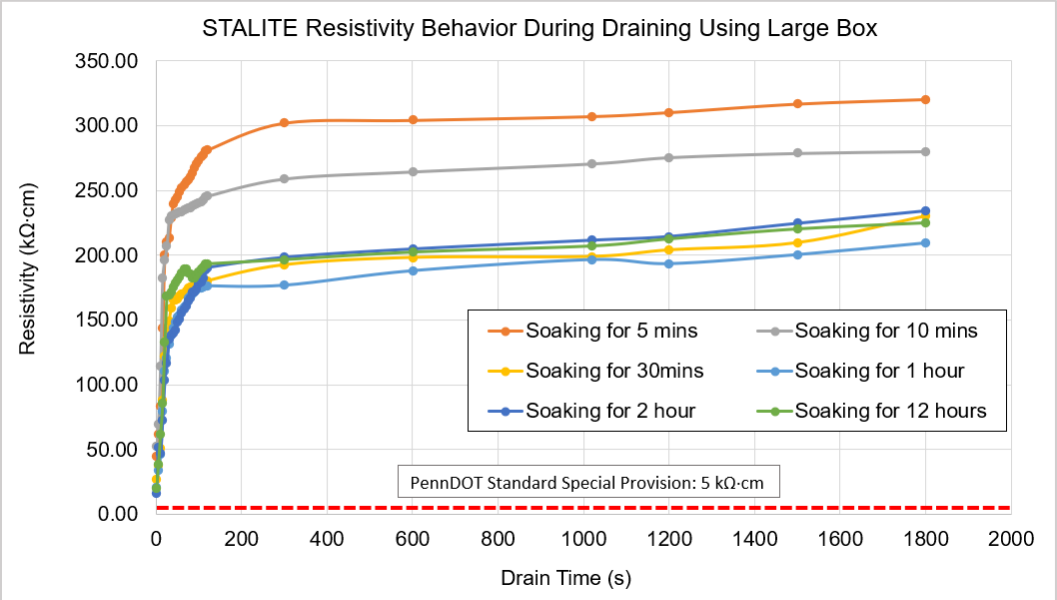
The resistivity testing results for Stalite aggregate are shown in Figures 4-5 and 4-6. The tests were conducted after various pre-soaking times for the samples in three custom boxes, providing insight into the influence of both electrode spacing and soaking duration on resistivity behavior during drainage. For most cases, the trends followed expected theoretical behavior, with resistivity increasing as water drained from the sample due to the reduction in conductive pathways within the aggregate. However, in the small box tests, an anomalous trend was observed where resistivity decreased during drainage. This behavior contradicts theoretical expectations and is most likely attributable to operational issues, such as the box not being perfectly level or uneven drainage patterns that altered electrode contact conditions during the measurement process.



(a) resistivity data during draining using the small box.



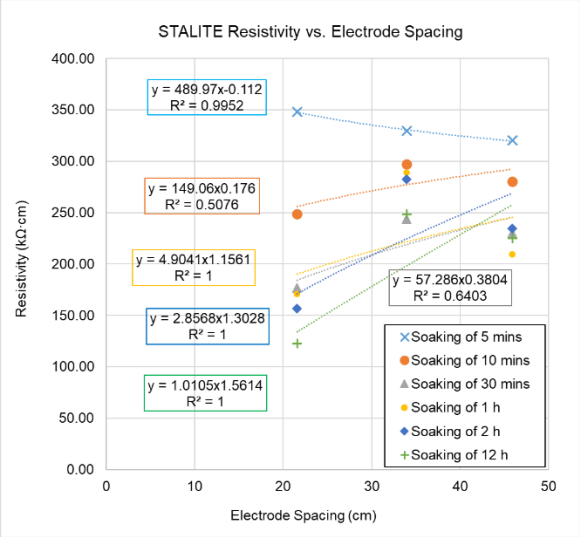
(b) resistivity data during draining using the medium box.



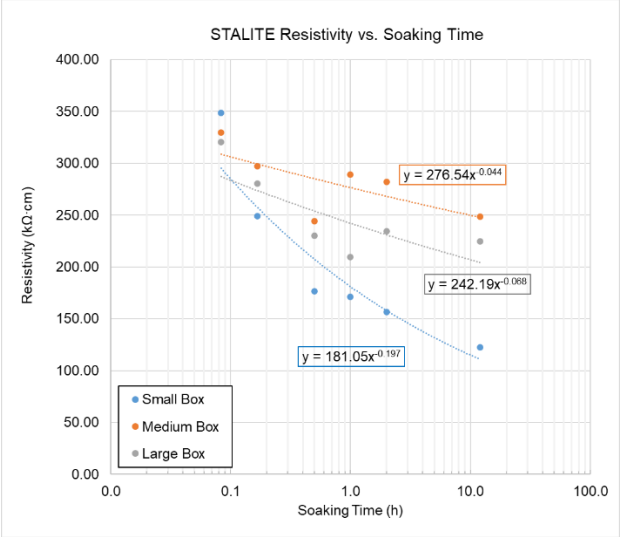
(c) resistivity data during draining using the large box.

Figure 4-42 Resistivity testing results for STALITE aggregate in drainage.

When excluding the small box anomalies, the results demonstrate a consistent relationship between electrode spacing and resistivity. Regression analysis in Figure 4-6(a) confirms the trend that at the same pre-soaking time, larger electrode spacing (as represented by the medium and large boxes) generally corresponded to lower measured resistivity. This is likely because larger boxes allow for a more representative bulk measurement of the aggregate mass, enhancing electrical conduction through the sample. In contrast, when the box is too small, the measurement may be dominated by the influence of a few large particles, which can restrict conductive pathways and artificially increase the resistivity reading. In terms of soaking duration, regression analysis in Figure 4-6(b) shows a clear inverse relationship: shorter pre-soaking times, such as 5 or 10 minutes, resulted in significantly higher initial resistivity values, while longer soaking times, up to 12 hours, led to lower resistivity. This can be attributed to the increased saturation of internal pores with prolonged soaking, which reduces the proportion of air-filled voids and enhances the continuity of conductive pathways, thus lowering resistivity. These results emphasize that both electrode spacing and pre-soaking time are critical parameters in aggregate resistivity testing, and their combined influence should be considered when interpreting field or laboratory measurements.



(a) Resistivity-electrode spacing relationship

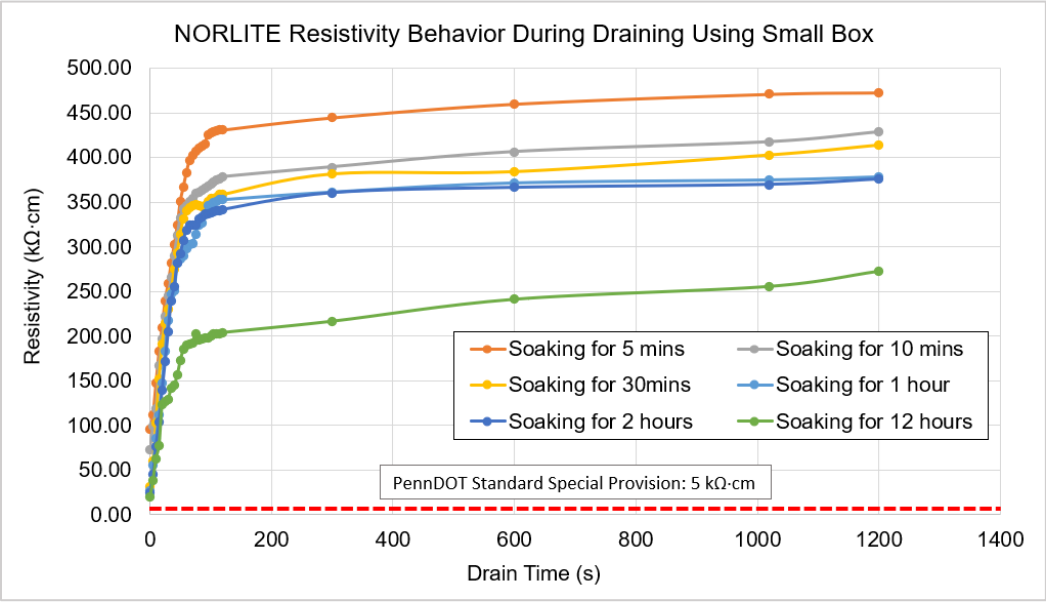


(b) Resistivity-soaking time relationship

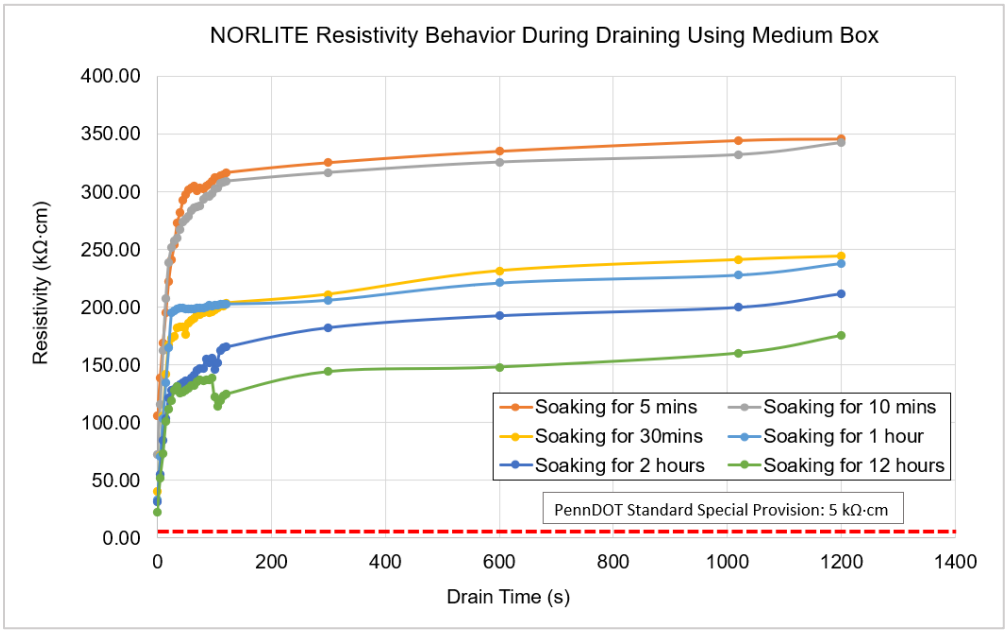
Figure 4-43 Relationships between resistivity and influencing factors of STALITE aggregates.

It is evident that all measured resistivity values in this study were substantially higher than the specification control range of 3-5 kΩ·cm, typically ranging from around 100 kΩ·cm to over 300 kΩ·cm depending on the test configuration. This indicates that the Stalite aggregate tested under these laboratory conditions exhibits extremely low ionic conductivity and high electrical resistivity, far exceeding the minimum durability thresholds defined in the standards.

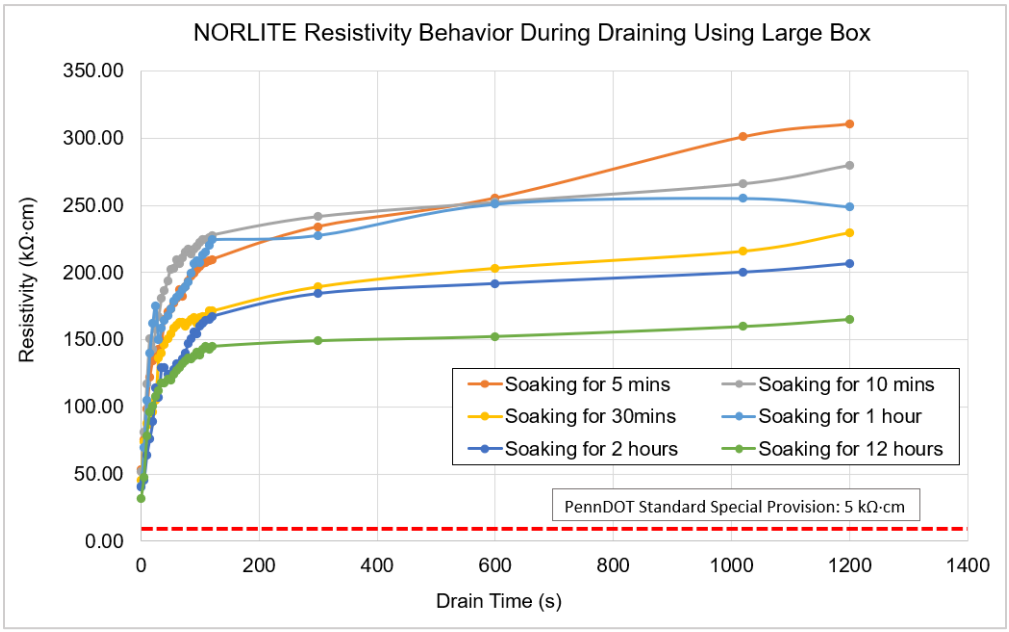
The resistivity testing results for Norlite aggregate are shown in Figures 4-7 and 4-8. The measurements were also carried out after different pre-soaking times using three custom testing boxes of varying sizes, enabling the comparison of resistivity behavior under different electrode spacings. Unlike the case of Stalite, the unexpected phenomenon of resistivity decreasing during water drainage was not observed for Norlite aggregates; instead, all curves followed the pattern that resistivity generally increased as water drained from the samples. This trend reflects the progressive reduction of water films and the corresponding decrease in ionic conduction paths, leading to higher resistivity over time.



(a) NORLITE resistivity data during draining using the small box.



(b) NORLITE resistivity data during draining using the medium box.

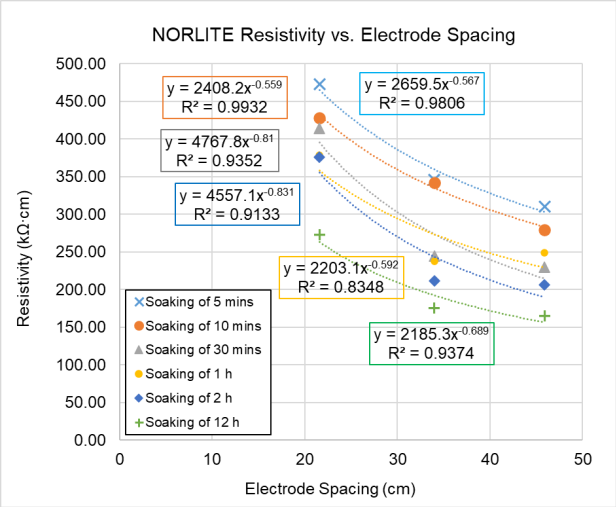


(c) NORLITE resistivity data during draining using the large box.

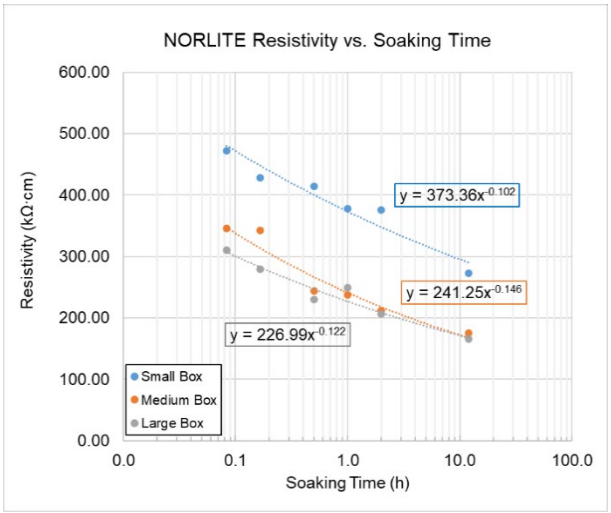
Figure 4-44 Resistivity testing results of NORLITE aggregate in drainage.

When comparing the results across electrode spacings, the collected data again demonstrated that, at the same pre-soaking time, larger electrode spacing tended to yield lower measured resistivity values. The plots of resistivity versus electrode spacing showed consistent decreasing trends for all

soaking durations, with fitted power-law relationships. The influence of soaking time followed the same general pattern: resistivity decreased as soaking time increased. This effect was more pronounced in the smaller box, where the impact of moisture penetration is magnified due to the smaller test volume. The relationships between resistivity and soaking time also followed power-law decay, indicating a diminishing marginal reduction in resistivity with extended soaking.



(a) Resistivity-electrode spacing relationship

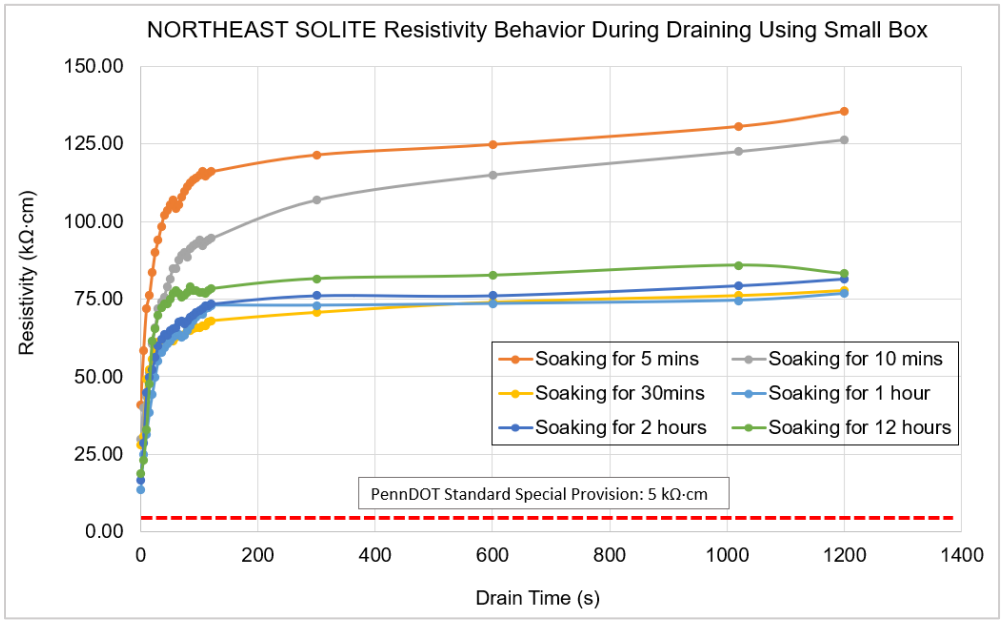


(b) Resistivity-soaking time relationship

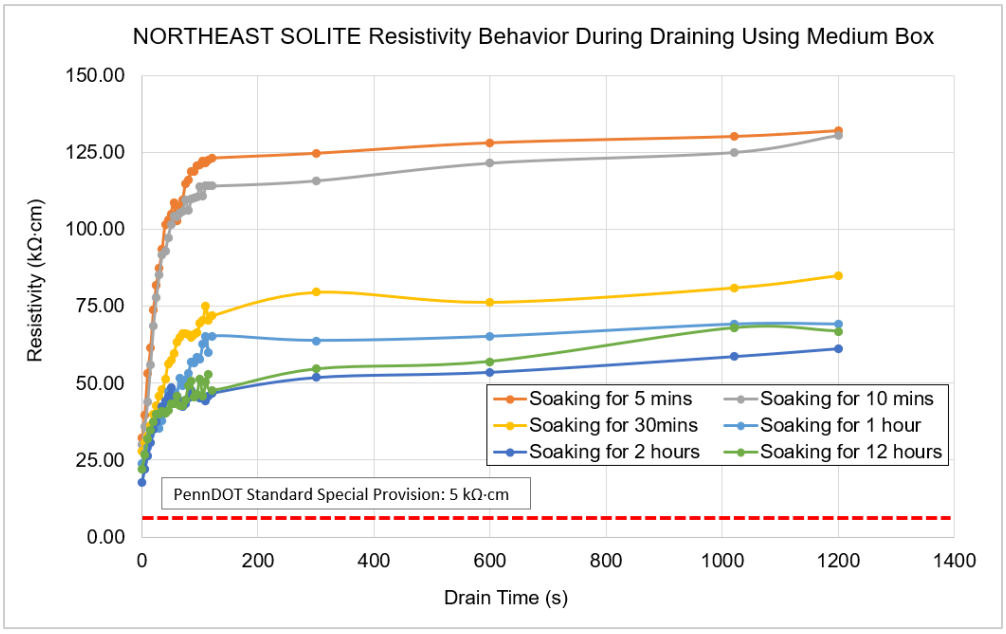
Figure 4-45 Relationships between resistivity and influencing factors of NORLITE aggregates.

The measured resistivity values for Norlite were also significantly higher than the threshold cited in standards, even at the longest soaking durations and largest electrode spacing, which indicates that Norlite aggregate possesses very high electrical resistivity under the tested conditions.

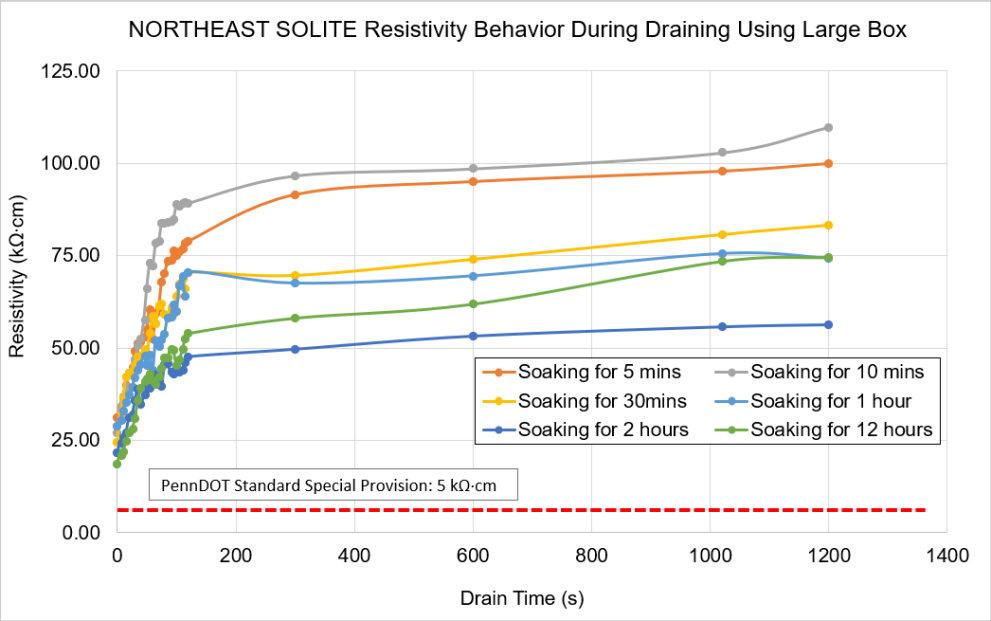
The resistivity testing results for Northeast Solite and Aero Aggregates samples are shown in Figures 4-9, 4-10, and 4-11, 4-12, respectively. Similar to the trends observed for Stalite and Norlite aggregates, resistivity increased rapidly during initial drainage and then stabilized as water drained out. With the same pre-soaking time, larger electrode spacing generally produced lower resistivity due to enhanced conductive pathways. Resistivity consistently decreased with longer soaking times. Across all test conditions, the measured values were far above the specification control range, indicating very high resistivity and confirming the material's suitability from a durability perspective.



(a) resistivity data during draining using the small box.

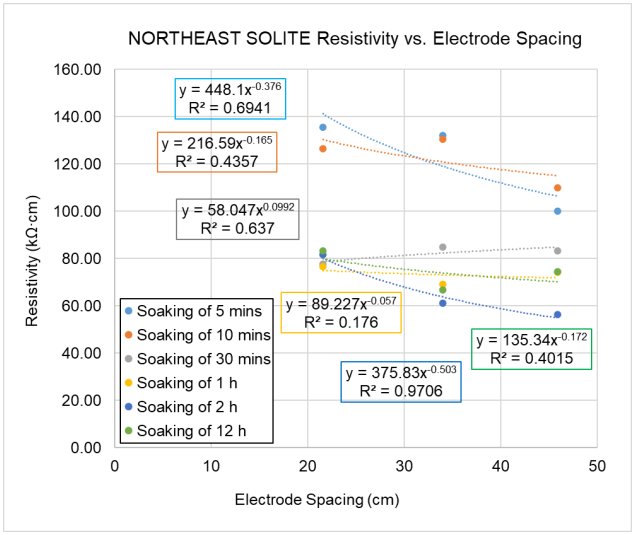


(b) resistivity data during draining using the medium box.

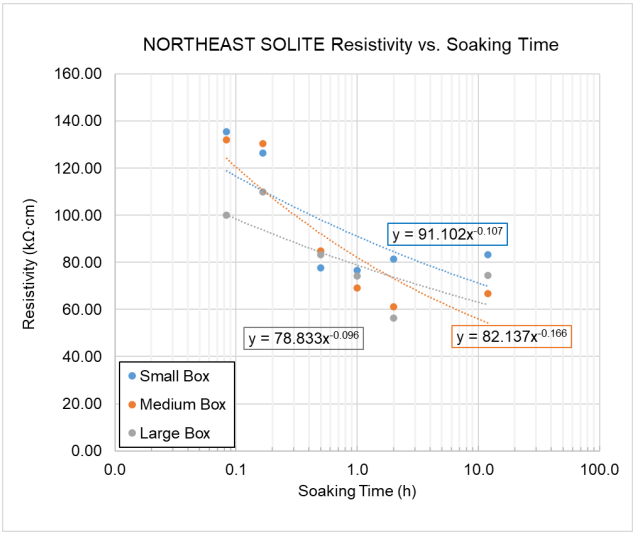


(c) resistivity data during draining using the large box.

Figure 4-46 Resistivity testing results of NORTHEAST SOLITE aggregate in drainage.

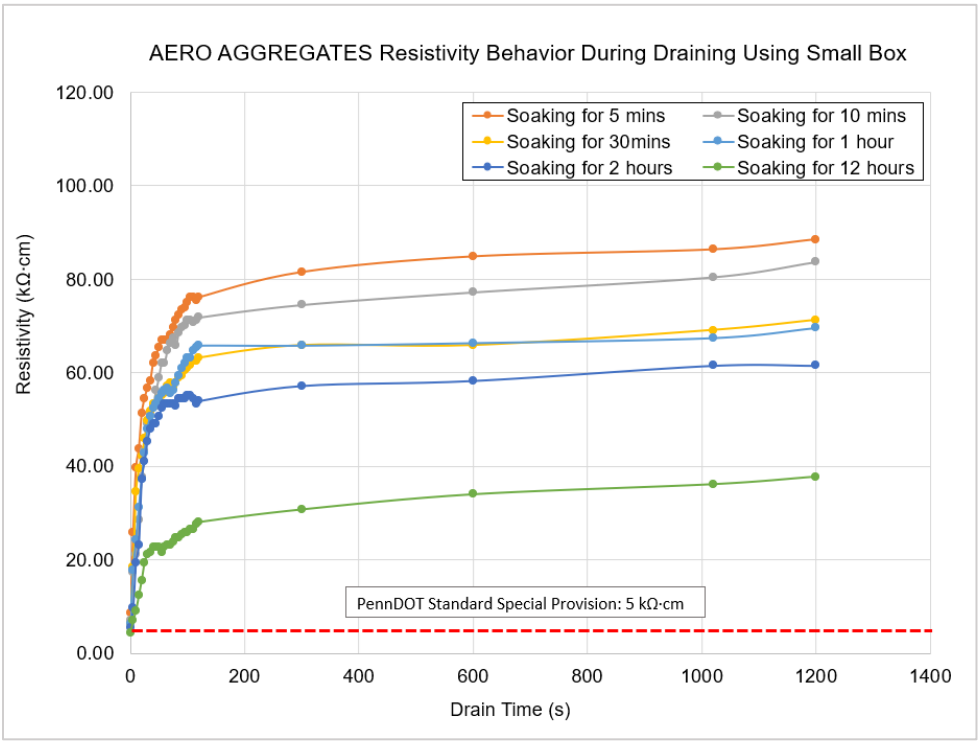


(a) Resistivity-electrode spacing relationship

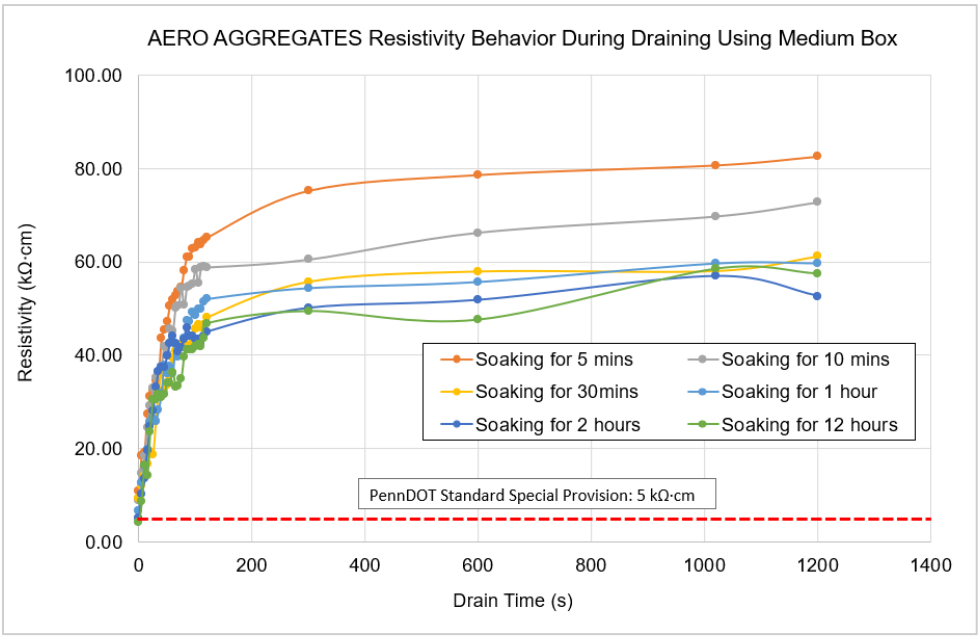


(b) Resistivity-soaking time relationship

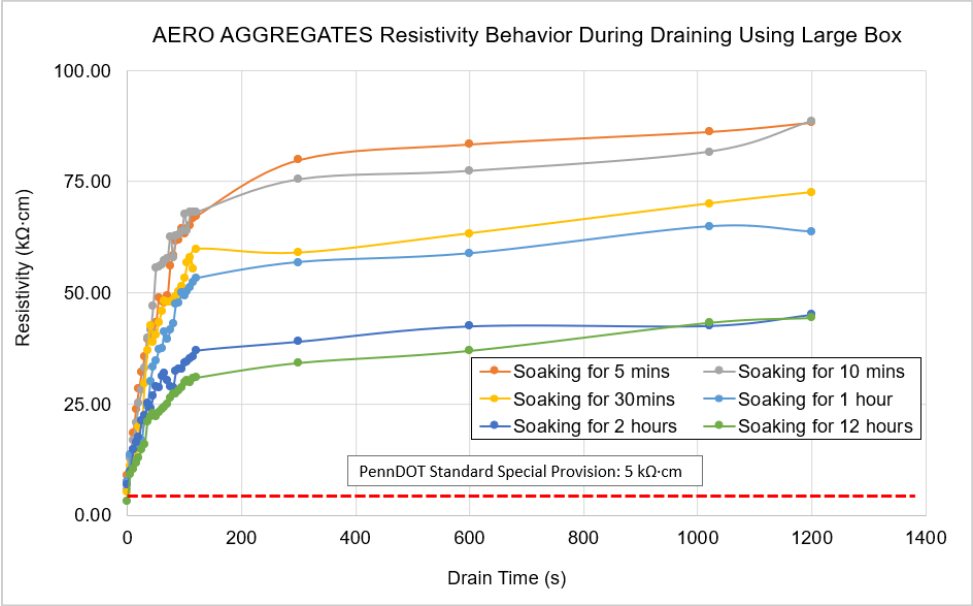
Figure 4-47 Relationships between resistivity and influencing factors for NORTHEAST SOLITE aggregates.



(a) resistivity data during draining using the small box.

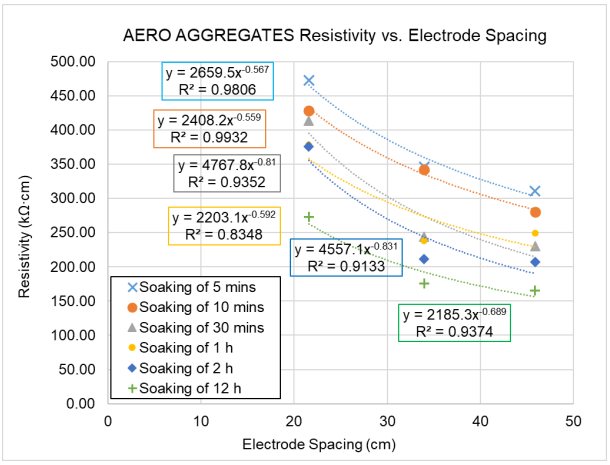


(b) resistivity data during draining using the medium box.

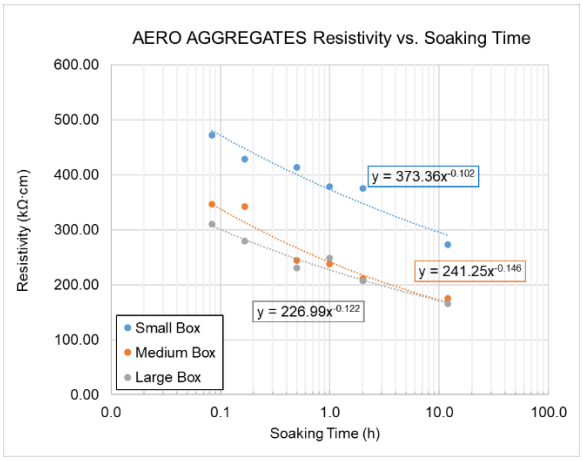


(c) resistivity data during draining using the large box.

Figure 4-48 Resistivity testing results of AERO AGGREGATES in drainage.



(a) Resistivity-electrode spacing relationship



(b) Resistivity-soaking time relationship

Figure 4-49 Relationships between resistivity and influencing factors of AERO AGGREGATES.

Across all tested LWAs, the resistivity measurements exhibited consistent overall patterns despite differences in absolute magnitude. For each material, resistivity rose quickly during the initial stages of water drainage before stabilizing. Larger electrode spacing, as achieved in the medium and large boxes, generally yielded lower resistivity values at the same soaking time due to enhanced conductive pathways and reduced dominance of single large particles. For all aggregates, increasing pre-soaking time led to lower resistivity, reflecting increased moisture and ion mobility within the

pore structure. The absolute resistivity values for all materials, under all tested conditions, remained well above the specification control range, indicating exceptionally high electrical resistivity.

Overall, the resistivity testing confirmed that both electrode spacing and pre-soaking time exert strong effects on the measured values. Larger electrode spacing consistently produced lower resistivity readings, while longer soaking times led to reductions due to greater pore saturation. Despite variations among materials, all results were well above the specification threshold, indicating that the LWAs tested exhibit very high resistivity and are unlikely to contribute to reinforcement corrosion under field conditions.

4.3 Data from Additional Electrical Resistivity Tests

4.3.1 Results of Long-term Effect of Moisture Change

The long-term resistivity monitoring results for Stalite and AERO AGGREGATE samples are presented in Figures 4-13 and 4-14. Each figure includes both the resistivity (solid lines, left axis) and corresponding water content (dashed lines, right axis) measured over a 48-hour drainage period. Two pre-soaking conditions (5 minutes and 12 hours) were also considered for each material to evaluate how the initial degree of saturation affects subsequent moisture loss and resistivity evolution.

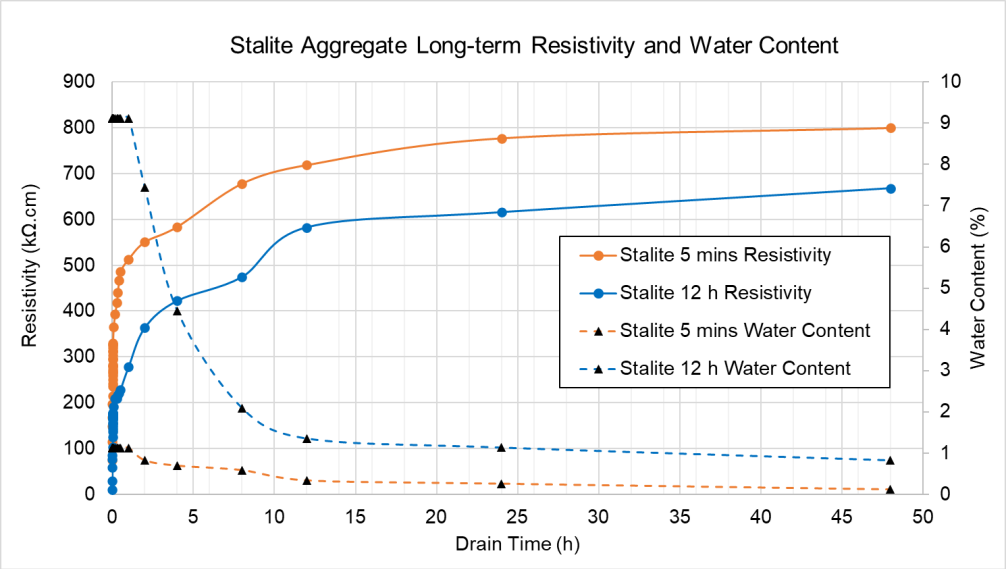


Figure 4-50 Long-term resistivity monitoring results for STALITE samples.

It can be found in Figure 4-13, for both soaking durations, resistivity increased steadily with drainage time, while water content decreased continuously, reflecting a typical drying and

desaturation process. Moisture content measurements discussed here were obtained from a separate companion sample prepared under identical conditions and monitored concurrently with the box used for resistivity measurements. The 5-minute soaking Stalite sample showed an initially higher resistivity that rose sharply to around 550-600 kΩ·cm within the first two hours. After about 12 hours, resistivity approached 750-800 kΩ·cm and eventually stabilized by the end of the 48-hour period. The corresponding water content decreased rapidly from about 1 % to below 0.1 %. The 12-hour soaking sample, starting at a much lower resistivity due to higher initial moisture, also exhibited a pronounced increase during the first several hours, reaching about 400-450 kΩ·cm by 4 hours, and gradually leveling off near 660-670 kΩ·cm after 48 hours. The water content decreased from approximately 9 % to below 1 % over the same period. The resistivity response of the samples as moisture changed shows three distinct phases: (i) a rapid rise during free drainage, (ii) a slower transition as capillary water is depleted, and (iii) a gradual plateau as only adsorbed water remains.

These results highlight the coupling of moisture and resistivity inherent in porous expanded shale. The open pore structure of Stalite promotes slow moisture release and delayed stabilization, producing the long tailing behavior observed beyond 24 hours. Short-soaked samples reach higher resistivity values more quickly because their initial moisture is limited to surface films and near-surface pores, allowing faster transition to a non-conductive state.

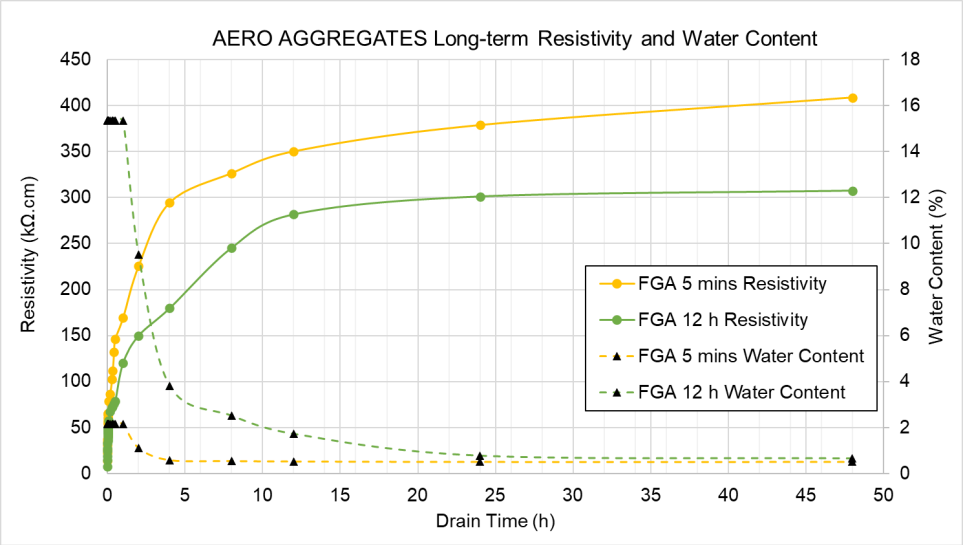


Figure 4-51 Long-term resistivity monitoring results for AERO AGGREGATES samples.

FGA showed a similar overall trend but at lower absolute resistivity levels and with faster stabilization. For the 5-minute soaking condition, resistivity increased from about 100 kΩ·cm to

nearly 350 kΩ·cm within 12 hours, after which the curve reached a stable plateau. The corresponding moisture content dropped sharply from about 1 % to below 0.1 % within 4-6 hours. For the 12-hour soaked sample, initial resistivity was lower due to high saturation, rising gradually to about 300 kΩ·cm after 48 hours, as moisture content fell to about 0.2 %.

FGA exhibits a shorter transition period and a smaller difference between short and long soaking conditions. This indicates that FGA's bulk conductivity is mainly controlled by surface conduction rather than pore-water connectivity.

Overall, the coupling between moisture and resistivity confirms that for future field or design evaluations, adopting resistivity values measured after 48 hours of drainage is recommended, as they represent the long-term steady state of the material.

4.3.2 Results of Compaction Effect

Figure 4-15 presents the resistivity response of Stalite aggregates under three compaction conditions tested in the medium box. The compaction levels are loose, medium, and dense. The results show that at any given drain time, resistivity decreases monotonically with increasing compaction. The loose sample yields the highest value of resistivity, the medium specimen is intermediate, and the dense specimen is lowest. Mechanistically, these trends are consistent with conduction in a three-phase granular aggregate where the pore water provides the dominant ionic pathway. Loosely packed materials typically retain larger air voids and discontinuous water films, leading to higher resistivity, whereas densely compacted materials are expected to exhibit more conductive behavior due to improved particle contact and continuous moisture pathways.

For each compaction state, the void ratio e was computed from the known box volume V_{box}, the measured specimen mass M, and the specific gravity of solids G_s (water density $\rho_w \approx 1{,}000$ kg/m^3): $V_{solid} = M/(\rho_w G_s)$, $V_{void} = V_{box} - V_{solid}$, $e = V_{void}/V_{solid}$. When plotted against time, resistivity systematically decreases with decreasing e (loose $e = 1.70$ > medium $e = 1.20$ > dense $e = 0.92$) under the same moisture and geometry, indicating that denser packing improves water-phase connectivity and thus lowers bulk resistivity.

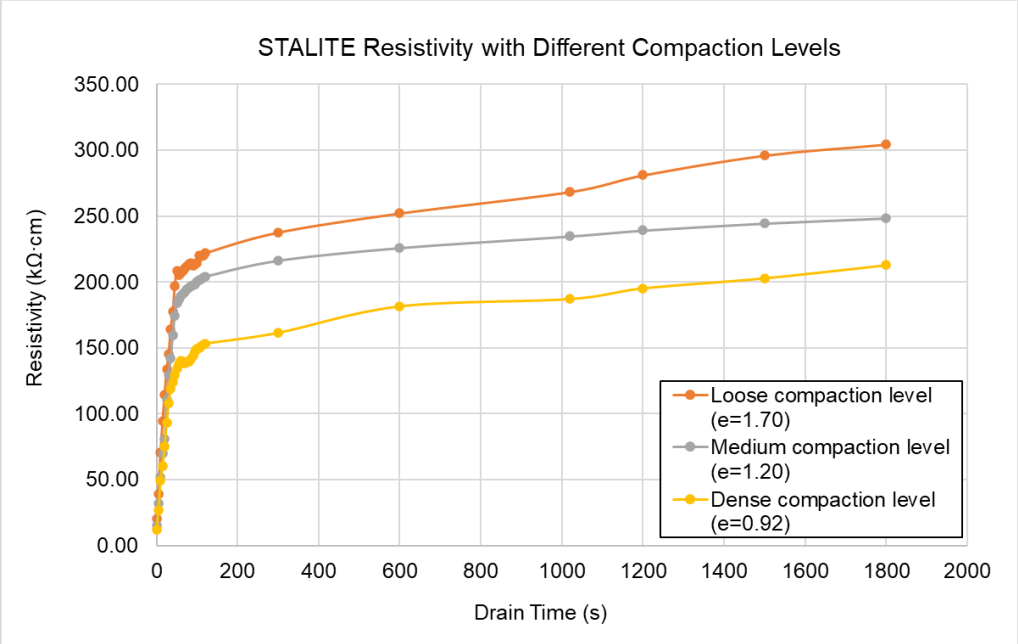


Figure 4-52 Effect of compaction level on resistivity results for STALITE samples.

The influence of compaction level on the resistivity of Aero Aggregate is shown in Figure 4-16. Similar to Stalite, all three placement conditions exhibit an initial rapid increase in resistivity during the first minute of drainage, followed by a more gradual rise. As drainage progresses, the loose specimen consistently produces the highest resistivity, the dense specimen the lowest, and the medium case lies in between. These trends indicate that looser placement leaves larger interparticle voids and more air gaps, interrupting water bridges, so that bulk resistivity is high. With increasing compaction, particles rearrange into a denser packing with smaller voids and more continuous water films, improving connection between the electrodes and lowering the apparent resistivity.

When compared with the results, Aero Aggregate exhibits the same qualitative dependence on compaction level, but the relative effect of compaction is stronger for Aero Aggregate. The loose condition is roughly a factor of two higher than the dense condition, compared with a ~30% difference for Stalite. This suggests that resistivity is more strongly controlled by macro packing and interparticle contacts for Aero Aggregate. It is also noted that the resistivity difference between the dense and medium compaction levels for Aero Aggregate is relatively small. This behavior can be attributed to the large particle size of the foam glass aggregates. Because of its low particle density and irregular, angular geometry, Aero Aggregate particles tend to form a framework that resists rearrangement under moderate compaction. In practice, the transition from loose to medium compaction results in only a minor reduction in void ratio (from e = 0.52 to e = 0.47). Consequently, the electrical pathways

governed by interstitial water films remain similar, producing comparable resistivity values for both conditions.

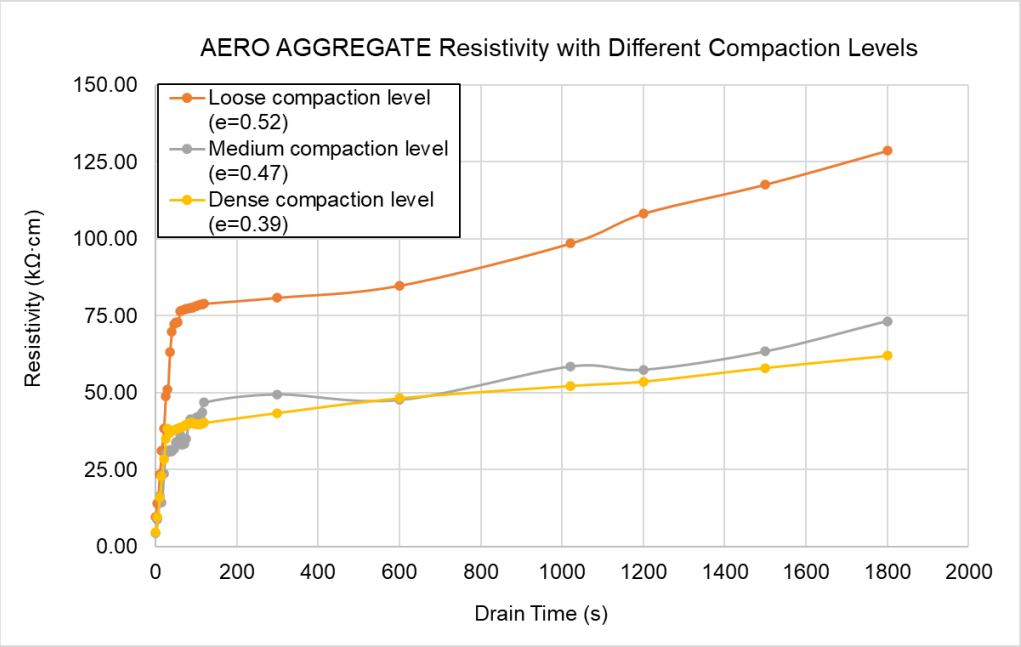


Figure 4-53 Effect of compaction level on resistivity results for AERO AGGREGATE samples.

4.3.3 Results of Gradation Effect

Figure 4-17 presents the resistivity response of Stalite aggregate under three gradation conditions: the as-received (medium) gradation, the finer gradation composed only of particles passing the 1/4-in. sieve, and the coarser gradation composed only of particles larger than 1/4 in. All tests were conducted in the medium box after 12 hours of soaking and under the same medium compaction procedure. A consistent ordering is observed that the coarse gradation yields the highest resistivity, the medium gradation is intermediate, and the fine gradation exhibits the lowest resistivity.

These results reflect the influence of particle size distribution on pore structure and moisture connectivity. Removing material finer than 1/4 in. produces an open, skeletal packing of large particles, and water is more easily drained from such a framework and water films are more readily broken, so that the ionic conduction network is fragmented and bulk resistivity is increased. In contrast, the finer gradation forms a much denser packing with more particle contacts. At the same initial saturation and compaction, this finer structure maintains more continuous water films and shorter conductive paths, which lowers the measured resistivity and slows its rate of increase with time.

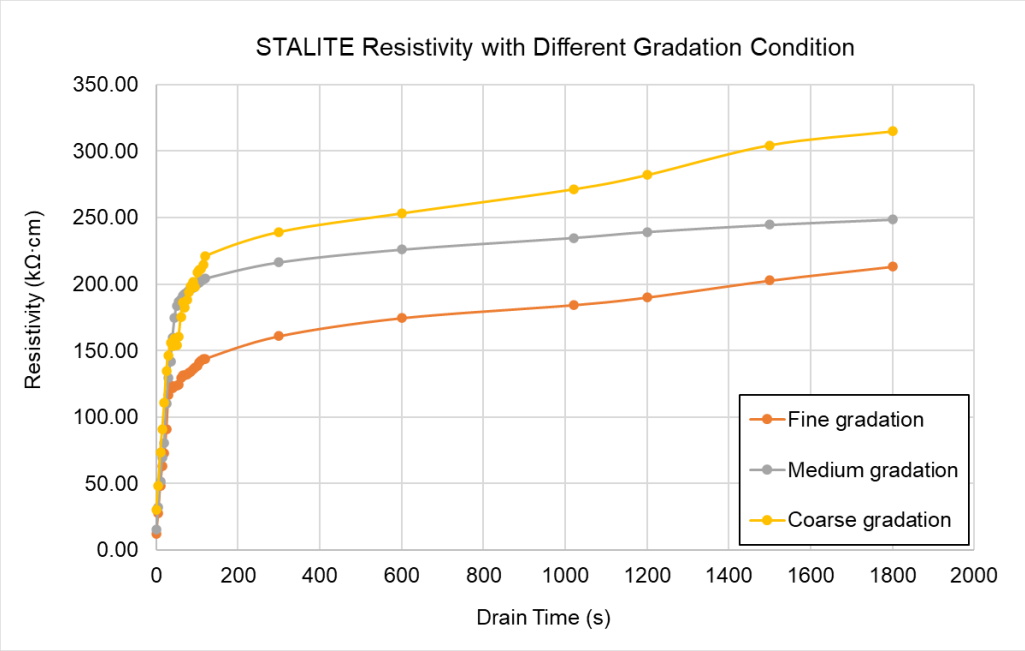


Figure 4-54 Effect of gradation conditions on resistivity results for STALITE samples.

Figure 4-18 shows results for Aero Aggregate tested under the same three gradation conditions, defined with a split at the 1 1/2-in. sieve. The fine gradation consistently produces the lowest resistivity, and the coarse gradation the highest, with the as-received gradation in between. It is also observed that the medium gradation curve for Aero aggregate lies slightly above the coarse curve at early times and then is overtaken as drainage proceeds. This minor crossing likely reflects subtle differences in initial packing and local water redistribution for these very large particles rather than a fundamental inversion of the gradation effect.

It is also observed that the resistivity values for the medium and coarse gradations of Aero Aggregate are relatively close throughout the entire testing period. This behavior contrasts with the results for the Stalite aggregate and can be explained by the dominant effect of particle size and geometry in the foam glass material. The AERO AGGREGATE particles are extremely large and limit rearrangement even when the gradation is modified. Because of this, removing the finer portion of the sample does not significantly alter the overall packing structure or the number of interparticle contacts compared with the as-received condition. In both cases, the structure is essentially governed by large particles that dominate the current pathways.

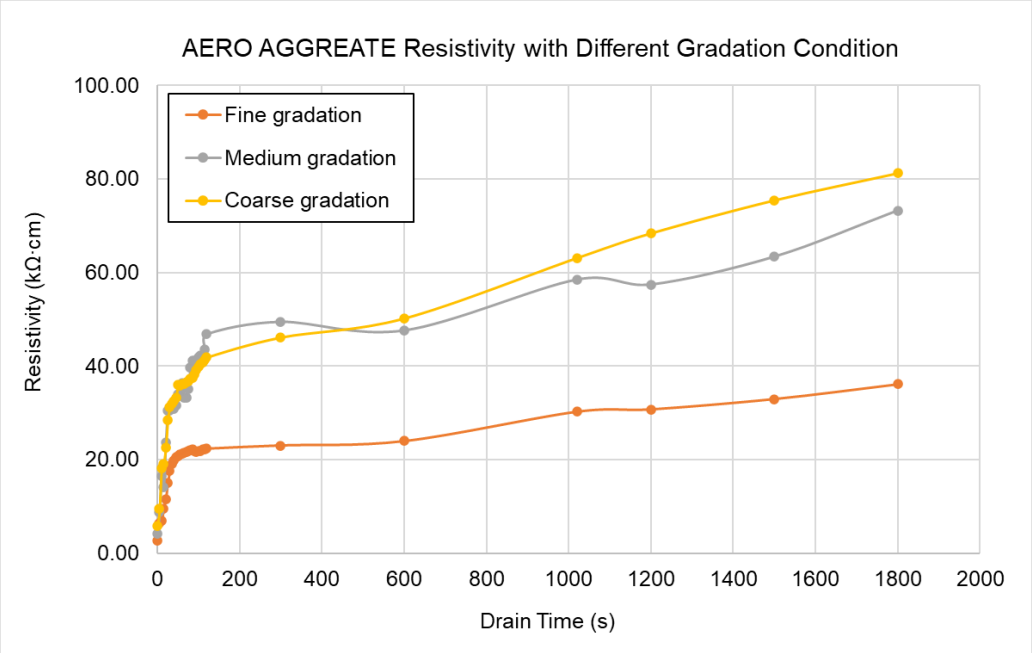


Figure 4-55 Effect of gradation conditions on resistivity results for AERO AGGREGATE samples.

4.4 Summary of the Testing Data

To provide a consolidated view of the experimental data, the results from the three major testing programs (sulfate and chloride content measurement, pH determination, and electrical resistivity testing) are compiled in tabular form in this section. The testing results of pH determination have been referenced in Table 4-1 and are referenced here for completeness alongside the summarized data for the other testing programs.

Table 4-26 Testing data from sulfate content measurement.

Extraction method / Materials	PTM No. 128	AASHTO T290/291 (× heating)	AASHTO T290/291 (√ heating)	AASHTO T260 (×heating)	AASHTO T260 (√ heating)
STALITE	19.70	73.00	166.10	101.00	167.40
NORLITE	23.80	41.60	173.90	152.00	198.20
NORTHEAST SOLITE	240.00	333.00	596.70	380.00	735.00
AERO AGGREGATES	-	6.20	15.40	43.90	48.80

Table 4-27 Testing data from chloride content measurement.

Materials \ Extraction method	PTM No. 128	AASHTO T290/291 (× heating)	AASHTO T290/291 (√ heating)	AASHTO T260 (×heating)	AASHTO T260 (√ heating)
STALITE	1.36	1.56	12.00	4.80	76.80
NORLITE	2.56	-	9.60	4.70	11.00
NORTHEAST SOLITE	2.13	-	-	5.23	38.30
AERO AGGREGATES	-	8.70	16.60	12.37	18.40

Table 4-28 Testing results for pH.

Materials \ Extraction method	Original size	Passing No. 10 sieve	Passing No. 50 sieve
STALITE	9.04	9.64	10.12
NORLITE	7.35	8.51	9.24
NORTHEAST SOLITE	7.68	8.45	8.99
AERO AGGREGATES	9.35	10.89	

Table 4-29 Resistivity testing results for STALITE aggregate.

Box	Electrode spacing (cm)	Pre-soaking time					
		5 min	10 min	30 min	1 h	2 h	12 h
Small box	21.59	348.30	248.94	176.58	171.02	156.38	122.42
Medium box	33.97	329.55	297.16	244.04	288.83	282.29	248.46
Large box	45.88	320.44	280.26	230.13	209.35	234.37	224.93

Table 4-30 Resistivity testing results for NORLITE aggregate.

Box	Electrode spacing (cm)	Pre-soaking time					
		5 min	10 min	30 min	1 h	2 h	12 h
Small box	21.59	472.60	428.40	413.95	378.25	375.70	272.85
Medium box	33.97	346.14	342.47	244.24	238.09	211.73	175.50
Large box	45.88	310.58	279.84	230.02	249.10	206.70	165.36

Table 4-31 Resistivity testing results for NORTHEAST SOLITE aggregate.

Box	Electrode spacing (cm)	Pre-soaking time					
		5 min	10 min	30 min	1 h	2 h	12 h
Small box	21.59	135.54	126.36	77.76	76.68	81.54	83.16
Medium box	33.97	131.94	130.56	84.98	69.12	61.20	66.81
Large box	45.88	99.99	109.82	83.27	74.32	56.30	74.58

Table 4-32 Resistivity testing results for AERO AGGREGATES aggregate.

Box	Electrode spacing (cm)	Pre-soaking time					
		5 min	10 min	30 min	1 h	2 h	12 h
Small box	21.59	88.56	83.70	71.28	69.66	61.56	37.80
Medium box	33.97	82.64	72.76	61.18	59.77	52.70	57.46
Large box	45.88	88.33	88.62	72.67	63.72	45.11	44.37

4.5 Summary Findings

Based on the experimental program and data evaluation conducted in this study, the following key findings and implications are identified with respect to PennDOT specifications, standards, and current practice related to MSE wall backfill materials:

a. Lightweight aggregates currently listed under PennDOT Bulletin 15 and Bulletin 14, including expanded shale and foamed glass aggregates evaluated in this study, generally satisfied applicable electrochemical specification requirements, and are considered suitable for use as MSE wall backfill materials from an electrochemical standpoint.

b. The MSE Wall special provision test methods for sulfates, chlorides, and Ph measurement were found to be applicable and representative for evaluating lightweight aggregates used as MSE wall backfill, provided that appropriate sample preparation procedures are followed.

c. Across the lightweight aggregates evaluated, an overall trend was observed in terms of exceedance of electrochemical specification limits. In general, the likelihood of approaching specification thresholds followed the order: sulfates > pH > chlorides > resistivity. This indicates that sulfate content represents the most critical electrochemical parameter for lightweight aggregates, whereas resistivity is less likely to control acceptance for MSE wall backfill applications.

d. Proper sample preparation in accordance with AASHTO test methods for sulfate, chloride, and pH testing is essential to ensure meaningful results. Testing materials in their as-received or as-manufactured gradation does not adequately reflect the soluble ion content of lightweight aggregates. Extraction procedures are required to promote the release of water-soluble ions from surface residues, pore water, and salts retained within internal voids of the aggregate particles. Although these preparation methods do not replicate the as-installed condition of MSE wall backfill, they provide a standardized and conservative basis for evaluating the electrochemical characteristics of finer particle fractions and for promoting mass transfer toward equilibrium conditions necessary for reliable measurement.

e. The results demonstrate that gradation and compaction condition significantly influence resistivity measurements. Coarser gradations generally exhibit higher resistivity, while finer gradations and increased compaction tend to reduce resistivity. Specifications and test procedures should therefore include clear, method-specific guidance regarding gradation selection and compaction control to improve consistency and comparability of resistivity test results.

f. For expanded shale lightweight aggregates, finer particle fractions (passing the No. 10 and No. 50 sieves) exhibited slightly higher pH values relative to the as-received gradation. This behavior is consistent with increased surface area and greater exposure of reactive mineral constituents. While pH values for many test conditions fell within the PennDOT MSE backfill specification range of 6.0 to 10.0, certain fine fractions exceeded this range. These results indicate that particle size influences pH response and that finer fractions may locally approach or exceed specification limits, which should be considered during material evaluation for MSE wall applications.

g. Gradation effects on resistivity were consistent across tested materials. Coarse gradations produced the highest resistivity values, medium gradations exhibited intermediate behavior, and fine gradations yielded the lowest resistivity. This finding reinforces the importance of considering gradation effects when interpreting resistivity results and when developing or refining MSE wall backfill testing specifications.

CHAPTER 5

Summary, Conclusions, and Recommendations

SUMMARY

PennDOT sponsored a research project to evaluate electrochemical testing protocols used to assess quality of lightweight aggregate (LWA) for use as backfill material for MSE walls. These tests are conducted to assess the quality of the aggregate in terms of reducing the risk of corrosion of the embedded metallic reinforcement. This report summarizes the work performed under this project.

Four different LWAs were selected for evaluation, including three expanded shale/slate and one foamed glass aggregate. The testing program comprised two main components: chemical testing (sulfate and chloride content measurement, and pH determination) and electrical resistivity testing. For the chemical tests, multiple extraction procedures and test protocols, particle sizes, and preparation methods were considered to evaluate their influence on measured ion concentrations and pH values. Electrical resistivity tests were performed on the aggregates received from the manufacturers in various conditions. For resistivity testing, custom fabricated boxes of three sizes were utilized to provide ability of changing electrode spacing. In addition to electrode spacing, the effect of several other factors was considered in resistivity testing: aggregate soak time, drainage time, moisture content, compaction level, and aggregate gradation.

CONCLUSIONS

The principal conclusions from this work are summarized below:

1. Influence of extraction method and particle size on sulfate and chloride content measurement

Measured sulfate and chloride content were shown to be sensitive to both extraction protocol and particle size. Procedures incorporating heating consistently produced higher ion concentrations than room-temperature extraction approach, indicating that a more aggressive extraction process mobilizes additional water-soluble salts from the LWA. For all materials, finer particle sizes (e.g.,

passing No. 10 or No. 50 sieves) yielded higher measured sulfate and chloride contents than as-received gradations, reflecting increased surface area and shorter diffusion distances. Among the four materials, Northeast Solite tended to produce the highest sulfate concentrations, especially under heated extraction, with some combinations exceeding the 200 mg/L sulfate control value. Stalite and Norlite generally remained below this threshold under most methods, and AERO AGGREGATE typically showed lower sulfate levels but still responded to aggressive extraction. Chloride contents were generally low for all LWAs. In several cases, the chloride test produced under-range readings (below the 1 mg/L detection limit) even after repeated trials, indicating very low chloride availability.

Overall, the results demonstrate that the choice of test protocol can affect whether a given aggregate appears to meet or marginally exceed specification limits, especially for sulfate. Heated and more aggressive methods should be recognized as conservative in terms of extracted ion content, and any specification based on a particular method needs to be explicit about the extraction procedure and particle size.

2. pH determination behavior

The pH tests conducted on multiple particle sizes showed that all LWAs produced moderate alkaline solutions, with pH values typically in the range of roughly 7.4-10.9, depending on material and particle size. For the expanded shale/slate, finer fractions (passing No. 10 and No. 50 sieve size) tended to yield slightly higher pH than the as-received gradation, again consistent with increased surface area and greater exposure of reactive minerals. Aero Aggregates FGA generally produced higher pH values compared with expanded shales. Although particle size induced measurable differences, the overall pH range remained favorable for metallic reinforcement passivation. None of the materials showed persistently low pH values that would be expected to accelerate steel corrosion, even under the more aggressive extraction conditions.

3. Baseline resistivity behavior for as-received gradations

Electrical resistivity tests were conducted on as-received gradations using custom small, medium, and large boxes to vary electrode spacing. The results showed that all four LWAs exhibit very high resistivity relative to specification thresholds. For all materials, resistivity increased as drainage proceeded, following a characteristic pattern that a rapid rise in the first minutes as free water drained, followed by a slower increase as the material transitioned from capillary to adsorbed

water. AERO AGGREGATE showed the same qualitative behavior but at lower absolute resistivity levels. With the exception of some anomalous behavior in the small box (where resistivity initially decreased during drainage, likely due to test setup artifacts and sensitivity to large particles in a small volume), resistivity was generally higher for smaller electrode spacing and lower for larger boxes. Pre-soaking time had a strong and systematic influence on the value resistivity. For all materials, longer pre-soaking (up to 12 h) reduced the initial resistivity because higher pore water content and greater saturation produced a more continuous conductive phase.

4. Effect of long-term drying considering water content effect

Long-term monitoring of Stalite and AERO AGGREGATE over 48 hours showed that resistivity continued to increase as moisture content declined, eventually approaching stable plateaus once water content fell below roughly 0.5-1% by mass. Short-term soaked specimens (5 min. soaking) started at lower saturation but reached higher resistivity values more quickly, while 12-hour soaked specimens started at lower resistivity and converged toward the similar high resistivity state over time.

The strong coupling between moisture content and resistivity confirmed that 48 hours of drying is generally sufficient to reach a steady electrochemical condition for these materials. For specification or design purposes, resistivity values measured after at least two days of drainage provide a more realistic representation of long-term behavior than very short time readings.

5. Influence of compaction level

Tests on Stalite and AERO AGGREGATE at three compaction levels (loose, medium, dense) demonstrated a consistent trend: looser packing produced higher resistivity, and denser packing produced lower resistivity, when pre-soaking, box size, and test duration were held constant.

For Stalite, reducing void ratio from about e = 1.70 (loose) to e = 0.92 (dense) lowered resistivity by roughly 30% at a given drainage time. For AERO AGGREGATE, the same qualitative pattern was observed, but the difference between loose and dense compaction was proportionally larger, with the loose state yielding nearly double the resistivity of the dense state by the end of the test. However, the medium and loose states were relatively close, because the very large foam glass particles are difficult to significantly rearrange under moderate compaction effort. These results indicate that resistivity measurements on LWAs are influenced by compaction and void ratio, and that laboratory or field data should always be interpreted in the context of placement density.

6. Influence of gradation conditions

For both Stalite and AERO AGGREGATE, gradation had a systematic effect on resistivity when tested in the medium box after 12 h soaking. Specimens prepared with coarse gradations (retaining only particles larger than a specified sieve) exhibited the highest resistivity, as the open and skeletal frameworks drained rapidly and left large, poorly connected voids. Specimens prepared with fine gradations (using only material passing a specified sieve) showed the lowest resistivity and a slower rise over time, because the smaller particles formed denser packings with smaller pores and more robust water films, maintaining better electrical connectivity at a given moisture content. The as-received gradations plotted between these two cases.

For Stalite, the separation between coarse, medium, and fine gradations was pronounced with final resistivities differing by roughly 20-30%. For AERO AGGREGATE, the medium and coarse gradations were closer to one another, reflecting the dominance of large particles and the relatively small role of changes in fines content. These findings confirm that particle size distribution is an important factor on resistivity, in addition to moisture content, compaction, and material type.

RECOMMENDATIONS

1. Use of heated or aggressive extraction methods

Electrochemical test methods referenced by AASHTO and PennDOT for evaluating MSE wall backfill materials are generally conducted without heating and are intended to provide standardized, repeatable measurements representative of typical service conditions. In contrast, TxDOT Tex-620-J incorporates extraction steps with elevated temperature. They constitute a more aggressive procedure and can result in substantially higher measured soluble ion concentrations due to enhanced dissolution and mass transfer.

Results from this study demonstrate that heating during extraction can lead to notable differences in measured ion content. However, even under these aggressive extraction conditions, the lightweight aggregates evaluated generally satisfied the PennDOT Standard Special Provision requirements for MSE wall backfill.

Heated or aggressive extraction methods are not recommended for routine acceptance testing of lightweight aggregates. Nevertheless, such methods may be considered as an upper-bound

assessment tool under limited and specific circumstances where conservative evaluation is considered. These circumstances may include the following:

(a) Elevated or exposure construction temperatures. In regions subject to high temperatures, during summer construction, or in situations where backfill materials experience limited ventilation and solar heating, elevated temperatures can accelerate ion dissolution and transport processes. Heated extraction may serve as a conservative means of evaluating the potential upper bound of soluble ion release under such conditions.

(b) Accelerated approach for long-term ion release. Lightweight aggregates such as expanded shale and foamed glass aggregates are produced through high-temperature processes that create internal pore structures capable of retaining soluble salts within micro voids. Heated extraction can be used as an accelerated approach to assess the potential long-term release of ions that may otherwise be slowly liberated over extended service periods.

(c) Extreme service scenarios involving combined temperature and moisture effects. In conditions where elevated temperatures coincide with prolonged wetting, such as drainage or impervious membrane failure, flooding near stream environments, or sustained high groundwater levels, ion mobility and dissolution rates may be enhanced. In these cases, heated extraction may provide a conservative approximation of worst-case chemical exposure conditions.

(d) When used, heated extraction methods should be clearly identified as aggressive procedures intended to establish an upper-bound estimate of soluble ion release, and results should be interpreted accordingly within the context of MSE wall performance expectations.

2. Consideration of sample preparation and gradation

Electrochemical test methods that require preparation of an aqueous solution, such as sulfate and chloride testing, inherently necessitate alteration of the original aggregate gradation and therefore cannot fully represent field conditions of MSE backfill. The PTM sample preparation method, while sometimes perceived as more representative, still requires material to be processed to pass the No. 8 sieve and thus does not reflect the as-received gradation of lightweight aggregates.

Parameters such as pH and resistivity can be measured directly on aggregate materials without solution extraction. The results of this study indicate that testing using the as-received gradation provides the most appropriate and representative results for evaluating field performance. Accordingly, as-received gradation is recommended for routine pH and resistivity testing of

lightweight aggregates used as MSE wall backfill. Current criteria on pH put the upper limit at 10. It is recommended that this limit be maintained as long as testing for pH is conducted on the as-received material. In case of testing pulverized material, the upper limit on pH may be increased to 11.

For chemical content testing (e.g., sulfates and chlorides), sample pulverization and solution-based extraction are unavoidable in order to transfer soluble ions from the solid aggregate to an aqueous phase suitable for measurement. Within this context, PTM sample preparation represents the least aggressive of the commonly used solution-based methods, as it imposes a coarser particle size requirement (passing the No. 8 sieve) compared to other procedures that require material to pass the No. 10 or No. 50 sieves.

PTM sample preparation may be considered appropriate when sulfate or chloride testing is required and when the intent is to minimize particle size reduction while still achieving adequate ion release for analysis. PTM should not be interpreted as fully representative of field conditions, but rather as a practical compromise between preserving aggregate structure and satisfying the methodological requirements of solution-based chemical testing.

The resistivity box size and use of pulverized material for determination of minimum laboratory soil resistivity according to AASHTO T 288 may not be appropriate for determination of electrical resistivity of lightweight aggregates. It is recommended that as-received material, without alteration of gradation, be used in a larger box size. A proposed test protocol, using a larger box size, for measuring electrical resistivity of LWA accompanies this research report as an independent document.

3. Compaction considerations in resistivity testing

Finger pressure packing of aggregates in laboratory resistivity test boxes is considered appropriate for standardized and repeatable testing, particularly for lightweight aggregates. However, results from this study confirm that lightweight aggregate resistivity, especially for FGA, is highly sensitive to compaction level and void ratio.

Laboratory resistivity testing conducted using finger pressure packing generally represents a relatively loose placement condition compared to typical field-installed MSE wall backfill, where compactive effort is greater and void ratios are lower. As a result, the resistivity measured in laboratory may be higher than the values under actual field compaction conditions. This difference

should be recognized when interpreting laboratory resistivity results for acceptance or design purposes.

While this study demonstrates clear trends relating resistivity to compaction and gradation, the results do not support modification of existing resistivity acceptance criteria or design guidance (e.g., DM-4) at this time. Establishing revised acceptance limits or correction factors would require:

(1) systematic field measurements of in-place resistivity for lightweight aggregate backfill,

(2) paired laboratory and field testing under controlled compaction conditions,

(3) development of empirical relationships linking laboratory resistivity measurements to field performance.

Until such data are available, current resistivity criteria should continue to be applied using standardized laboratory preparation methods, with the understanding that laboratory test results may represent an upper-bound estimate of resistivity relative to field conditions.

4. Influence of moisture content on resistivity and implications for drainage and corrosion protection

Results from this study demonstrate that increasing moisture content significantly reduces the electrical resistivity of lightweight aggregates, which may increase the potential for corrosion of metallic reinforcement elements within MSE wall systems. Exposed reinforcement components, such as steel straps or connectors, are particularly susceptible to accelerated corrosion under moist conditions due to reduced resistivity and enhanced electrochemical activity.

Given the strong sensitivity of resistivity to moisture content, effective drainage design and construction are critical to maintaining favorable electrochemical conditions within MSE wall backfill. Standards and specifications should continue to emphasize requirements related to drainage provisions, including drainage layers, filters, outlets, and long-term maintenance considerations to prevent water accumulation within the reinforced zone.

For MSE wall applications located in environments prone to sustained wetting, such as areas with high groundwater tables, poor surface drainage, proximity to streams, or potential flooding, additional corrosion mitigation measures should be considered. These may include increased considerations of site drainage conditions during design, enhanced inspection of drainage performance during construction, and corrosion protection strategies such as epoxy-coated reinforcement or other protective systems for exposed metallic elements.

While this study does not support changes to existing resistivity acceptance criteria at this time, the findings underscore the importance of drainage performance as a controlling factor in long-term electrochemical behavior. Accordingly, careful evaluation of drainage conditions and moisture exposure should remain an integral part of MSE wall specification, particularly when lightweight aggregates are used as backfill.

Across all tested conditions, the four LWAs generally exhibited low sulfate and chloride availability, moderately alkaline pH, and very high electrical resistivity. Certain combinations of aggressive extraction and fine particle size produced sulfate concentrations near or above the 200 mg/L limit for some materials, most notably for Northeast Solite, suggesting that protocol choice matters and that some LWAs may be classified with respect to existing chemical limits under worst case testing conditions. In contrast, chloride contents were usually well below the 100 mg/L criterion, and many test results fell below the analytical detection limit. Electrical resistivity results were favorable as even under short soaking, loose placement, coarse gradation, and early-time conditions, measured resistivities were one to two orders of magnitude higher than the specification threshold range of 3-5 kΩ·cm. This indicates that, from a resistivity standpoint, all four materials provide a highly resistive environment for metallic reinforcement, with substantial safety margin under realistic field conditions.

Overall, the data show that expanded shale LWAs and foamed glass aggregate can be electrochemically compatible with MSE wall applications, provided that material selection and acceptance testing consider the sensitivity of measured sulfate, chloride, and resistivity to test protocol, gradation, and compaction. The study also highlights the need for clear and method-specific notes in specifications and supports the use of standardized compaction and gradation conditions when resistivity is used as an important parameter for quality control.

The study clearly indicates the significant impact of water content on resistivity. High water content decreases resistivity significantly, and prolonged retainage of water behind the MSE wall may result in the corrosion of metallic rebars. In case of using metallic rebars, taking protective measures to reduce corrosion potential is essential. Such measures may include using waterproof coating of rebars if applicable but ensuring proper drainage behind the wall remains a very crucial step.

It was demonstrated that both chemical and electrical resistivity measured values are affected by the test protocol used to measure the response. The difference among results is sometimes significant and cannot be ignored. Hence, specification should be considerate of this impact, and the

established limits should be appropriate for the selected test procedure. The maximum limit for chloride and sulfate contents needs to be higher if more aggressive testing protocols are opted. Similarly, the minimum resistivity limits may need to be decreased if the test conditions create a harsher condition, reducing the electrical resistivity within the tested material.

All four materials tested in this research appear to be suitable for MSE wall backfill with respect to the current PennDOT EC limits under the current PennDOT test protocols as well as other test methods discussed in this research, except, in some cases, the sulfate content when material heating and high temperature testing is involved. It is recommended that in case of using metallic rebars in MSE walls, the Department monitor the long-term field performance to determine any potential problems requiring revision of either test protocols or the specification limits. PennDOT may decide to be conservative in setting the limits without creating a situation of eliminating good performing materials.

References

Aabøe, R. and Øiseth, E. (2004). "Foamed glass: an alternative lightweight and insulating material." Sustainable Waste Management and Recycling: Glass Waste. *Proc. of the International Conference Organized by the Concrete and Masonry Research*, Kingston University, London, pp. 167–176. Thomas Telford Publishing, London, UK.

Aabøe, R., and Øiseth, E., and Hägglund, J. (2005). "Granulated foamed glass for civil engineering applications." *Workshop NR 2: Recycled Materials in Road and Airfield Pavements*, 25 June 2005, Oslo, Norway. Seventh International Conference on the Bearing Capacity of Roads, Railways, and Airfields, 27-29 June 2005, Trondheim, Norway.

AASHTO (2017). LRFD Bridge Construction Specifications, 4th edition.

AASHTO T 288. (2023). Standard Method of Test for Determining Minimum Laboratory Soil Resistivity. American Association of State Highway and Transportation Officials, Washington, DC.

AASHTO T 289. (2022). Standard Method of Test for Determining pH of Soil for Use in Corrosion Testing. American Association of State Highway and Transportation Officials, Washington, DC.

AASHTO T 290. (2020). Standard Method of Test for Determining Water-Soluble Sulfate Ion Content in Soil. American Association of State Highway and Transportation Officials, Washington, DC.

AASHTO T 291. (2022). Standard Method of Test for Determining Water-Soluble Chloride Ion Content in Soil. American Association of State Highway and Transportation Officials, Washington, DC.

Arciniega, J.L. (2017). "Invited student paper—Impact of grain size distribution on resistivity of mechanically stabilized earth wall backfill materials." *Proc., Transportation Research Board Annual Meeting*. Washington, DC: Transportation Research Board.

Arciniega, J.L., Walker, W.S., Nazarian, S., and Fishman, K.L. (2018). "A process for optimizing gradation of marginal backfill of mechanically stabilized earth walls to achieve acceptable resistivity." *Proc. Transportation Research Board Annual Meeting*. Washington, DC: Transportation Research Board.

ASTM D4972-19. (2019). Standard Test Methods for pH of Soils. ASTM International, West Conshohocken, PA.

ASTM WK24621. (2015). Test Method for Measurement of Coarse Aggregate Resistivity Using the Two- Electrode Soil Box. Draft Document, 08-28-2015, for consideration by ASTM Subcommittee C-09.20.

Agrawal Y., Gupta, T., Sharma R., Panwar, N.L., and Siddique S. (2021). A Comprehensive Review on the Performance of Structural Lightweight Aggregate Concrete for Sustainable Construction. Construction Materials. 1. 39-62. 10.3390/constrmater1010003.

Ardakani A., and Yazdani M. (2014). The relation between particle density and static elastic moduli of lightweight expanded clay aggregates. Appl. Clay Sci. 2014 (93-94), 28-34.

Arioz, K.O., and Karasu, K. (2008), A preliminary research on the properties of lightweight expanded clay aggregate. J. Aust. Ceram. Soc., 69, 23-30.

Arulrajah, A., Disfani, M.M., Maghoolpilehood, F., Horpibulsuk, S., Udonchai, A., and Du, Y.J. (2015a). "Engineering and environmental properties of foamed recycled glass as a lightweight engineering material." *Journal of Cleaner Production*, 94(a), 369-375.

Arulrajah, A., Horpibulsuk, S., Maghoolpilehood, F., Samingthong, W., Du, Y.J., and Shen, S.L. (2015b). "Evaluation of Interface Shear Strength Properties of Geogrid Reinforced Foamed Recycled Glass Using a Large Direct Shear Testing Apparatus." *Advances in Materials Science and Engineering*, 2015(2), 1-7.

ASTM International. (2017). ASTM C331/C331M-17: Standard Specification for Lightweight Aggregates for Concrete Masonry Units1.

Barbosa F.S., Farage M.C.R., Beaucour A.L., and Ortola S. (2012). Evaluation of aggregate gradation in lightweight concrete via image processing. Construction and Building Materials. 29:7-11.

Betti, G., Pinori, U., and Marradi, A. (2014). "The Use of Recycled Glassfoam Aggregates for Lightweight Embankment." *3rd International Conference on Transportation Infrastructure*, ICTI 2014 Pisa, 22-25 April 2014.

Boarder R.F.W., Owens P.L., and Khatib J.M. (2016). 10 - The sustainability of lightweight aggregates manufactured from clay wastes for reducing the carbon footprint of structural and foundation concrete. Woodhead Publishing Series in Civil and Structural Engineering, Sustainability of Construction Materials (Second Edition), 209-244.

Bogas J.A., Carriço A., and Pontes J. (2019). Influence of cracking on the capillary absorption and carbonation of structural lightweight aggregate concrete, Cem. Concr. Compos. 104, 103382.
Chia K.S., and Zhang M. (2002). Water permeability and chloride penetrability of high-strength lightweight aggregate concrete. Cement and Concrete Research, 32, 639-645.

Borrok, D., Bronson, A., Rocha, S., and Nazarian, B. (2013). Characterization of Coarse Backfill Materials for Prevention of Corrosion of MSE Metallic Wall Reinforcement. FHWA/TX-11/0-6359-1. Center for Transportation Infrastructure Systems, University of Texas at El Paso.

Borthakur A., Chhour K.L., Gayle H.L., Prehn S.R., Stenstrom M.K., and Mohanty S.K. (2022). Natural aging of expanded shale, clay, and slate (ESCS) amendment with heavy metals in stormwater

increases its antibacterial properties: Implications on biofilter design. J Hazard Mater. 2022 May 5;429:128309. doi: 10.1016/j.jhazmat.2022.128309.

Boudaghpour S., and Hashemi S. (2008). Study on Light Expended Clay Aggregate (LECA) in a Geotechnical View and its Application on Greenhouse and Greenroof Cultivation International Journal of Geology. 2:59–63.

Cabrera, D. (2018). "Invited student paper—Monitoring rate of corrosion of metallic reinforcements in backfill material for mechanically stabilized walls." *Proc., Transportation Research Board Annual Meeting*. Washington, DC: Transportation Research Board.

Chandra S., Berntsson L. (2002). Lightweight Aggregate Concrete Science, Technology, and Applications. Noyes Publications, New York.

Das, T.K., Raoelison, O.D., Rehman, H., Zhang, Y., Chau, W., Thamiz, L., Stenstrom, M. K., Mohanty, S.K. (2023). Use of expanded shale, clay, and slate aggregates and biochar in the clear zone of road infrastructures for sustainable treatment of stormwater. J. Clean. Prod. 428, 139443 https://doi.org/10.1016/j. jclepro.2023.139443.

EPA (1999). National Primary Drinking Water Standards. EPA-F-94-001. Environment Protection Agency, Washington, USA.

EPA (2007). Information Update for EPA 996. Environmental Protection Agency of Victoria, Australia, Victoria, Australia.

EPA (2009). Solid Industrial Waste Hazard Categorization and Management, Industrial Waste Resource Guidelines. Publication No. IWRG 631. Environmental Protection Agency of Victoria, Australia, Victoria, Australia.

Frydenlund, T.E. and Aabøe, R. (2003). "Foamglass – A New Vision in Road Construction." *The XXIInd PIARC World Road Congress*, 19-25 October 2003, Durban, South Africa.

Fishman, K.L., Nazarian, S., Walker, S., and Bronson, A. (2021a). Electrochemical Test Methods to Evaluate the Corrosion Potential of Earthen Materials. Washington, DC: The National Academies Press. https://doi.org/10.17226/26076.

Fishman, K.L., Fakhri, H., Nazarian, S., Walker S., and Bronson, A. (2021b). "Evaluation of Test Methods for Characterizing Steel Corrosion Potential in MSE Wall Fill." *Proceedings of Corrosion 2021 Conference*, April 19-30.

Geosystems Consultants, Inc. (2013). "Geotechnical Laboratory Testing Results, Lightweight Aggregate." 8 May, 2013.

Holm, T. A., and Ries, J. P. (2007). ESCSI's Reference Manual for the Properties and Applications of Expanded Shale, Clay, and Slate Lightweight Aggregate. Expanded Shale, Clay and Slate Institute.

Holm, T.A., and Valsangkar A.J. (1993). Lightweight aggregate soil mechanics: properties and applications. Transportation Research Record: 7-13.

Kokusho, T. and Esashi, Y. (1981). "Cyclic triaxial test on sands and coarse materials." *Proceedings of the 10th international conference on soil mechanics and foundation engineering,* Stockholm, Sweden, vol. 1. Rotterdam, The Netherlands: A. A. Balkema; p. 673–6.

Krc, K. (2015). An investigation of shear-friction of lightweight aggregate concretes (2015). Master's Theses. 7468. https://scholarsmine.mst.edu/masters_theses/7468.

Lenart, S. and Kaynia, A.M. (2019). "Dynamic properties of lightweight foamed glass and their effect on railway vibration." *Transportation Geotechnicas*, 21, 100276, https://doi.org/10.1016/j.trgeo.2019.100276.

Lotfy, A., Hossain, K.M.A. and Lachemi, M. Lightweight Self-consolidating Concrete with Expanded Shale Aggregates: Modelling and Optimization. *International Journal of Concrete Structures and Materials*. 9, 185–206 (2015). https://doi.org/10.1007/s40069-015-0096-5.

Loux, T., Laspee, H.E., and Filshill, A. (2018). "Foamed glass aggregate: A lightweight fill alternative finds the U.S. market," *Practice on the Cutting Edge*, ASCE Metropolitan Section, May 10, New York City.

Loux, T., Filshill, A., and Zhang, Z. (2019). "Foamed glass aggregate lightweight fill over compressible soils," *GeoSt. John's Under Land & Sea Conference*, September 29 – October 2, St. John's, CA.

Loux, T., McInnes, S., Crawford, R., and Filshill, A. (2021). "Design and Construction of a Geosynthetic Reinforced MSE Structure with Foamed Glass Aggregate Lightweight Backfill." *7th European Geosynthetics Conference*, 4-7 September 2022, Warsaw, Poland.

Lu J.X., Shen. P., Ali H.A., and Poon C.S. (2021). Development of high performance lightweight concrete using ultra high performance cementitious composite and different lightweight aggregates, Cem. Concr. Compos. 124, 104277.

Lu, J.X. (2023). Recent advances in high strength lightweight concrete: from development strategies to practical applications. Construct. Build. Mater. 400, 132905.

Mohammed,T., Aguayo, F., Nodehi, M., and Ozbakkaloglu, T. (2022). Engineering properties of structural lightweight concrete containing expanded shale and clay with high volume class F and class C fly ash. Struct. Concr.

Mustafa, W.S., Szendefy J., and Nagy B. (2023) Thermal performance of foam glass aggregate at different compaction ratios, MDPI Build. 13 1–21.

Nicks, J.E., Ghaaowd I.I., and Adams, M.T. (2024) Strength-Deformation Characteristics of Two Different Foamed Glass Aggregates under a Static Design Load. Geotech. Test. J. 47 (1): 351–370. https://doi.org/10.1520/GTJ20220258.

Nilsen A.U., Monteiro P.J.M., Gjørv O.E. (1995). Estimation of the elastic moduli of lightweight aggregate. Cement Concr. Res. 25 (2), 276–280.

Nishio, N, Tamaoki, K, and Machida, Y. (1985). "Dynamic deformation characteristics of crushed gravel by means of large-size triaxial test apparatus." *Proceedings of the 20th annual convention*, Japanese society of soil mechanics and foundation engineering, Tokyo, Japan. p. 603–4.

Nodehi, M. (2021) A comparative review on foam-based versus lightweight aggregate-based alkali-activated materials and geopolymer. Innov. Infrastruct. Solut. 6, 231. https://doi.org/10.1007/s41062-021-00595-w.

Parsons, R.L., Brady, Z., Walkenbach, T.N., Han, J., Kulesza, S., and Brennan, J. (2020). "Resistivity measurement of backfill for mechanically stabilized earth walls," *Journal of Materials in Civil Engineering*, 32(3), 04019367.

Prange, B. (1981). "Resonant Column Testing of Railroad Ballast." *Proceedings of the 10th international conference on soil mechanics and foundation engineering*, Stockholm, Sweden, Vol. 3. Rotterdam, The Netherlands: A. A. Balkema; p. 273–82.

Rahman, M.A., Arulrajah, A., Piratheepan, J., Bo, M.W., and Imteaz, M.A. (2014a). "Resilient modulus and permanent deformation responses of geogrid-reinforced construction and demolition materials." *J. Mater. Civ. Eng*. 26, 512e519.

Rahman, M.A., Imteaz, M., Arulrajah, A., and Disfani, M.M. (2014b). "Suitability of recycled construction and demolition aggregates as alternative pipe backfilling materials." *J. Clean. Prod*. 66, 75e84.

Rumšys D., Bacinskas D., Spudulis E., and Meškėnas A. (2017). Comparison of Material Properties of Lightweight Concrete with Recycled Polyethylene and Expanded Clay Aggregates. Procedia Engineering, 172, 937-944.

Selman S.M., and Abbas Z.K. (2022). The Use of Lightweight Aggregate in Concrete: A Review. Journal of Engineering, 28(1-13). https://doi.org/10.31026/j.eng.2022.11.01.

Shafigh P., Mahmud H.B., Jumaat M.Z.B., Ahmmad R., and Bahri S. (2014). Structural lightweight aggregate concrete using two types of waste from the palm oil industry as aggregate. Journal of Cleaner Production, 80: 187-196.

Skogstad, H.B., Geving, S., and Hägglund, J. (2005). "Hygrothermal material properties for granulated cellular glass used in ground constructions." *Proceedings of the 7th Symposium on Building Physics in the Nordic Countries*. 13-15 June 2005, Reykjavík, Iceland.

Stoll R.D., and Holm T.A., (1985). Expanded Shale Lightweight Fill: Geotechnical Properties. Journal of Geotechnical Engineering. 111(8): 1023-1027.

Sveindottir, E.L., Maage, M., Poot, S., Hansen, E.A., Bennenk, H.W., Helland, S., Norden, G., Kwint, E., Milencovic, A., Smeplass, S., et al.(1998). LWAC Material Properties-State-of-the-Art. BriteEuram Proj. Euro Lightcon. 111. doi:10.13140/RG.2.2.31783.70566.

Swan, R.H., Yeom, S., Sjoblom, K.J., Stark, T.D., and Filshill, A. (2016). "Engineering Properties of Foamed Recycled Glass as a Lightweight Fill." Proceedings of the Geo-Chicago 2016 Conference, https://doi.org/10.1061/9780784480151.002.

Tanaka, Y, Kudo, K, Yoshida, Y, and Ikemi, M. (1987). "A study on the mechanical properties of sandy gravel-Dynamic properties of reconstituted sample." Research report No. U87019. Abiko, Japan; Central Research Institute of Electric Power Industry, in Japanese.

Tehrani F.M. (2021). Non-Corrosivity of Expanded Shale, Clay and Slate Aggregate in Mechanically Stabilized Earth Fills. E-newsletters Archive, ESCSI. https://www.escsi.org/e-newsletter/non-corrosivity-of-expanded-shale-clay-and-slate-aggregate-in-mechanically-stabilized-earth-fills/.

Tex-128-E. (1999). Determining Soil pH. Texas Department of Transportation, Austin, TX.

Tex-129-E. (1999). Measuring the Resistivity of Soil Materials. Texas Department of Transportation, Austin, TX.

Tex-129-M. (2018). Test Procedure for Measuring the Resistivity of Soils and Aggregates. Texas Department of Transportation, Austin, TX.

Tex-620-J. (2005). Determining Chloride and Sulfate Contents in Soil. Texas Department of Transportation, Austin, TX.

Tex-620-M. (2018). Test Procedure for Determining the Conductivity, pH, Sulfate Content, and Chloride Content of Soil and Coarse Aggregate. Texas Department of Transportation, Austin, TX.

Thienel, K.C., Haller, T., and Beuntner, N. (2020). Lightweight Concrete-From Basics to Innovations. Materials, 13, 1120. https://doi.org/10.3390/ma13051120.

Valsangkar A.J., and Holm T.A. (1990). Geotechnical Properties of Expanded Shale Lightweight Aggregate. Geotechnical Testing Journal. 13, 10-15.

Vilda, W.S. III. (2009). Corrosion in the Soil Environment: Soil Resistivity and pH Measurements. Final Report, NCHRP Project 21-06. http://onlinepubs.trb.org/onlinepubs/nchrp/docs/NCHRP21-06_FR.pdf.

Wall J., and Castrodale R. (2019) ESCS lightweight aggregate geotechnical fill. North Carolina Department of Transportation GEO3T2 Conference Cary, North Carolina

Wartman, J., Grubb, D.G., and Nasim, A.S.M. (2004). “Select engineering characteristics of crushed glass.” *J. Mater. Civ. Eng*. 16, 526e539.

Wu T., Wei H., Liu X., and Xing G. (2016). Factor Influencing the mechanical properties of lightweight aggregates concrete. Indian Journal of Engineering and Material Sciences 23 301-11.

Yoon, J.Y., Kim, J.H., Hwang, Y.Y., and Shin, D.K. (2015). Lightweight Concrete Produced Using a Two-Stage Casting Process. Materials. 8, 1384-1397. https://doi.org/10.3390/ma8041384.

Youm K.S., Moon, J., Cho J.Y., and Kim J.J. (2016). Experimental study on strength and durability of lightweight aggregate concrete containing silica fume, Constr. Build. Mater. 114, 517–527.

Zegowitz, A. (2010). “Cellular Glass Aggregate Serving as Thermal Insulation and a Drainage Layer.” *Proceedings of Thermal Performance of Exterior Envelopes of Whole Buildings XI*, Florida, USA.

Zhang B., and Poon, C.S. (2015). Use of Furnace Bottom Ash for producing lightweight aggregate concrete with thermal insulation properties. Journal of Cleaner Production, 99, 94-100.

Zukri, A., Nazir, R., Said, K.N., and Moayedi, H. (2018). Physical and Mechanical Properties of Lightweight Expanded Clay Aggregate (LECA). MATEC Web of Conferences, 250. DOI: 10.1051/matecconf/201825001016.

Proposed Test Method Protocol

Electrical Resistivity Testing of Lightweight Aggregates (LWA)

for Mechanically Stabilized Earth (MSE) Wall Backfill

Draft prepared for PennDOT LWA Project

1. Scope

1.1 This test method covers the determination of bulk electrical resistivity of lightweight aggregate (LWA) materials intended for use as mechanically stabilized earth (MSE) wall backfill.

1.2 The procedure is intended for coarse, granular LWAs (e.g., expanded shale and foamed glass aggregate) tested in their as-received gradation to better reflect field particle size distribution and packing conditions.

1.3 The method measures electrical resistance using a two-electrode box configuration and converts the measured resistance to bulk resistivity using the geometric characteristics of the test box.

1.4 The method provides (a) a resistivity measurement at a standardized drained condition and (b) optional resistivity-time behavior during drainage for research/diagnostic purposes.

1.5 The values stated in SI units are to be regarded as standard. Inch-pound units may be used in parallel where required by project specifications.

2. Referenced Documents

2.1 AASHTO Standards:

- T 288 Standard Method of Test for Determining Minimum Laboratory Soil Resistivity
- T 255 Standard Method of Test for Total Evaporable Moisture Content of Aggregate by Drying
- T 19 Standard Method of Test for Bulk Density (“Unit Weight”) and Voids in Aggregate (optional for documenting packing)

2.2 Other references:

- Agency specifications: PennDOT Standard Special Provision for MSE Backfill

3. Terminology

3.1 Definitions

3.1.1 electrical resistance (R) — the measured opposition to the flow of alternating current through the specimen, in ohms (Ω).

3.1.2 bulk electrical resistivity (ρ) — the material property describing resistance to current flow through a specimen of known geometry, in ohm-centimeters (Ω·cm) or ohm-meters (Ω·m).

3.1.3 electrode spacing (L) — the distance between the inner faces of the two electrode plates, in centimeters (cm).

3.1.4 cross-sectional area (A) — the internal cross-sectional area of the specimen normal to current flow, in square centimeters (cm^2).

3.1.5 geometric box factor (K) — the ratio A/L, used to convert resistance to resistivity ($\rho = R \times K$).

3.1.6 as-received gradation — material gradation as delivered for construction, without laboratory crushing/pulverizing or sieve separation.

3.1.7 drained condition — specimen condition after gravity drainage with the drain port open for a defined time period, representing a partially drained backfill condition.

4. Summary of Test Method

4.1 A representative mass of LWA in its as-received gradation is pre-soaked for a defined time to establish a repeatable initial moisture condition. The specimen is placed into a custom resistivity box in lifts and packed to a standardized condition. Electrical resistance is measured under (a) a saturated condition and (b) during gravity drainage. Resistance is converted to bulk resistivity using the box geometry.

4.2 A standardized drained-condition resistivity is reported at a prescribed drainage time (recommended: 24 h) or at stabilization, whichever occurs first, to balance practicality with repeatability for LWAs with high internal porosity.

5. Significance and Use

5.1 Electrical resistivity is used as an indicator of the potential corrosivity of backfill materials in contact with metallic reinforcement in MSE wall systems. Higher resistivity generally indicates lower ionic conductivity and reduced likelihood of corrosion.

5.2 Conventional AASHTO soil-box resistivity testing was developed primarily for soils and backfills finer than the No. 10 sieve. For coarse LWAs, forcing particles into a small soil box can alter packing and bias results. This protocol therefore specifies testing on as-received LWA gradation using a larger custom box to preserve particle arrangement.

5.3 The protocol is intended for material acceptance testing and comparative evaluation across LWA sources. Optional drainage-curve data may be collected for research, forensic evaluation, or to support field-laboratory correlation.

6. Apparatus

6.1 Resistivity Measurement Instrument — An LCR meter or equivalent resistance meter capable of measuring resistance using AC excitation at 97 Hz (or comparable frequency specified by the agency).

6.2 Custom Resistivity Box — A rigid, nonconductive box fitted with two stainless steel plate electrodes on opposing ends and a closable drainage port near the base.

6.2.1 Recommended box selection: the MEDIUM box configuration

- Rationale: provides conservative (lower) resistivity compared with short soaking in smaller configurations, while approaching results observed in larger boxes.
- Reduces sensitivity to single large-particle bridging and edge effects common in undersized boxes.
- Practical specimen mass and handling compared with the largest configuration.
- Box dimensions (length × width × height): 33.97 × 16.83 × 17.15 cm (measure and record the actual dimensions for each box).

6.2.2 Cross-sectional area (A): measure the internal width and height of the filled specimen section; compute A = width × height (cm^2).

6.3 Drainage System — A gravity-drain outlet with removable stopper; collection tray for drain water.

6.4 Balance — capable of measuring specimen mass to 0.1 g or better.

6.5 Containers — nonreactive soaking container(s) of sufficient volume to fully submerge the specimen mass.

6.6 Thermometer — ambient and water temperature measurement (±1 °C) to document test conditions.

6.7 Optional: companion box for moisture-content sampling (to avoid disturbing the box used for continuous resistivity monitoring).

7. Reagents and Water

7.1 Water — distilled or deionized (DI) water with resistivity greater than 20,000 Ω·cm.

7.2 Cleaning — DI water and non-ionic detergent for washing the box and electrodes; lint-free wipes for drying.

8. Sampling

8.1 Obtain a representative sample of the LWA in accordance with agency sampling requirements.

8.2 Maintain the sample in sealed containers to preserve as-received moisture condition prior to testing.

8.3 Do not crush, pulverize, or otherwise reduce particle size for resistivity testing under this protocol.

9. Test Specimen Preparation

9.1 Use the as-received material gradation. If the delivered material includes oversize particles exceeding the box capacity or causing bridging, note this and select a box meeting minimum dimension criteria (see 6.2) or document a justified trimming approach.

9.2 Determine and record the maximum particle size (D_{max}) of the as-received material.

9.3 Recommended minimum box sizing guidance: electrode spacing $\geqslant 8\times D_{max}$ and specimen height $\geqslant 3\times D_{max}$ to reduce particle-scale artifacts.

9.4 Pre-soaking condition.

9.4.1 Place sufficient as-received LWA mass in a clean container and add DI water until fully submerged.

9.4.2 Mix gently to dislodge entrapped air and promote uniform wetting without crushing particles.

9.4.3 Allow the specimen to soak for at least 12 hours to establish a repeatable and conservative moisture condition for acceptance testing.

Note: shorter pre-soak periods can yield higher resistivity due to incomplete wetting of internal pores of LWAs; 12 h is intended to reduce variability and represent a conservative low-resistivity condition.

10. Procedure

10.1 Box Preparation

10.1.1 Verify the box is clean and dry; ensure electrode plates are securely mounted and free of corrosion or deposits.

10.1.2 Measure and record box internal width and height (for A) and electrode spacing L.

10.1.3 Close the drainage port with the stopper and confirm watertight seal.

10.2 Specimen Placement and Standardized Packing

10.2.1 Remove the pre-soaked specimen from the soaking container and allow free water to drain briefly without shaking or squeezing.

10.2.2 Place the material into the box in three approximately equal lifts.

10.2.3 For each lift, apply moderate finger pressure packing (or an agency-specified equivalent) to achieve a consistent arrangement without particle crushing. Level the surface before placing the next lift.

10.2.4 After the final lift, level the top surface to ensure full contact to the electrode plates along the specimen height.

10.2.5 Influence of Packing and Compaction Level:

The electrical resistivity is strongly influenced by particle contact conditions and void ratio. Increased compaction generally results in lower resistivity due to improved particle contact and reduced pore space. The finger pressure packing specified in this procedure represents a standardized and repeatable laboratory placement condition and is not intended to replicate field-installed compaction levels. As a result, resistivity values measured using this method may be higher than those achieved under typical field compaction conditions and should be interpreted as a conservative indicator for acceptance and comparative evaluation.

10.3 Saturated Resistance Measurement

10.3.1 With the drain port sealed, connect the meter leads to the electrode terminals.

10.3.2 Measure resistance at 97 Hz AC (or specified frequency) and record the stabilized resistance R_{sat} (Ω). Record temperature.

10.4 Drainage Phase and Drained-Condition Measurement

10.4.1 Immediately after the saturated reading, open the drainage port and allow gravity drainage. Collect drainage water if desired for documentation.

10.4.2 Record resistance R(t) at the following minimum time points after opening the drain: 5s, 10s, 30s, 1min, 2min, 5 min, 10 min, 30 min, 1 h, 2 h, 4 h, 8 h, 12 h, and 24 h.

10.4.3 Standard acceptance reporting time: 24 h after opening the drain (R_{24h}), unless stabilization occurs earlier.

10.4.4 Stabilization criterion (optional): if the resistance change is less than 2% over a 60-minute period after 12 h drainage, the specimen may be considered stabilized and the stabilized resistance R_{stab} may be reported.

10.4.5 If the specimen has not stabilized by 24 h and the agency requires a near-dry endpoint, continue monitoring to 48 h and report both R_{24h} and R_{48h}.

10.5 Optional Moisture Content Measurements

10.5.1 To relate resistivity change to moisture content without disturbing the resistivity specimen, conduct moisture sampling using a companion box prepared and drained in parallel under identical conditions.

10.5.2 At selected time points (e.g., 1 h, 2 h, 4 h, 8 h, 12 h, 24 h, 48 h), remove a representative subsample from the companion box and determine gravimetric moisture content per AASHTO T 255.

11. Calculation

11.1 Compute geometric box factor K (cm): $K = A / L$, where A is specimen cross-sectional area (cm^2) and L is electrode spacing (cm).

11.2 Compute bulk resistivity ρ ($\Omega \cdot cm$): $\rho = R \times K = R \times A / L$.

11.3 Report resistivity at saturated condition (ρ_{sat}) using R_{sat}, and at standardized drained condition (ρ_{24h}) using R_{24h} (or ρ_{stab} if stabilization criterion is used).

11.4 If multiple readings are taken, plot ρ versus time and identify characteristic phases (rapid early change during free-water drainage followed by slower change as capillary/adsorbed water dominates).

12. Report

12.1 Report the following information:

- Material identification (supplier, product, lot number, source location, date received).
- As-received gradation description and D_{max}.

- Box configuration used (recommended: medium), measured electrode spacing L (cm), internal width and height, computed area A (cm^2), and box factor K (cm).
- Pre-soak time (recommended: 12 h) and water type (DI water resistivity).
- Packing method used (e.g. finger pressure packing; number of lifts).
- Resistance readings: R_{sat} and R(t) at specified times, including R_{24h} (and R_{48h} if collected).
- Computed resistivity values: ρ_{sat}, ρ_{24h} (and ρ_{48h} if collected).
- Ambient and water temperature during testing.
- Any deviations from this protocol and rationale (e.g., box size changes due to particle size or bridging).

13. Precision and Bias

13.1 Precision for this protocol should be established by the implementing laboratory. At minimum, perform duplicate tests on the same lot and report the mean and percent difference.

13.2 Bias: As with resistivity testing generally, the measured value is sensitive to specimen geometry, packing, electrode contact, and moisture condition. Using standardized box configuration, pre-soak time, and packing procedure is intended to reduce inter-laboratory variability.

14. Notes and Annex

14.1 Rationale for as-received gradation — Resistivity of granular backfill is governed by packing structure and pore connectivity; altering particle size distribution can produce resistivity values not representative of field placement.

14.2 Rationale for medium box selection — Project testing showed that resistivity outcomes vary with electrode spacing and box size; medium and large boxes typically provide more representative bulk behavior than an undersized box, while remaining practical for routine testing.

14.3 Suggested agency acceptance reporting — For routine acceptance, reporting a standardized drained-condition resistivity (ρ_{24h}) plus a saturated value (ρ_{sat}) provides a conservative bracket of behavior under wet-to-drained conditions.

14.4 Future refinement — If agency practice requires direct prediction of field resistivity from laboratory values, a paired laboratory-field dataset under documented compaction and moisture conditions is recommended to develop a conversion relationship.